

SEVENTH EDITION

PRINCIPLES OF

# FOUNDATION ENGINEERING



BRAJA DAS

**Principles of Foundation Engineering****Seventh Edition****Author Braja M. Das**

Publisher, Global Engineering:

Christopher M. Shortt

Senior Developmental Editor: Hilda Gowans

Editorial Assistant: Tanya Altieri

Team Assistant: Carly Rizzo

Marketing Manager: Lauren Betzos

Production Manager: Patricia M. Boies

Content Project Manager: Darrell Frye

Production Service: RPK Editorial Services, Inc.

Copyeditor: Shelly Gerger-Knechtel

Proofreader: Martha McMaster

Indexer: Braja M. Das

Compositor: Integra

Senior Art Director: Michelle Kunkler

Internal Designer: Carmela Pereira

Cover Designer: Andrew Adams

Cover Images:

Courtesy of ADSC : The International Association of Foundation Drillers, Dallas, Texas D. B. M. Contractors, Inc., Federal Way, Washington

Nicholson Construction Company, Cuddy, Pennsylvania

Image Permissions Researcher: Deanna Ettinger

Text Permissions Researcher: Katie Huha

Text and Image Permissions Researcher: Kristiina Paul

First Print Buyer: Arethea Thomas

©2011, 2007 Cengage Learning

ALL RIGHTS RESERVED. No part of this work covered by the copyright herein may be reproduced, transmitted, stored, or used in any form or by any means graphic, electronic, or mechanical, including but not limited to photocopying, recording, scanning, digitizing, taping, web distribution, information networks, or information storage and retrieval systems, except as permitted under Section 107 or 108 of the 1976 United States Copyright Act, without the prior written permission of the publisher.

For product information and technology assistance,  
contact us at **Cengage Learning Customer &  
Sales Support, 1-800-354-9706**

For permission to use material from this text or product,  
submit all requests online at [cengage.com/permissions](http://cengage.com/permissions)  
Further permissions questions can be emailed to  
[permissionrequest@cengage.com](mailto:permissionrequest@cengage.com)

Library of Congress Control Number: 2009940220

ISBN-13: 978-0-495-66810-7

ISBN-10: 0-49566810-9

**Cengage Learning**200 First Stamford Place, Suite 400  
Stamford, CT 06902  
USA

Cengage Learning is a leading provider of customized learning solutions with office locations around the globe, including Singapore, the United Kingdom, Australia, Mexico, Brazil, and Japan. Locate your local office at:  
[international.cengage.com/region](http://international.cengage.com/region)

Cengage Learning products are represented in Canada by Nelson Education Ltd.

For your course and learning solutions, visit  
[www.cengage.com/engineering](http://www.cengage.com/engineering)

Purchase any of our products at your local college store or at our preferred online store [www.CengageBrain.com](http://www.CengageBrain.com)

# 1

# Geotechnical Properties of Soil

## 1.1

## Introduction

The design of foundations of structures such as buildings, bridges, and dams generally requires a knowledge of such factors as (a) the load that will be transmitted by the superstructure to the foundation system, (b) the requirements of the local building code, (c) the behavior and stress-related deformability of soils that will support the foundation system, and (d) the geological conditions of the soil under consideration. To a foundation engineer, the last two factors are extremely important because they concern soil mechanics.

The geotechnical properties of a soil—such as its grain-size distribution, plasticity, compressibility, and shear strength—can be assessed by proper laboratory testing. In addition, recently emphasis has been placed on the *in situ* determination of strength and deformation properties of soil, because this process avoids disturbing samples during field exploration. However, under certain circumstances, not all of the needed parameters can be or are determined, because of economic or other reasons. In such cases, the engineer must make certain assumptions regarding the properties of the soil. To assess the accuracy of soil parameters—whether they were determined in the laboratory and the field or whether they were assumed—the engineer must have a good grasp of the basic principles of soil mechanics. At the same time, he or she must realize that the natural soil deposits on which foundations are constructed are not homogeneous in most cases. Thus, the engineer must have a thorough understanding of the geology of the area—that is, the origin and nature of soil stratification and also the groundwater conditions. Foundation engineering is a clever combination of soil mechanics, engineering geology, and proper judgment derived from past experience. To a certain extent, it may be called an art.

When determining which foundation is the most economical, the engineer must consider the superstructure load, the subsoil conditions, and the desired tolerable settlement. In general, foundations of buildings and bridges may be divided into two major categories: (1) *shallow foundations* and (2) *deep foundations*. *Spread footings*, *wall footings*, and *mat foundations* are all shallow foundations. In most shallow foundations, *the depth of embedment can be equal to or less than three to four times the width of the foundation*. *Pile* and *drilled shaft* foundations are deep foundations. They are used when top layers have poor

load-bearing capacity and when the use of shallow foundations will cause considerable structural damage or instability. The problems relating to shallow foundations and mat foundations are considered in Chapters 3, 4, 5, and 6. Chapter 11 discusses pile foundations, and Chapter 12 examines drilled shafts.

This chapter serves primarily as a review of the basic geotechnical properties of soils. It includes topics such as grain-size distribution, plasticity, soil classification, effective stress, consolidation, and shear strength parameters. It is based on the assumption that you have already been exposed to these concepts in a basic soil mechanics course.

## 1.2

## Grain-Size Distribution

In any soil mass, the sizes of the grains vary greatly. To classify a soil properly, you must know its *grain-size distribution*. The grain-size distribution of *coarse-grained* soil is generally determined by means of *sieve analysis*. For a *fine-grained* soil, the grain-size distribution can be obtained by means of *hydrometer analysis*. The fundamental features of these analyses are presented in this section. For detailed descriptions, see any soil mechanics laboratory manual (e.g., Das, 2009).

### Sieve Analysis

A sieve analysis is conducted by taking a measured amount of dry, well-pulverized soil and passing it through a stack of progressively finer sieves with a pan at the bottom. The amount of soil retained on each sieve is measured, and the cumulative percentage of soil passing through each is determined. This percentage is generally referred to as *percent finer*. Table 1.1 contains a list of U.S. sieve numbers and the corresponding size of their openings. These sieves are commonly used for the analysis of soil for classification purposes.

**Table 1.1** U.S. Standard Sieve Sizes

Sieve No.	Opening (mm)
4	4.750
6	3.350
8	2.360
10	2.000
16	1.180
20	0.850
30	0.600
40	0.425
50	0.300
60	0.250
80	0.180
100	0.150
140	0.106
170	0.088
200	0.075
270	0.053

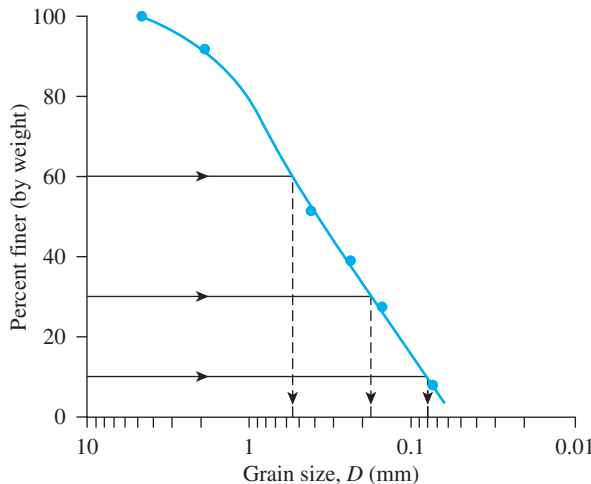


**Figure 1.1** Grain-size distribution curve of a coarse-grained soil obtained from sieve analysis

The percent finer for each sieve, determined by a sieve analysis, is plotted on *semilogarithmic graph paper*, as shown in Figure 1.1. Note that the grain diameter,  $D$ , is plotted on the *logarithmic scale* and the percent finer is plotted on the *arithmetic scale*.

Two parameters can be determined from the grain-size distribution curves of coarse-grained soils: (1) the *uniformity coefficient* ( $C_u$ ) and (2) the *coefficient of gradation*, or *coefficient of curvature* ( $C_c$ ). These coefficients are

$$C_u = \frac{D_{60}}{D_{10}} \quad (1.1)$$

and

$$C_c = \frac{D_{30}^2}{(D_{60})(D_{10})} \quad (1.2)$$

where  $D_{10}$ ,  $D_{30}$ , and  $D_{60}$  are the diameters corresponding to percents finer than 10, 30, and 60%, respectively.

For the grain-size distribution curve shown in Figure 1.1,  $D_{10} = 0.08$  mm,  $D_{30} = 0.17$  mm, and  $D_{60} = 0.57$  mm. Thus, the values of  $C_u$  and  $C_c$  are

$$C_u = \frac{0.57}{0.08} = 7.13$$

and

$$C_c = \frac{0.17^2}{(0.57)(0.08)} = 0.63$$

Parameters  $C_u$  and  $C_c$  are used in the *Unified Soil Classification System*, which is described later in the chapter.

### Hydrometer Analysis

Hydrometer analysis is based on the principle of sedimentation of soil particles in water. This test involves the use of 50 grams of dry, pulverized soil. A *deflocculating agent* is always added to the soil. The most common deflocculating agent used for hydrometer analysis is 125 cc of 4% solution of sodium hexametaphosphate. The soil is allowed to soak for at least 16 hours in the deflocculating agent. After the soaking period, distilled water is added, and the soil–deflocculating agent mixture is thoroughly agitated. The sample is then transferred to a 1000-ml glass cylinder. More distilled water is added to the cylinder to fill it to the 1000-ml mark, and then the mixture is again thoroughly agitated. A hydrometer is placed in the cylinder to measure the specific gravity of the soil–water suspension in the vicinity of the instrument's bulb (Figure 1.2), usually over a 24-hour period. Hydrometers are calibrated to show the amount of soil that is still in suspension at any given time  $t$ . The largest diameter of the soil particles still in suspension at time  $t$  can be determined by Stokes' law,

$$D = \sqrt{\frac{18\eta}{(G_s - 1)\gamma_w}} \sqrt{\frac{L}{t}} \quad (1.3)$$

where

$D$  = diameter of the soil particle

$G_s$  = specific gravity of soil solids

$\eta$  = viscosity of water

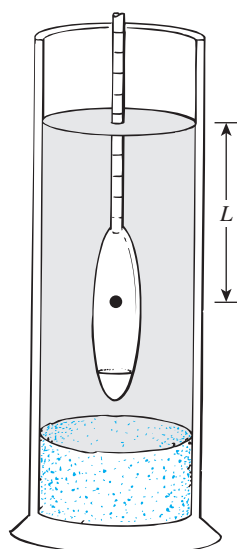


Figure 1.2 Hydrometer analysis

$\gamma_w$  = unit weight of water

$L$  = effective length (i.e., length measured from the water surface in the cylinder to the center of gravity of the hydrometer; see Figure 1.2)

$t$  = time

Soil particles having diameters larger than those calculated by Eq. (1.3) would have settled beyond the zone of measurement. In this manner, with hydrometer readings taken at various times, the soil *percent finer* than a given diameter  $D$  can be calculated and a grain-size distribution plot prepared. The sieve and hydrometer techniques may be combined for a soil having both coarse-grained and fine-grained soil constituents.

### 1.3

## Size Limits for Soils

Several organizations have attempted to develop the size limits for *gravel*, *sand*, *silt*, and *clay* on the basis of the grain sizes present in soils. Table 1.2 presents the size limits recommended by the American Association of State Highway and Transportation Officials (AASHTO) and the Unified Soil Classification systems (Corps of Engineers, Department of the Army, and Bureau of Reclamation). The table shows that soil particles smaller than 0.002 mm have been classified as *clay*. However, clays by nature are cohesive and can be rolled into a thread when moist. This property is caused by the presence of *clay minerals* such as *kaolinite*, *illite*, and *montmorillonite*. In contrast, some minerals, such as *quartz* and *feldspar*, may be present in a soil in particle sizes as small as clay minerals, but these particles will not have the cohesive property of clay minerals. Hence, they are called *clay-size particles*, not *clay particles*.

### 1.4

## Weight–Volume Relationships

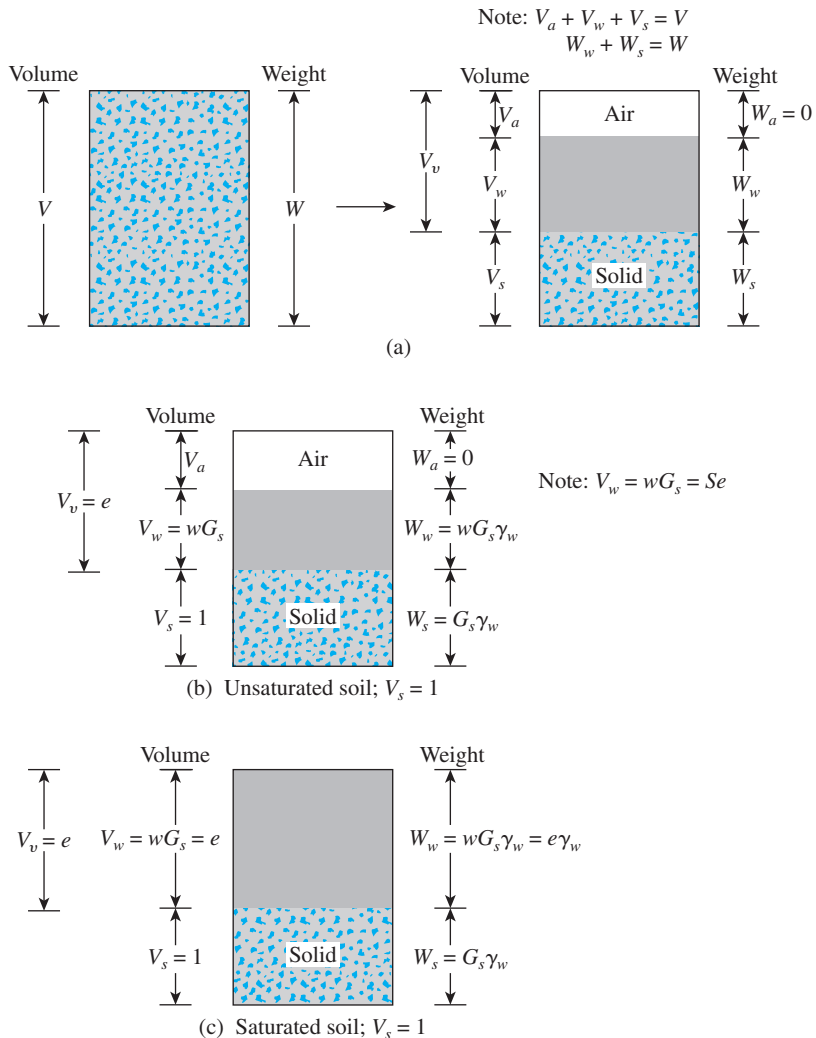
In nature, soils are three-phase systems consisting of solid soil particles, water, and air (or gas). To develop the *weight–volume relationships* for a soil, the three phases can be separated as shown in Figure 1.3a. Based on this separation, the volume relationships can then be defined.

The *void ratio*,  $e$ , is the ratio of the volume of voids to the volume of soil solids in a given soil mass, or

$$e = \frac{V_v}{V_s} \quad (1.4)$$

**Table 1.2** Soil-Separate Size Limits

Classification system	Grain size (mm)
Unified	Gravel: 75 mm to 4.75 mm Sand: 4.75 mm to 0.075 mm Silt and clay (fines): <0.075 mm
AASHTO	Gravel: 75 mm to 2 mm Sand: 2 mm to 0.05 mm Silt: 0.05 mm to 0.002 mm Clay: <0.002 mm

**Figure 1.3** Weight–volume relationships

where

$$V_v = \text{volume of voids}$$

$$V_s = \text{volume of soil solids}$$

The *porosity*,  $n$ , is the ratio of the volume of voids to the volume of the soil specimen, or

$$n = \frac{V_v}{V} \quad (1.5)$$

where

$$V = \text{total volume of soil}$$

Moreover,

$$n = \frac{V_v}{V} = \frac{V_v}{V_s + V_v} = \frac{\frac{V_v}{V_s}}{\frac{V_s}{V_s} + \frac{V_v}{V_s}} = \frac{\frac{V_v}{V_s}}{1 + e} \quad (1.6)$$

The *degree of saturation*,  $S$ , is the ratio of the volume of water in the void spaces to the volume of voids, generally expressed as a percentage, or

$$S(\%) = \frac{V_w}{V_v} \times 100 \quad (1.7)$$

where

$V_w$  = volume of water

Note that, for saturated soils, the degree of saturation is 100%.

The weight relationships are *moisture content*, *moist unit weight*, *dry unit weight*, and *saturated unit weight*, often defined as follows:

$$\text{Moisture content} = w(\%) = \frac{W_w}{W_s} \times 100 \quad (1.8)$$

where

$W_s$  = weight of the soil solids

$W_w$  = weight of water

$$\text{Moist unit weight} = \gamma = \frac{W}{V} \quad (1.9)$$

where

$W$  = total weight of the soil specimen =  $W_s + W_w$

The weight of air,  $W_a$ , in the soil mass is assumed to be negligible.

$$\text{Dry unit weight} = \gamma_d = \frac{W_s}{V} \quad (1.10)$$

When a soil mass is completely saturated (i.e., all the void volume is occupied by water), the moist unit weight of a soil [Eq. (1.9)] becomes equal to the *saturated unit weight* ( $\gamma_{\text{sat}}$ ). So  $\gamma = \gamma_{\text{sat}}$  if  $V_v = V_w$ .

More useful relations can now be developed by considering a representative soil specimen in which the volume of soil solids is equal to *unity*, as shown in Figure 1.3b. Note that if  $V_s = 1$ , then, from Eq. (1.4),  $V_v = e$ , and the weight of the soil solids is

$$W_s = G_s \gamma_w$$

where

$G_s$  = specific gravity of soil solids

$\gamma_w$  = unit weight of water ( $9.81 \text{ kN/m}^3$ , or  $62.4 \text{ lb/ft}^3$ )

Also, from Eq. (1.8), the weight of water  $W_w = wW_s$ . Thus, for the soil specimen under consideration,  $W_w = wW_s = wG_s\gamma_w$ . Now, for the general relation for moist unit weight given in Eq. (1.9),

$$\gamma = \frac{W}{V} = \frac{W_s + W_w}{V_s + V_v} = \frac{G_s\gamma_w(1 + w)}{1 + e} \quad (1.11)$$

Similarly, the dry unit weight [Eq. (1.10)] is

$$\gamma_d = \frac{W_s}{V} = \frac{W_s}{V_s + V_v} = \frac{G_s\gamma_w}{1 + e} \quad (1.12)$$

From Eqs. (1.11) and (1.12), note that

$$\gamma_d = \frac{\gamma}{1 + w} \quad (1.13)$$

According to Eq. (1.7), degree of saturation is

$$S = \frac{V_w}{V_v}$$

Now, referring to Fig. 1.3(b),

$$V_w = wG_s$$

and

$$V_v = e$$

Thus,

$$S = \frac{V_w}{V_v} = \frac{wG_s}{e} \quad (1.14)$$

For a saturated soil,  $S = 1$ . So

$$e = wG_s \quad (1.15)$$

The saturated unit weight of soil then becomes

$$\gamma_{\text{sat}} = \frac{W_s + W_w}{V_s + V_v} = \frac{G_s\gamma_w + e\gamma_w}{1 + e} \quad (1.16)$$

In SI units, Newton or kiloNewton is weight and is a derived unit, and g or kg is mass. The relationships given in Eqs. (1.11), (1.12) and (1.16) can be expressed as moist, dry, and saturated densities as follow:

$$\rho = \frac{G_s \rho_w (1 + w)}{1 + e} \quad (1.17)$$

$$\rho_d = \frac{G_s \rho_w}{1 + e} \quad (1.18)$$

$$\rho_{\text{sat}} = \frac{\rho_w (G_s + e)}{1 + e} \quad (1.19)$$

where  $\rho$ ,  $\rho_d$ ,  $\rho_{\text{sat}}$  = moist density, dry density, and saturated density, respectively  
 $\rho_w$  = density of water ( $= 1000 \text{ kg/m}^3$ )

Relationships similar to Eqs. (1.11), (1.12), and (1.16) in terms of porosity can also be obtained by considering a representative soil specimen with a unit volume (Figure 1.3c). These relationships are

$$\gamma = G_s \gamma_w (1 - n) (1 + w) \quad (1.20)$$

$$\gamma_d = (1 - n) G_s \gamma_w \quad (1.21)$$

and

$$\gamma_{\text{sat}} = [(1 - n) G_s + n] \gamma_w \quad (1.22)$$

Table 1.3 gives a summary of various forms of relationships that can be obtained for  $\gamma$ ,  $\gamma_d$ , and  $\gamma_{\text{sat}}$ .

**Table 1.3** Various Forms of Relationships for  $\gamma$ ,  $\gamma_d$ , and  $\gamma_{\text{sat}}$

Unit-weight relationship	Dry unit weight	Saturated unit weight
$\gamma = \frac{(1 + w) G_s \gamma_w}{1 + e}$	$\gamma_d = \frac{\gamma}{1 + w}$	$\gamma_{\text{sat}} = \frac{(G_s + e) \gamma_w}{1 + e}$
$\gamma = \frac{(G_s + Se) \gamma_w}{1 + e}$	$\gamma_d = \frac{G_s \gamma_w}{1 + e}$	$\gamma_{\text{sat}} = [(1 - n) G_s + n] \gamma_w$
$\gamma = \frac{(1 + w) G_s \gamma_w}{1 + \frac{wG_s}{S}}$	$\gamma_d = G_s \gamma_w (1 - n)$	$\gamma_{\text{sat}} = \left( \frac{1 + w}{1 + wG_s} \right) G_s \gamma_w$
$\gamma = G_s \gamma_w (1 - n)(1 + w)$	$\gamma_d = \frac{G_s}{1 + \frac{wG_s}{S}} \gamma_w$	$\gamma_{\text{sat}} = \left( \frac{e}{w} \right) \left( \frac{1 + w}{1 + e} \right) \gamma_w$
	$\gamma_d = \frac{e S \gamma_w}{(1 + e) w}$	$\gamma_{\text{sat}} = \gamma_d + n \gamma_w$
	$\gamma_d = \gamma_{\text{sat}} - n \gamma_w$	$\gamma_{\text{sat}} = \gamma_d + \left( \frac{e}{1 + e} \right) \gamma_w$
	$\gamma_d = \gamma_{\text{sat}} - \left( \frac{e}{1 + e} \right) \gamma_w$	

**Table 1.4** Specific Gravities of Some Soils

Type of soil	$G_s$
Quartz sand	2.64–2.66
Silt	2.67–2.73
Clay	2.70–2.9
Chalk	2.60–2.75
Loess	2.65–2.73
Peat	1.30–1.9

Except for peat and highly organic soils, the general range of the values of specific gravity of soil solids ( $G_s$ ) found in nature is rather small. Table 1.4 gives some representative values. For practical purposes, a reasonable value can be assumed in lieu of running a test.

## 1.5 Relative Density

In *granular soils*, the degree of compaction in the field can be measured according to the *relative density*, defined as

$$D_r(\%) = \frac{e_{\max} - e}{e_{\max} - e_{\min}} \times 100 \quad (1.23)$$

where

$e_{\max}$  = void ratio of the soil in the loosest state

$e_{\min}$  = void ratio in the densest state

$e$  = *in situ* void ratio

The relative density can also be expressed in terms of dry unit weight, or

$$D_r(\%) = \left\{ \frac{\gamma_d - \gamma_{d(\min)}}{\gamma_{d(\max)} - \gamma_{d(\min)}} \right\} \frac{\gamma_{d(\max)}}{\gamma_d} \times 100 \quad (1.24)$$

where

$\gamma_d$  = *in situ* dry unit weight

$\gamma_{d(\max)}$  = dry unit weight in the *densest* state; that is, when the void ratio is  $e_{\min}$

$\gamma_{d(\min)}$  = dry unit weight in the *loosest* state; that is, when the void ratio is  $e_{\max}$

The denseness of a granular soil is sometimes related to the soil's relative density. Table 1.5 gives a general correlation of the denseness and  $D_r$ . For naturally occurring sands, the magnitudes of  $e_{\max}$  and  $e_{\min}$  [Eq. (1.23)] may vary widely. The main reasons for such wide variations are the uniformity coefficient,  $C_u$ , and the roundness of the particles.

**Table 1.5** Denseness of a Granular Soil

Relative density, $D_r(\%)$	Description
0–20	Very loose
20–40	Loose
40–60	Medium
60–80	Dense
80–100	Very dense

### Example 1.1

The moist weight of 0.1 ft<sup>3</sup> of soil is 12.2 lb. If the moisture content is 12% and the specific gravity of soil solids is 2.72, find the following:

- a. Moist unit weight (lb/ft<sup>3</sup>)
- b. Dry unit weight (lb/ft<sup>3</sup>)
- c. Void ratio
- d. Porosity
- e. Degree of saturation (%)
- f. Volume occupied by water (ft<sup>3</sup>)

#### Solution

Part a

From Eq. (1.9),

$$\gamma = \frac{W}{V} = \frac{12.2}{0.1} = 122 \text{ lb/ft}^3$$

Part b

From Eq. (1.13),

$$\gamma_d = \frac{\gamma}{1 + w} = \frac{122}{1 + \frac{12}{100}} = 108.93 \text{ lb/ft}^3$$

Part c

From Eq. (1.12),

$$\gamma_d = \frac{G_s \gamma_w}{1 + e}$$

or  $108.93 = \frac{(2.72)(62.4)}{1 + e}$

$$e = 0.56$$

Part d

From Eq. (1.6),

$$n = \frac{e}{1 + e} = \frac{0.56}{1 + 0.56} = \mathbf{0.359}$$

Part e

From Eq. (1.14),

$$S = \frac{wG_s}{e} = \frac{(0.12)(2.72)}{0.56} = \mathbf{0.583}$$

Part f

From Eq. (1.12),

$$W_s = \frac{W}{1 + w} = \frac{12.2 \text{ lb}}{1.12} = 10.89 \text{ lb}$$

$$W_w = W - W_s = 12.2 - 10.89 = 1.31 \text{ lb}$$

$$V_w = \frac{1.31}{62.4} = \mathbf{0.021 \text{ ft}^3}$$

■

## Example 1.2

The dry density of a sand with a porosity of 0.387 is  $1600 \text{ kg/m}^3$ . Find the void ratio of the soil and the specific gravity of the soil solids.

### Solution

Void ratio

Given:  $n = 0.387$ . From Eq. (1.6),

$$e = \frac{n}{1 - n} = \frac{0.387}{1 - 0.387} = \mathbf{0.631}$$

Specific gravity of soil solids

From Eq. (1.18),

$$\rho_d = \frac{G_s \rho_w}{1 + e}$$

$$1600 = \frac{G_s(1000)}{1.631}$$

$$G_s = \mathbf{2.61}$$

■

### Example 1.3

The moist unit weight of a soil is  $19.2 \text{ kN/m}^3$ . Given  $G_s = 2.69$  and moisture content  $w = 9.8\%$ , determine

- a. Dry unit weight ( $\text{kN/m}^3$ )
- b. Void ratio
- c. Porosity
- d. Degree of saturation (%)

#### Solution

Part a

From Eq. (1.13),

$$\gamma_d = \frac{\gamma}{1 + w} = \frac{19.2}{1 + \frac{9.8}{100}} = \mathbf{17.49 \text{ kN/m}^3}$$

Part b

From Eq. (1.12),

$$\begin{aligned}\gamma_d &= 17.49 \text{ kN/m}^3 = \frac{G_s \gamma_w}{1 + e} = \frac{(2.69)(9.81)}{1 + e} \\ e &= \mathbf{0.509}\end{aligned}$$

Part c

From Eq. (1.6),

$$n = \frac{e}{1 + e} = \frac{0.509}{1 + 0.509} = \mathbf{0.337}$$

Part d

From Eq. (1.14),

$$S = \frac{wG_s}{e} = \left[ \frac{(0.098)(2.69)}{0.509} \right] (100) = \mathbf{51.79\%}$$

### Example 1.4

For a saturated soil, given  $w = 40\%$  and  $G_s = 2.71$ , determine the saturated and dry unit weights in  $\text{lb/ft}^3$  and  $\text{kN/m}^3$ .

#### Solution

For saturated soil, from Eq. (1.15),

$$e = wG_s = (0.4)(2.71) = 1.084$$

From Eq. (1.16),

$$\gamma_{\text{sat}} = \frac{(G_s + e)\gamma_w}{1 + e} = \frac{(2.71 + 1.084)62.4}{1 + 1.084} = \mathbf{113.6 \text{ lb/ft}^3}$$

Also

$$\gamma_{\text{sat}} = (113.6) \left( \frac{9.81}{62.4} \right) = \mathbf{17.86 \text{ kN/m}^3}$$

From Eq. (1.12),

$$\gamma_d = \frac{G_s \gamma_w}{1 + e} = \frac{(2.71)(62.4)}{1 + 1.084} = 81.2 \text{ lb/ft}^3$$

Also,

$$\gamma_d = (81.2) \left( \frac{9.81}{62.4} \right) = \mathbf{12.76 \text{ kN/m}^3}$$

■

### Example 1.5

The mass of a moist soil sample collected from the field is 465 grams, and its oven dry mass is 405.76 grams. The specific gravity of the soil solids was determined in the laboratory to be 2.68. If the void ratio of the soil in the natural state is 0.83, find the following:

- a. The moist density of the soil in the field ( $\text{kg/m}^3$ )
- b. The dry density of the soil in the field ( $\text{kg/m}^3$ )
- c. The mass of water, in kilograms, to be added per cubic meter of soil in the field for saturation

#### Solution

Part a

From Eq. (1.8),

$$w = \frac{W_w}{W_s} = \frac{465 - 405.76}{405.76} = \frac{59.24}{405.76} = 14.6\%$$

From Eq. (1.17),

$$\begin{aligned} \rho &= \frac{G_s \rho_w + w G_s \rho_w}{1 + e} = \frac{G_s \rho_w (1 + w)}{1 + e} = \frac{(2.68)(1000)(1.146)}{1.83} \\ &= \mathbf{1678.3 \text{ kg/m}^3} \end{aligned}$$

Part b

From Eq. (1.18),

$$\rho_d = \frac{G_s \rho_w}{1 + e} = \frac{(2.68)(1000)}{1.83} = \mathbf{1468.48 \text{ kg/m}^3}$$

## Part c

Mass of water to be added =  $\rho_{\text{sat}} - \rho$

From Eq. (1.19),

$$\rho_{\text{sat}} = \frac{G_s \rho_w + e \rho_w}{1 + e} = \frac{\rho_w (G_s + e)}{1 + e} = \frac{(1000)(2.68 + 0.83)}{1.83} = 1918 \text{ kg/m}^3$$

So, mass of water to be added =  $1918 - 1678.3 = 239.7 \text{ kg/m}^3$ . ■

**Example 1.6**

The maximum and minimum dry unit weights of a sand are  $17.1 \text{ kN/m}^3$  and  $14.2 \text{ kN/m}^3$ , respectively. The sand in the field has a relative density of 70% with a moisture content of 8%. Determine the moist unit weight of the sand in the field.

**Solution**

From Eq. (1.24),

$$D_r = \left[ \frac{\gamma_d - \gamma_{d(\min)}}{\gamma_{d(\max)} - \gamma_{d(\min)}} \right] \left[ \frac{\gamma_{d(\max)}}{\gamma_d} \right]$$

$$0.7 = \left[ \frac{\gamma_d - 14.2}{17.1 - 14.2} \right] \left[ \frac{17.1}{\gamma_d} \right]$$

$$\gamma_d = 16.11 \text{ kN/m}^3$$

$$\gamma = \gamma_d(1 + w) = 16.11 \left( 1 + \frac{8}{100} \right) = 17.4 \text{ kN/m}^3$$

**1.6****Atterberg Limits**

When a clayey soil is mixed with an excessive amount of water, it may flow like a *semiliquid*. If the soil is gradually dried, it will behave like a *plastic*, *semisolid*, or *solid* material, depending on its moisture content. The moisture content, in percent, at which the soil changes from a liquid to a plastic state is defined as the *liquid limit* (LL). Similarly, the moisture content, in percent, at which the soil changes from a plastic to a semisolid state and from a semisolid to a solid state are defined as the *plastic limit* (PL) and the *shrinkage limit* (SL), respectively. These limits are referred to as *Atterberg limits* (Figure 1.4):

- The *liquid limit* of a soil is determined by Casagrande's liquid device (ASTM Test Designation D-4318) and is defined as the moisture content at which a groove closure of 12.7 mm (1/2 in.) occurs at 25 blows.
- The *plastic limit* is defined as the moisture content at which the soil crumbles when rolled into a thread of 3.18 mm (1/8 in.) in diameter (ASTM Test Designation D-4318).

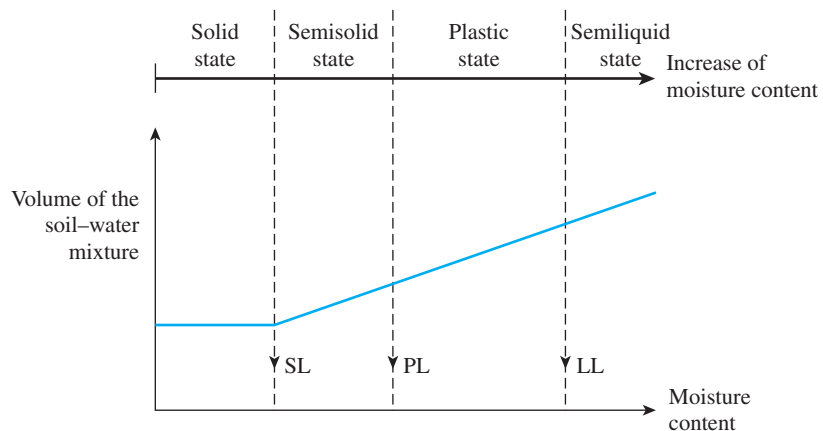


**Figure 1.4** Definition of Atterberg limits

- The *shrinkage limit* is defined as the moisture content at which the soil does not undergo any further change in volume with loss of moisture (ASTM Test Designation D-427).

The difference between the liquid limit and the plastic limit of a soil is defined as the *plasticity index* (PI), or

$$\text{PI} = \text{LL} - \text{PL} \quad (1.25)$$

## 1.7 Liquidity Index

The relative consistency of a cohesive soil in the natural state can be defined by a ratio called the *liquidity index*, which is given by

$$\text{LI} = \frac{w - \text{PL}}{\text{LL} - \text{PL}} \quad (1.26)$$

where  $w$  = *in situ* moisture content of soil.

The *in situ* moisture content for a sensitive clay may be greater than the liquid limit. In this case,

$$\text{LI} > 1$$

These soils, when remolded, can be transformed into a viscous form to flow like a liquid.

Soil deposits that are heavily overconsolidated may have a natural moisture content less than the plastic limit. In this case,

$$LI < 0$$

## 1.8 Activity

Because the plasticity of soil is caused by the adsorbed water that surrounds the clay particles, we can expect that the type of clay minerals and their proportional amounts in a soil will affect the liquid and plastic limits. Skempton (1953) observed that the plasticity index of a soil increases linearly with the percentage of clay-size fraction (% finer than  $2 \mu\text{m}$  by weight) present. The correlations of PI with the clay-size fractions for different clays plot separate lines. This difference is due to the diverse plasticity characteristics of the various types of clay minerals. On the basis of these results, Skempton defined a quantity called *activity*, which is the slope of the line correlating PI and % finer than  $2 \mu\text{m}$ . This activity may be expressed as

$$A = \frac{\text{PI}}{(\% \text{ of clay-size fraction, by weight})} \quad (1.27)$$

Activity is used as an index for identifying the swelling potential of clay soils. Typical values of activities for various clay minerals are given in Table 1.6.

## 1.9 Soil Classification Systems

Soil classification systems divide soils into groups and subgroups based on common engineering properties such as the *grain-size distribution*, *liquid limit*, and *plastic limit*. The two major classification systems presently in use are (1) the *American Association of State Highway and Transportation Officials (AASHTO) System* and (2) the *Unified Soil Classification System* (also ASTM). The AASHTO system is used mainly for the classification of highway subgrades. It is not used in foundation construction.

**Table 1.6** Activities of Clay Minerals

Mineral	Activity ( <i>A</i> )
Smectites	1–7
Illite	0.5–1
Kaolinite	0.5
Halloysite ( $4\text{H}_2\text{O}$ )	0.5
Halloysite ( $2\text{H}_2\text{O}$ )	0.1
Attapulgite	0.5–1.2
Allophane	0.5–1.2

### AASHTO System

The AASHTO Soil Classification System was originally proposed by the Highway Research Board's Committee on Classification of Materials for Subgrades and Granular Type Roads (1945). According to the present form of this system, soils can be classified according to eight major groups, A-1 through A-8, based on their grain-size distribution, liquid limit, and plasticity indices. Soils listed in groups A-1, A-2, and A-3 are coarse-grained materials, and those in groups A-4, A-5, A-6, and A-7 are fine-grained materials. Peat, muck, and other highly organic soils are classified under A-8. They are identified by visual inspection.

The AASHTO classification system (for soils A-1 through A-7) is presented in Table 1.7. Note that group A-7 includes two types of soil. For the A-7-5 type, the plasticity

**Table 1.7** AASHTO Soil Classification System

General classification	Granular materials (35% or less of total sample passing No. 200 sieve)						
	A-1		A-2				
Group classification	A-1-a	A-1-b	A-3	A-2-4	A-2-5	A-2-6	A-2-7
Sieve analysis (% passing)							
No. 10 sieve	50 max						
No. 40 sieve	30 max	50 max	51 min				
No. 200 sieve	15 max	25 max	10 max	35 max	35 max	35 max	35 max
For fraction passing							
No. 40 sieve							
Liquid limit (LL)				40 max	41 min	40 max	41 min
Plasticity index (PI)	6 max		Nonplastic	10 max	10 max	11 min	11 min
Usual type of material	Stone fragments, gravel, and sand		Fine sand			Silty or clayey gravel and sand	
Subgrade rating						Excellent to good	
Silt-clay materials (More than 35% of total sample passing No. 200 sieve)							
General classification	A-4		A-5	A-6	A-7		
Group classification						A-7-5 <sup>a</sup>	A-7-6 <sup>b</sup>
Sieve analysis (% passing)							
No. 10 sieve							
No. 40 sieve							
No. 200 sieve		36 min		36 min		36 min	36 min
For fraction passing							
No. 40 sieve							
Liquid limit (LL)		40 max		41 min		40 max	41 min
Plasticity index (PI)		10 max		10 max		11 min	11 min
Usual types of material			Mostly silty soils			Mostly clayey soils	
Subgrade rating					Fair to poor		

<sup>a</sup>If PI  $\leq$  LL - 30, the classification is A-7-5.

<sup>b</sup>If PI > LL - 30, the classification is A-7-6.

index of the soil is less than or equal to the liquid limit minus 30. For the A-7-6 type, the plasticity index is greater than the liquid limit minus 30.

For qualitative evaluation of the desirability of a soil as a highway subgrade material, a number referred to as the *group index* has also been developed. The higher the value of the group index for a given soil, the weaker will be the soil's performance as a subgrade. A group index of 20 or more indicates a very poor subgrade material. The formula for the group index is

$$GI = (F_{200} - 35)[0.2 + 0.005(LL - 40)] + 0.01(F_{200} - 15)(PI - 10) \quad (1.28)$$

where

$F_{200}$  = percent passing No. 200 sieve, expressed as a whole number

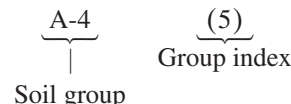
LL = liquid limit

PI = plasticity index

When calculating the group index for a soil belonging to group A-2-6 or A-2-7, use only the partial group-index equation relating to the plasticity index:

$$GI = 0.01(F_{200} - 15)(PI - 10) \quad (1.29)$$

The group index is rounded to the nearest whole number and written next to the soil group in parentheses; for example, we have



The group index for soils which fall in groups A-1-a, A-1-b, A-3, A-2-4, and A-2-5 is always zero.

### Unified System

The Unified Soil Classification System was originally proposed by A. Casagrande in 1942 and was later revised and adopted by the United States Bureau of Reclamation and the U.S. Army Corps of Engineers. The system is currently used in practically all geotechnical work.

In the Unified System, the following symbols are used for identification:

Symbol	G	S	M	C	O	Pt	H	L	W	P
Description	Gravel	Sand	Silt	Clay	Organic silts and clay	Peat and highly organic soils	High plasticity	Low plasticity	Well graded	Poorly graded

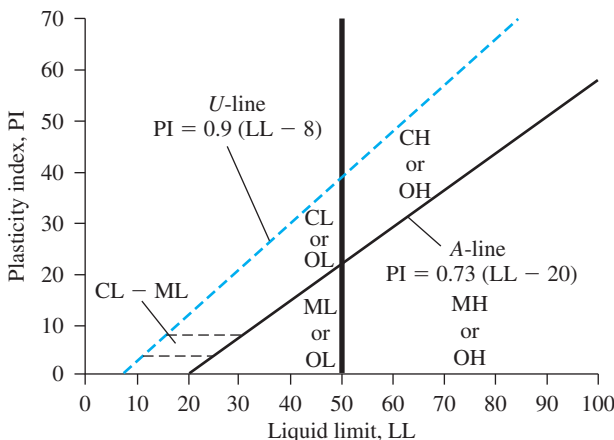


**Figure 1.5** Plasticity chart

The plasticity chart (Figure 1.5) and Table 1.8 show the procedure for determining the group symbols for various types of soil. When classifying a soil be sure to provide the group name that generally describes the soil, along with the group symbol. Figures 1.6, 1.7, and 1.8 give flowcharts for obtaining the group names for coarse-grained soil, inorganic fine-grained soil, and organic fine-grained soil, respectively.

### Example 1.7

Classify the following soil by the AASHTO classification system.

Percent passing No. 4 sieve = 92  
 Percent passing No. 10 sieve = 87  
 Percent passing No. 40 sieve = 65  
 Percent passing No. 200 sieve = 30  
 Liquid limit = 22  
 Plasticity index = 8

### Solution

Table 1.7 shows that it is a granular material because less than 35% is passing a No. 200 sieve. With LL = 22 (that is, less than 40) and PI = 8 (that is, less than 10), the soil falls in group A-2-4.

The soil is **A-2-4(0)**. ■

**Table 1.8** Unified Soil Classification Chart (after ASTM, 2009) (ASTM D2487-98: Standard Practice for Classification of Soils for Engineering Purposes (Unified Soil Classification). Copyright ASTM INTERNATIONAL. Reprinted with permission.)

		Soil classification		
		Group symbol	Group name <sup>b</sup>	
Criteria for assigning group symbols and group names using laboratory tests <sup>a</sup>				
<b>Coarse-grained soils</b>				
Gravels	Clean Gravels More than 50% of coarse fraction retained on No. 4 sieve	$C_u \geq 4$ and $1 \leq C_c \leq 3^e$ $C_u < 4$ and/or $1 > C_c > 3^e$	GW GP	Well-graded gravel/ Poorly graded gravel <sup>f</sup>
	Gravels with Fines More than 12% fines <sup>c</sup>	Fines classify as ML or MH Fines classify as CL or CH	GM GC	Silty gravel <sup>f,g,h</sup>
Sands	Clean Sands 50% or more of coarse fraction passes No. 4 sieve	$C_u \geq 6$ and $1 \leq C_c \leq 3^e$ $C_u < 6$ and/or $1 > C_c > 3^e$	SW SP	Well-graded sand <sup>i</sup> Poorly graded sand <sup>j</sup>
	Sand with Fines More than 12% fines <sup>d</sup>	Fines classify as ML or MH Fines classify as CL or CH	SM SC	Silty sand <sup>g,h,i</sup> Clayey sand <sup>g,h,i</sup>
<b>Fine-grained soils</b>				
Silts and Clays	Inorganic Liquid limit less than 50	PI > 7 and plots on or above "A" line <sup>j</sup> PI < 4 or plots below "A" line <sup>j</sup>	CL ML	Lean clay <sup>k,l,m</sup> Silt <sup>k,l,m</sup>
	Organic	Liquid limit—oven dried Liquid limit—not dried < 0.75	OL	Organic clay <sup>k,l,m,n</sup> Organic silt <sup>k,l,m,o</sup>
Silts and Clays	Inorganic Liquid limit 50 or more	PI plots on or above "A" line PI plots below "A" line	CH MH	Fat clay <sup>k,l,m</sup> Elastic silt <sup>k,l,m</sup>
	Organic	Liquid limit—oven dried Liquid limit—not dried < 0.75	OH	Organic clay <sup>k,l,m,p</sup> Organic silt <sup>k,l,m,q</sup>
<b>Highly organic soils</b>		Primarily organic matter, dark in color, and organic odor	PT	Peat
<sup>a</sup> Based on the material passing the 75-mm. (3-in) sieve.				
<sup>b</sup> If field sample contained cobbles or boulders, or both, add "with cobbles or boulders, or both" to group name.				
<sup>c</sup> Gravels with 5 to 12% fines require dual symbols: GW-GM well-graded gravel with silt; GW-GC well-graded gravel with clay; GP-GM poorly graded gravel with silt; GP-GC poorly graded gravel with clay.				
<sup>d</sup> Sands with 5 to 12% fines require dual symbols: SW-SM well-graded sand with silt; SW-SC well-graded sand with clay; SP-SM poorly graded sand with silt; SP-SC poorly graded sand with clay.				
<sup>e</sup> $C_u = D_{60}/D_{10}$ $C_c = \frac{(D_{30})^2}{D_{10} \times D_{60}}$				
<sup>f</sup> If soil contains $\geq 15\%$ sand, add "with sand" to group name.				
<sup>g</sup> If fines classify as CL-ML, use dual symbol GC-GM or SC-SM.				
<sup>h</sup> If fines are organic, add "with organic fines" to group name.				
<sup>i</sup> If soil contains $\geq 30\%$ plus No. 200, predominantly gravel, add "gravelly" to group name.				
<sup>j</sup> PI $\geq 4$ and plots on or above "A" line.				
<sup>k</sup> PI $< 4$ or plots below "A" line.				
<sup>l</sup> PI plots on or above "A" line.				
<sup>m</sup> PI plots below "A" line.				
<sup>n</sup> If Atterberg limits plot in hatched area, soil is a CL-ML, silty clay.				

<sup>a</sup>Based on the material passing the 75-mm. (3-in) sieve.  
<sup>b</sup>If field sample contained cobbles or boulders, or both, add "with cobbles or boulders, or both" to group name.  
<sup>c</sup>Gravels with 5 to 12% fines require dual symbols: GW-GM well-graded gravel with silt; GW-GC well-graded gravel with clay; GP-GM poorly graded gravel with silt; GP-GC poorly graded gravel with clay.  
<sup>d</sup>Sands with 5 to 12% fines require dual symbols: SW-SM well-graded sand with silt; SW-SC well-graded sand with clay; SP-SM poorly graded sand with silt; SP-SC poorly graded sand with clay.  
<sup>e</sup> $C_u = D_{60}/D_{10}$     $C_c = \frac{(D_{30})^2}{D_{10} \times D_{60}}$   
<sup>f</sup>If soil contains  $\geq 15\%$  sand, add "with sand" to group name.  
<sup>g</sup>If fines classify as CL-ML, use dual symbol GC-GM or SC-SM.  
<sup>h</sup>If fines are organic, add "with organic fines" to group name.  
<sup>i</sup>If soil contains  $\geq 15\%$  gravel, add "with gravel" to group name.  
<sup>j</sup>If Atterberg limits plot in hatched area, soil is a CL-ML, silty clay.

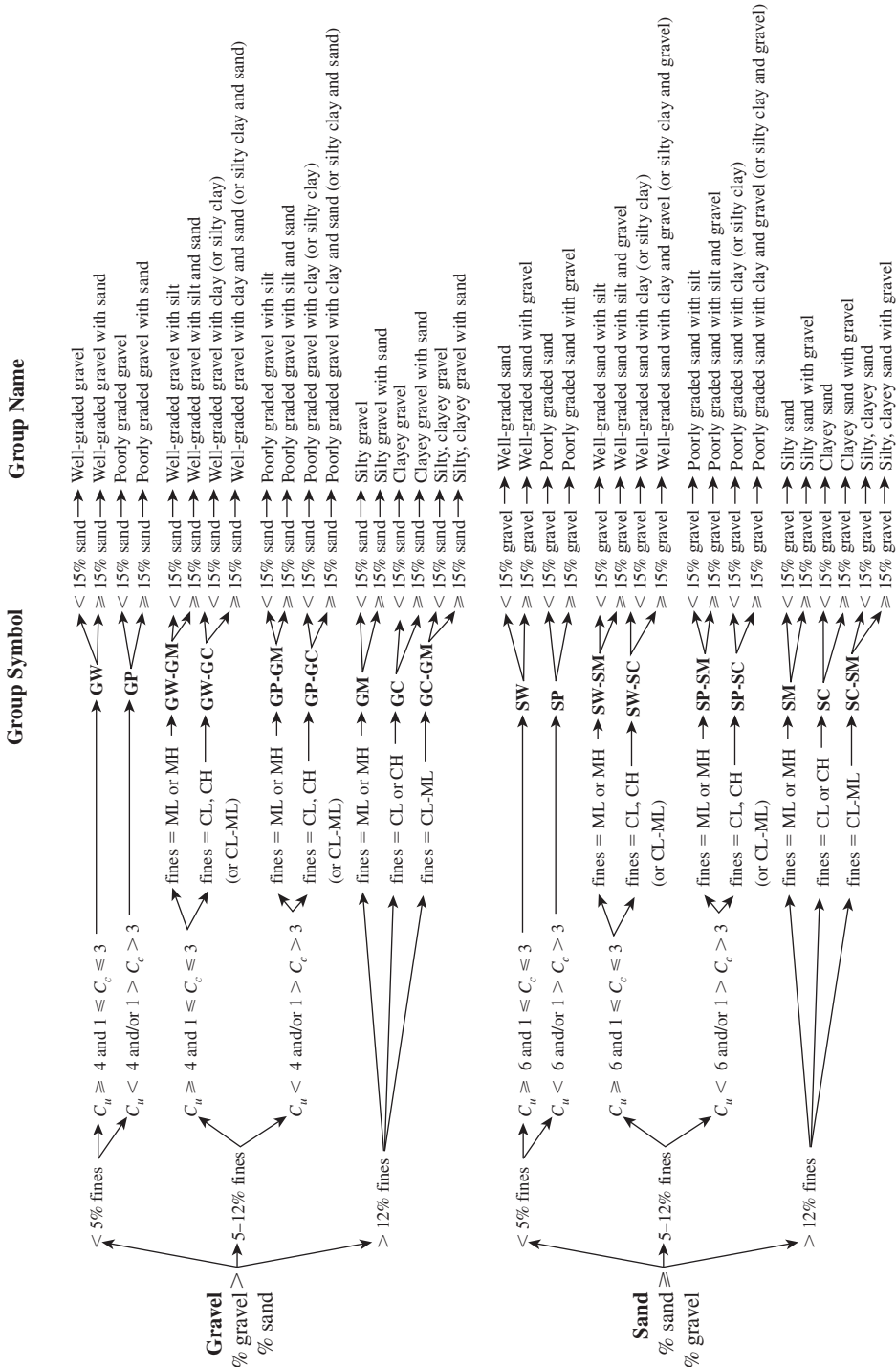


**Figure 1.6** Flowchart for classifying coarse-grained soils (more than 50% retained on No. 200 Sieve) (After ASTM, 2009) (ASTM D2487-98: Standard Practice for Classification of Soils for Engineering Purposes (Unified Soil Classification). Copyright ASTM INTERNATIONAL. Reprinted with permission.)

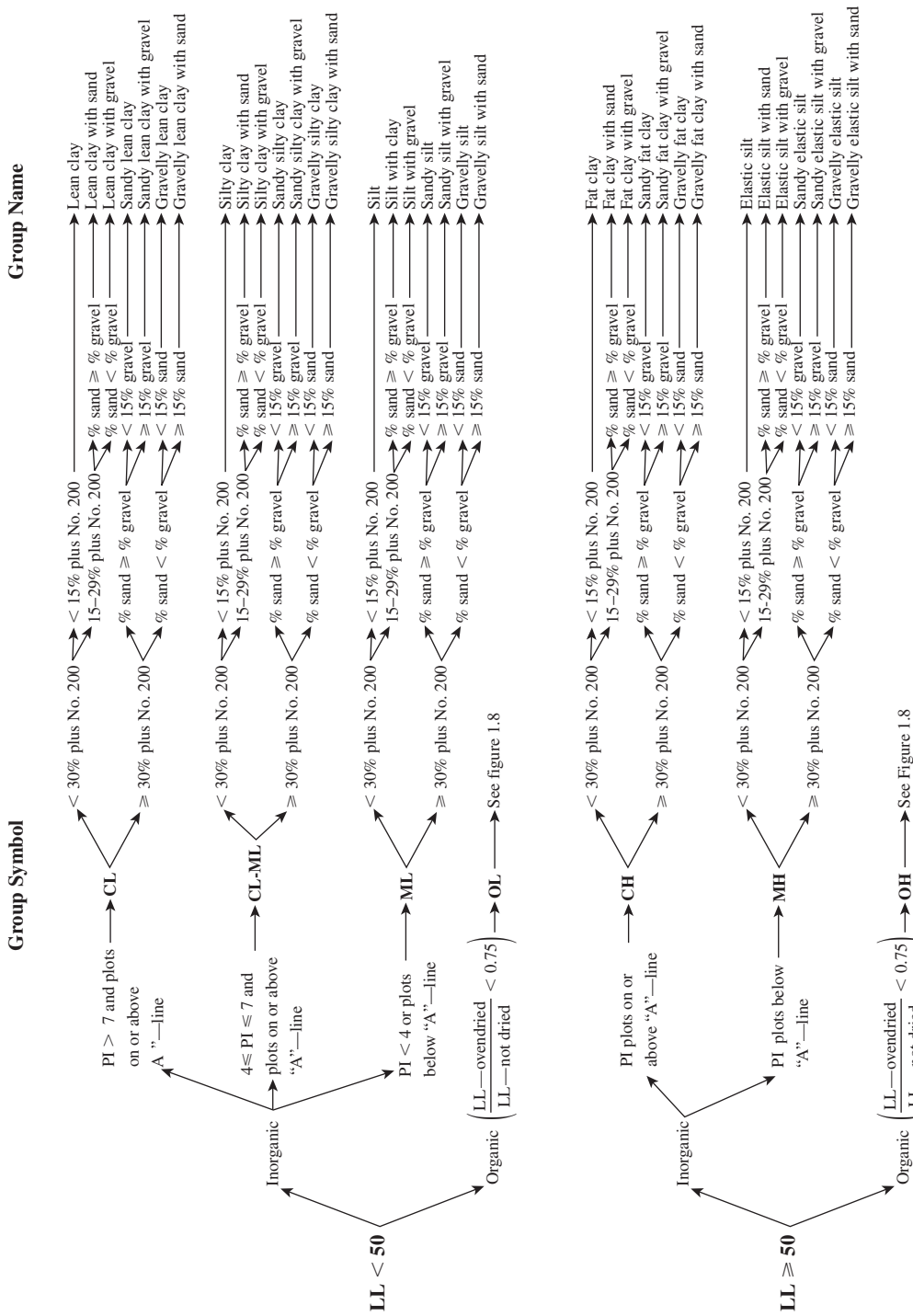


**Figure 1.7** Flowchart for classifying fine-grained soil (50% or more passes No. 200 Sieve) (After ASTM, 2009)(ASTM D2487-98: Standard Practice for Classification of Soils for Engineering Purposes (Unified Soil Classification). Copyright ASTM INTERNATIONAL. Reprinted with permission.)

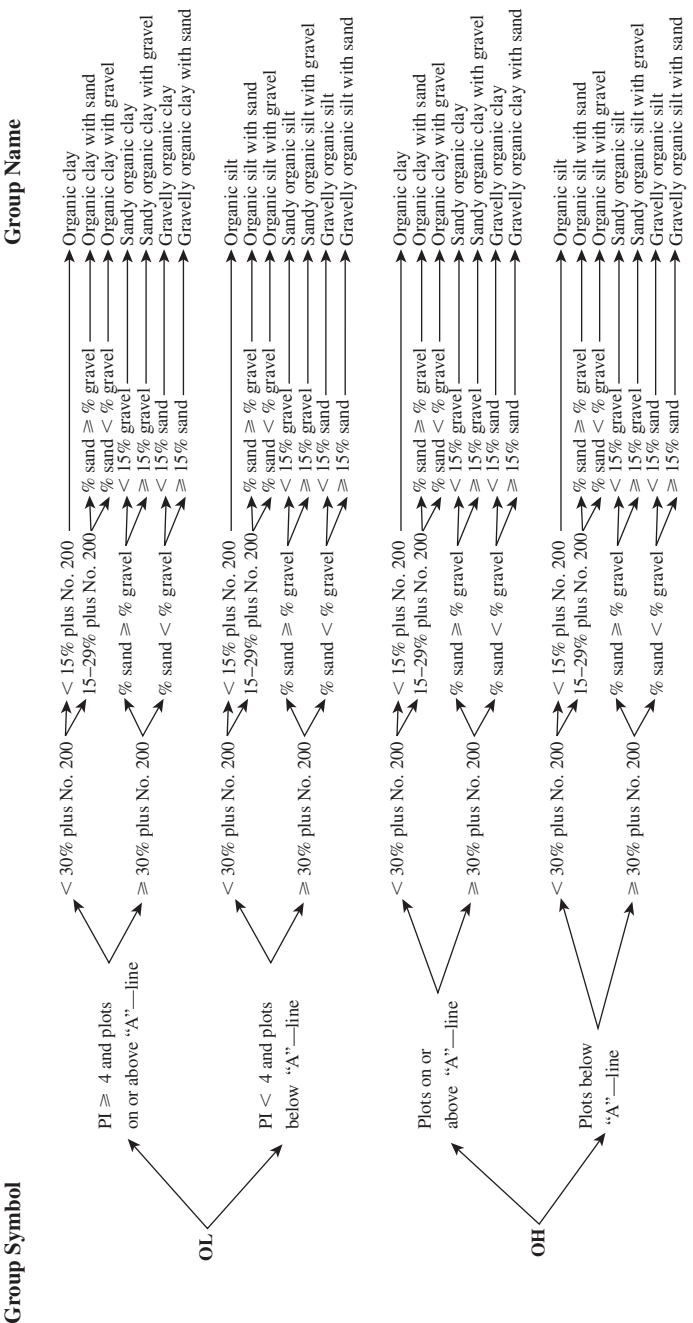


**Figure 1.8** Flowchart for classifying organic fine-grained soil (50% or more passes No. 200 Sieve) (After ASTM, 2009)  
 (ASTM D2487-98: Standard Practice for Classification of Soils for Engineering Purposes (Unified Soil Classification). Copyright ASTM INTERNATIONAL. Reprinted with permission.)

### Example 1.8

Classify the following soil by the Unified Soil Classification System:

Percent passing No. 4 sieve = 82  
 Percent passing No. 10 sieve = 71  
 Percent passing No. 40 sieve = 64  
 Percent passing No. 200 sieve = 41  
 Liquid limit = 31  
 Plasticity index = 12

#### Solution

We are given that  $F_{200} = 41$ , LL = 31, and PI = 12. Since 59% of the sample is retained on a No. 200 sieve, the soil is a coarse-grained material. The percentage passing a No. 4 sieve is 82, so 18% is retained on No. 4 sieve (gravel fraction). The coarse fraction passing a No. 4 sieve (sand fraction) is  $59 - 18 = 41\%$  (which is more than 50% of the total coarse fraction). Hence, the specimen is a sandy soil.

Now, using Table 1.8 and Figure 1.5, we identify the group symbol of the soil as **SC**.

Again from Figure 1.6, since the gravel fraction is greater than 15%, the group name is **clayey sand with gravel**. ■

## 1.10

### Hydraulic Conductivity of Soil

The void spaces, or pores, between soil grains allow water to flow through them. In soil mechanics and foundation engineering, you must know how much water is flowing through a soil per unit time. This knowledge is required to design earth dams, determine the quantity of seepage under hydraulic structures, and dewater foundations before and during their construction. Darcy (1856) proposed the following equation (Figure 1.9) for calculating the velocity of flow of water through a soil:

$$v = ki \quad (1.30)$$

In this equation,

$v$  = Darcy velocity (unit: cm/sec)

$k$  = hydraulic conductivity of soil (unit: cm/sec)

$i$  = hydraulic gradient

The hydraulic gradient is defined as

$$i = \frac{\Delta h}{L} \quad (1.31)$$

where

$\Delta h$  = piezometric head difference between the sections at AA and BB

$L$  = distance between the sections at AA and BB

(Note: Sections AA and BB are perpendicular to the direction of flow.)

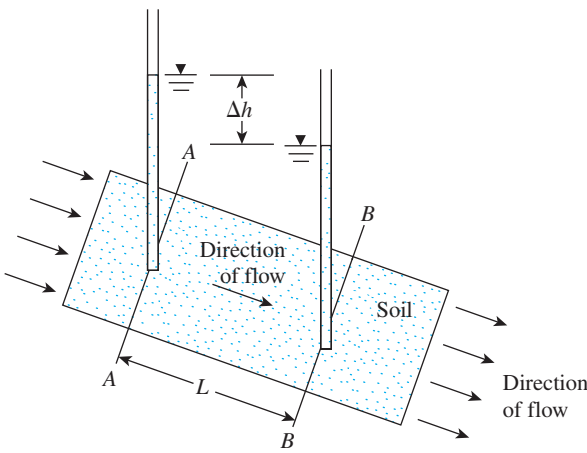


**Figure 1.9** Definition of Darcy's law

Darcy's law [Eq. (1.30)] is valid for a wide range of soils. However, with materials like clean gravel and open-graded rockfills, the law breaks down because of the turbulent nature of flow through them.

The value of the hydraulic conductivity of soils varies greatly. In the laboratory, it can be determined by means of *constant-head* or *falling-head* permeability tests. The constant-head test is more suitable for granular soils. Table 1.9 provides the general range for the values of  $k$  for various soils. In granular soils, the value depends primarily on the void ratio. In the past, several equations have been proposed to relate the value of  $k$  to the void ratio in granular soil. However the author recommends the following equation for use (also see Carrier, 2003):

$$k \propto \frac{e^3}{1 + e} \quad (1.32)$$

where

$k$  = hydraulic conductivity

$e$  = void ratio

Chapuis (2004) proposed an empirical relationship for  $k$  in conjunction with Eq. (1.32) as

$$k(\text{cm/s}) = 2.4622 \left[ D_{10}^2 \frac{e^3}{(1 + e)} \right]^{0.7825} \quad (1.33)$$

where  $D$  = effective size (mm).

**Table 1.9** Range of the Hydraulic Conductivity for Various Soils

Type of soil	Hydraulic conductivity, $k$ (cm/sec)
Medium to coarse gravel	Greater than $10^{-1}$
Coarse to fine sand	$10^{-1}$ to $10^{-3}$
Fine sand, silty sand	$10^{-3}$ to $10^{-5}$
Silt, clayey silt, silty clay	$10^{-4}$ to $10^{-6}$
Clays	$10^{-7}$ or less

The preceding equation is valid for natural, uniform sand and gravel to predict  $k$  that is in the range of  $10^{-1}$  to  $10^{-3}$  cm/s. This can be extended to natural, silty sands without plasticity. It is not valid for crushed materials or silty soils with some plasticity.

Based on laboratory experimental results, Amer and Awad (1974) proposed the following relationship for  $k$  in granular soil:

$$k = 3.5 \times 10^{-4} \left( \frac{e^3}{1 + e} \right) C_u^{0.6} D_{10}^{2.32} \left( \frac{\rho_w}{\eta} \right) \quad (1.34)$$

where

$k$  is in cm/sec

$C_u$  = uniformity coefficient

$D_{10}$  = effective size (mm)

$\rho_w$  = density of water (g/cm<sup>3</sup>)

$\eta$  = viscosity (g·s/cm<sup>2</sup>)

At 20°C,  $\rho_w = 1$  g/cm<sup>3</sup> and  $\eta \approx 0.1 \times 10^{-4}$  g·s/cm<sup>2</sup>. So

$$k = 3.5 \times 10^{-4} \left( \frac{e^3}{1 + e} \right) C_u^{0.6} D_{10}^{2.32} \left( \frac{1}{0.1 \times 10^{-4}} \right)$$

or

$$k \text{ (cm/sec)} = 35 \left( \frac{e^3}{1 + e} \right) C_u^{0.6} D_{10}^{2.32} \quad (1.35)$$

### Hydraulic Conductivity of Cohesive Soil

According to their experimental observations, Samarasinghe, Huang, and Drnevich (1982) suggested that the hydraulic conductivity of normally consolidated clays could be given by the equation

$$k = C \frac{e^n}{1 + e} \quad (1.36)$$

where  $C$  and  $n$  are constants to be determined experimentally.

Some other empirical relationships for estimating the hydraulic conductivity in clayey soils are given in Table 1.10. One should keep in mind, however, that any empirical

**Table 1.10** Empirical Relationships for Estimating Hydraulic Conductivity in Clayey Soil

Type of soil	Source	Relationship <sup>a</sup>
Clay	Mesri and Olson (1971)	$\log k = A' \log e + B'$
	Taylor (1948)	$\log k = \log k_0 - \frac{e_0 - e}{C_k}$
		$C_k \approx 0.5e_0$

<sup>a</sup> $k_0$  = *in situ* hydraulic conductivity at void ratio  $e_0$

$k$  = hydraulic conductivity at void ratio  $e$

$C_k$  = hydraulic conductivity change index

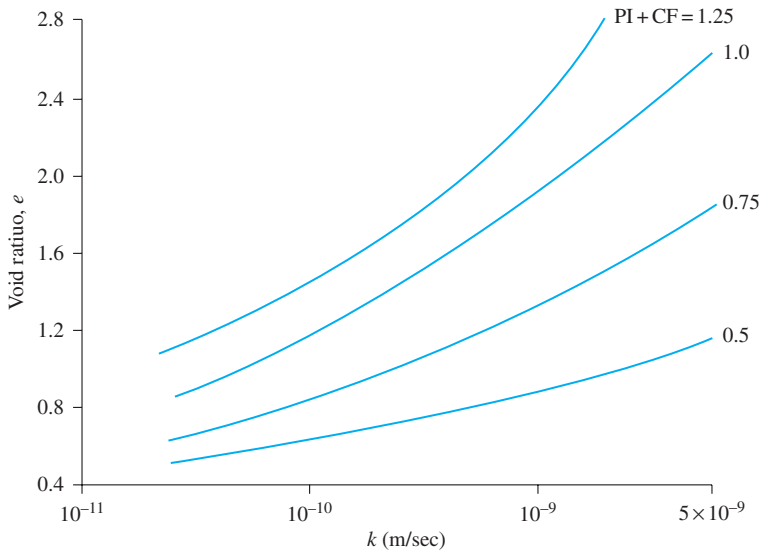


**Figure 1.10** Variation of void ratio with hydraulic conductivity of clayey soils (Based on Tavenas, *et al.*, 1983)

relationship of this type is for estimation only, because the magnitude of  $k$  is a highly variable parameter and depends on several factors.

Tavenas, *et al.* (1983) also gave a correlation between the void ratio and the hydraulic conductivity of clayey soil. This correlation is shown in Figure 1.10. An important point to note, however, is that in Figure 6.10, PI, the plasticity index, and CF, the clay-size fraction in the soil, are in *fraction* (decimal) form.

## 1.11 Steady-State Seepage

For most cases of seepage under hydraulic structures, the flow path changes direction and is not uniform over the entire area. In such cases, one of the ways of determining the rate of seepage is by a graphical construction referred to as the *flow net*, a concept based on Laplace's theory of continuity. According to this theory, for a steady flow condition, the flow at any point A (Figure 1.11) can be represented by the equation

$$k_x \frac{\partial^2 h}{\partial x^2} + k_y \frac{\partial^2 h}{\partial y^2} + k_z \frac{\partial^2 h}{\partial z^2} = 0 \quad (1.37)$$

where

$k_x, k_y, k_z$  = hydraulic conductivity of the soil in the  $x$ ,  $y$ , and  $z$  directions, respectively  
 $h$  = hydraulic head at point A (i.e., the head of water that a piezometer placed at A would show with the *downstream water level* as *datum*, as shown in Figure 1.11)

For a two-dimensional flow condition, as shown in Figure 1.11,

$$\frac{\partial^2 h}{\partial^2 y} = 0$$

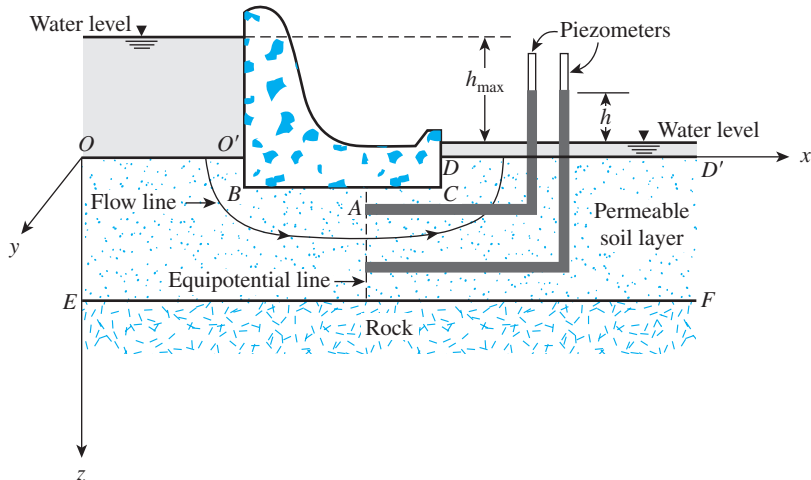


**Figure 1.11** Steady-state seepage

so Eq. (1.37) takes the form

$$k_x \frac{\partial^2 h}{\partial x^2} + k_z \frac{\partial^2 h}{\partial z^2} = 0 \quad (1.38)$$

If the soil is isotropic with respect to hydraulic conductivity,  $k_x = k_z = k$ , and

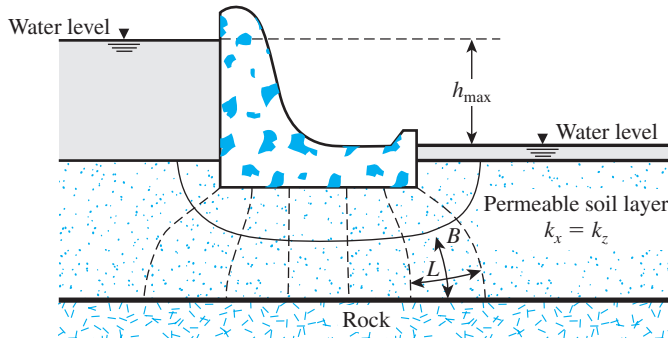
$$\frac{\partial^2 h}{\partial x^2} + \frac{\partial^2 h}{\partial z^2} = 0 \quad (1.39)$$

Equation (1.39), which is referred to as Laplace's equation and is valid for confined flow, represents two orthogonal sets of curves known as *flow lines* and *equipotential lines*. A flow net is a combination of numerous equipotential lines and flow lines. A flow line is a path that a water particle would follow in traveling from the upstream side to the downstream side. An equipotential line is a line along which water, in piezometers, would rise to the same elevation. (See Figure 1.11.)

In drawing a flow net, you need to establish the *boundary conditions*. For example, in Figure 1.11, the ground surfaces on the upstream ( $OO'$ ) and downstream ( $DD'$ ) sides are equipotential lines. The base of the dam below the ground surface,  $O'B'C'D'$ , is a flow line. The top of the rock surface,  $EF$ , is also a flow line. Once the boundary conditions are established, a number of flow lines and equipotential lines are drawn by trial and error so that all the flow elements in the net have the same length-to-width ratio ( $L/B$ ). In most cases,  $L/B$  is held to unity, that is, the flow elements are drawn as curvilinear "squares." This method is illustrated by the flow net shown in Figure 1.12. Note that all flow lines must intersect all equipotential lines at *right angles*.

Once the flow net is drawn, the seepage (in unit time per unit length of the structure) can be calculated as

$$q = kh_{\max} \frac{N_f}{N_d} n \quad (1.40)$$

**Figure 1.12** Flow net

where

$N_f$  = number of flow channels

$N_d$  = number of drops

$n$  = width-to-length ratio of the flow elements in the flow net ( $B/L$ )

$h_{\max}$  = difference in water level between the upstream and downstream sides

The space between two consecutive flow lines is defined as a *flow channel*, and the space between two consecutive equipotential lines is called a *drop*. In Figure 1.12,  $N_f = 2$ ,  $N_d = 7$ , and  $n = 1$ . When square elements are drawn in a flow net,

$$q = kh_{\max} \frac{N_f}{N_d} \quad (1.41)$$

## 1.12 Effective Stress

The *total stress* at a given point in a soil mass can be expressed as

$$\sigma = \sigma' + u \quad (1.42)$$

where

$\sigma$  = total stress

$\sigma'$  = effective stress

$u$  = pore water pressure

The effective stress,  $\sigma'$ , is the vertical component of forces at solid-to-solid contact points over a unit cross-sectional area. Referring to Figure 1.13a, at point A

$$\begin{aligned}\sigma &= \gamma h_1 + \gamma_{\text{sat}} h_2 \\ u &= h_2 \gamma_w\end{aligned}$$

where

$\gamma_w$  = unit weight of water

$\gamma_{\text{sat}}$  = saturated unit weight of soil

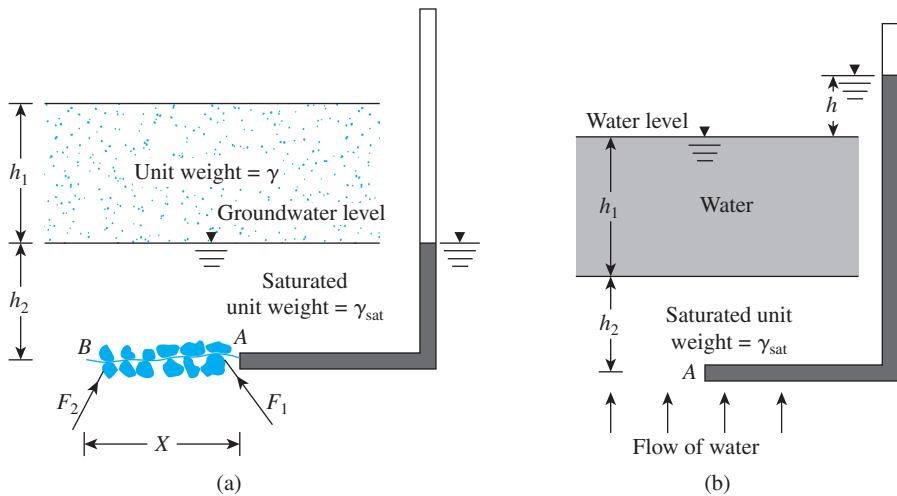


**Figure 1.13** Calculation of effective stress

So

$$\begin{aligned}\sigma' &= (\gamma h_1 + \gamma_{\text{sat}} h_2) - (h_2 \gamma_w) \\ &= \gamma h_1 + h_2(\gamma_{\text{sat}} - \gamma_w) \\ &= \gamma h_1 + \gamma' h_2\end{aligned}\quad (1.43)$$

where  $\gamma'$  = effective or submerged unit weight of soil.

For the problem in Figure 1.13a, there was *no seepage of water* in the soil. Figure 1.13b shows a simple condition in a soil profile in which there is upward seepage. For this case, at point A,

$$\sigma = h_1 \gamma_w + h_2 \gamma_{\text{sat}}$$

and

$$u = (h_1 + h_2 + h) \gamma_w$$

Thus, from Eq. (1.42),

$$\begin{aligned}\sigma' &= \sigma - u = (h_1 \gamma_w + h_2 \gamma_{\text{sat}}) - (h_1 + h_2 + h) \gamma_w \\ &= h_2(\gamma_{\text{sat}} - \gamma_w) - h \gamma_w = h_2 \gamma' - h \gamma_w\end{aligned}$$

or

$$\sigma' = h_2 \left( \gamma' - \frac{h}{h_2} \gamma_w \right) = h_2 (\gamma' - i \gamma_w) \quad (1.44)$$

Note in Eq. (1.44) that  $h/h_2$  is the hydraulic gradient  $i$ . If the hydraulic gradient is very high, so that  $\gamma' - i \gamma_w$  becomes zero, *the effective stress will become zero*. In other words, there is no contact stress between the soil particles, and the soil will break up. This situation is referred to as the *quick condition*, or *failure by heave*. So, for heave,

$$i = i_{\text{cr}} = \frac{\gamma'}{\gamma_w} = \frac{G_s - 1}{1 + e} \quad (1.45)$$

where  $i_{cr}$  = critical hydraulic gradient.

For most sandy soils,  $i_{cr}$  ranges from 0.9 to 1.1, with an average of about unity.

## 1.13 Consolidation

In the field, when the stress on a saturated clay layer is increased—for example, by the construction of a foundation—the pore water pressure in the clay will increase. Because the hydraulic conductivity of clays is very small, some time will be required for the excess pore water pressure to dissipate and the increase in stress to be transferred to the soil skeleton. According to Figure 1.14, if  $\Delta\sigma$  is a surcharge at the ground surface over a very large area, the increase in total stress at any depth of the clay layer will be equal to  $\Delta\sigma$ .

However, at time  $t = 0$  (i.e., immediately after the stress is applied), the excess pore water pressure at any depth  $\Delta u$  will equal  $\Delta\sigma$ , or

$$\Delta u = \Delta h_i \gamma_w = \Delta\sigma \text{ (at time } t = 0\text{)}$$

Hence, the increase in effective stress at time  $t = 0$  will be

$$\Delta\sigma' = \Delta\sigma - \Delta u = 0$$

Theoretically, at time  $t = \infty$ , when all the excess pore water pressure in the clay layer has dissipated as a result of drainage into the sand layers,

$$\Delta u = 0 \quad (\text{at time } t = \infty)$$

Then the increase in effective stress in the clay layer is

$$\Delta\sigma' = \Delta\sigma - \Delta u = \Delta\sigma - 0 = \Delta\sigma$$

This gradual increase in the effective stress in the clay layer will cause settlement over a period of time and is referred to as *consolidation*.

Laboratory tests on undisturbed saturated clay specimens can be conducted (ASTM Test Designation D-2435) to determine the consolidation settlement caused by various incremental loadings. The test specimens are usually 63.5 mm (2.5 in.) in diameter and 25.4 mm (1 in.) in height. Specimens are placed inside a ring, with one porous stone at the top

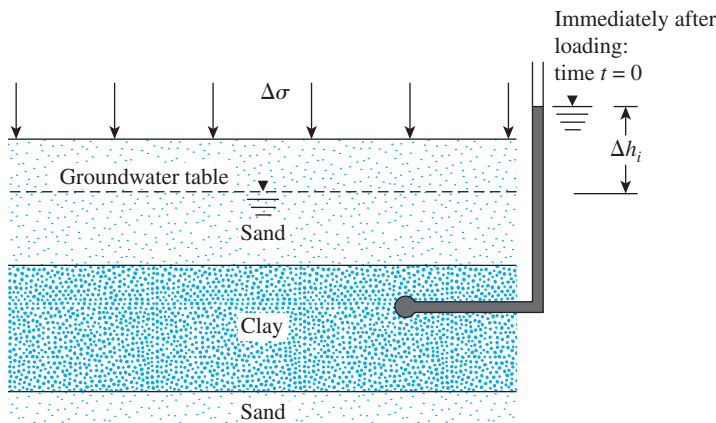


**Figure 1.14** Principles of consolidation

and one at the bottom of the specimen (Figure 1.15a). A load on the specimen is then applied so that the total vertical stress is equal to  $\sigma$ . Settlement readings for the specimen are taken periodically for 24 hours. After that, the load on the specimen is doubled and more settlement readings are taken. At all times during the test, the specimen is kept under water. The procedure is continued until the desired limit of stress on the clay specimen is reached.

Based on the laboratory tests, a graph can be plotted showing the variation of the void ratio  $e$  at the *end* of consolidation against the corresponding vertical effective stress  $\sigma'$ . (On a semilogarithmic graph,  $e$  is plotted on the arithmetic scale and  $\sigma'$  on the log scale.) The nature of the variation of  $e$  against  $\log \sigma'$  for a clay specimen is shown in Figure 1.15b. After the desired consolidation pressure has been reached, the specimen gradually can be unloaded, which will result in the swelling of the specimen. The figure also shows the variation of the void ratio during the unloading period.

From the  $e$ -log  $\sigma'$  curve shown in Figure 1.15b, three parameters necessary for calculating settlement in the field can be determined.

They are preconsolidation pressure ( $\sigma'_c$ ), compression index ( $C_c$ ), and the swelling index ( $C_s$ ). The following are more detailed descriptions for each of the parameters.

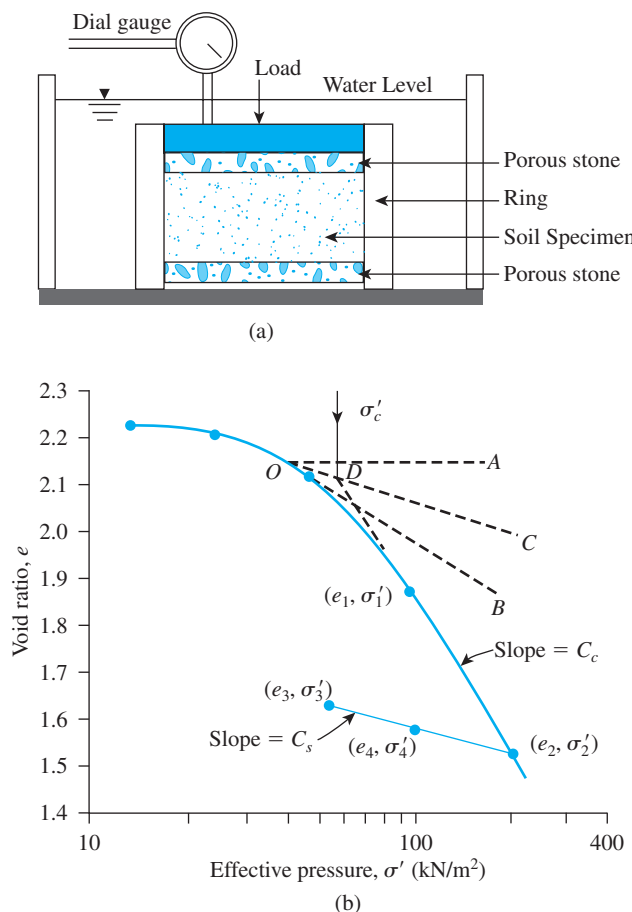


**Figure 1.15** (a) Schematic diagram of consolidation test arrangement; (b)  $e$ -log  $\sigma'$  curve for a soft clay from East St. Louis, Illinois (Note: At the end of consolidation,  $\sigma = \sigma'$ )

### Preconsolidation Pressure

The *preconsolidation pressure*,  $\sigma'_c$ , is the *maximum past effective overburden pressure* to which the soil specimen has been subjected. It can be determined by using a simple graphical procedure proposed by Casagrande (1936). The procedure involves five steps (see Figure 1.15b):

- a. Determine the point  $O$  on the  $e$ -log  $\sigma'$  curve that has the sharpest curvature (i.e., the smallest radius of curvature).
- b. Draw a horizontal line  $OA$ .
- c. Draw a line  $OB$  that is tangent to the  $e$ -log  $\sigma'$  curve at  $O$ .
- d. Draw a line  $OC$  that bisects the angle  $AOB$ .
- e. Produce the straight-line portion of the  $e$ -log  $\sigma'$  curve backwards to intersect  $OC$ . This is point  $D$ . The pressure that corresponds to point  $D$  is the preconsolidation pressure  $\sigma'_c$ .

Natural soil deposits can be *normally consolidated* or *overconsolidated* (or *preconsolidated*). If the present effective overburden pressure  $\sigma' = \sigma'_o$  is equal to the preconsolidated pressure  $\sigma'_c$  the soil is *normally consolidated*. However, if  $\sigma'_o < \sigma'_c$ , the soil is *overconsolidated*.

Stas and Kulhawy (1984) correlated the preconsolidation pressure with liquidity index in the following form:

$$\frac{\sigma'_c}{p_a} = 10^{(1.11 - 1.62 \text{ LI})} \quad (1.46)$$

where

$p_a$  = atmospheric pressure ( $\approx 2000 \text{ lb}/\text{ft}^2$  or  $100 \text{ kN}/\text{m}^2$ )

LI = liquidity index

A similar correlation has also been provided by Kulhawy and Mayne (1990), which is based on the work of Wood (1983) as

$$\sigma'_c = \sigma'_o \left\{ 10^{\left[ 1 - 2.5 \text{ LI} - 1.25 \log \left( \frac{\sigma'_o}{p_a} \right) \right]} \right\} \quad (1.47)$$

where  $\sigma'_o$  = *in situ* effective overburden pressure.

Nagaraj and Murthy (1985) gave a correlation between  $\sigma'_c$  and the *in situ* effective overburden pressure which can be expressed as

$$\log \sigma'_o (\text{kN}/\text{m}^2) = \frac{1.122 - \left( \frac{e_o}{e_L} \right) - 0.0463 \log \sigma'_c (\text{kN}/\text{m}^2)}{0.188} \quad (1.48)$$

where

$\sigma'_o$  = *in situ* effective overburden pressure

$e_o$  = *in situ* void ratio

$e_L$  = void ratio at liquid limit =  $\left[ \frac{\text{LL}(\%)}{100} \right] G_s$

$G_s$  = specific gravity of soil solids

### Compression Index

The *compression index*,  $C_c$ , is the slope of the straight-line portion (the latter part) of the loading curve, or

$$C_c = \frac{e_1 - e_2}{\log \sigma'_2 - \log \sigma'_1} = \frac{e_1 - e_2}{\log \left( \frac{\sigma'_2}{\sigma'_1} \right)} \quad (1.49)$$

where  $e_1$  and  $e_2$  are the void ratios at the end of consolidation under effective stresses  $\sigma'_1$  and  $\sigma'_2$ , respectively.

The *compression index*, as determined from the laboratory  $e$ -log  $\sigma'$  curve, will be somewhat different from that encountered in the field. The primary reason is that the soil remolds itself to some degree during the field exploration. The nature of variation of the  $e$ -log  $\sigma'$  curve in the field for a normally consolidated clay is shown in Figure 1.16. The curve, generally referred to as the *virgin compression curve*, approximately intersects the laboratory curve at a void ratio of  $0.42e_o$  (Terzaghi and Peck, 1967). Note that  $e_o$  is the void ratio of the clay in the field. Knowing the values of  $e_o$  and  $\sigma'_c$ , you can easily construct the virgin curve and calculate its compression index by using Eq. (1.49).

The value of  $C_c$  can vary widely, depending on the soil. Skempton (1944) gave an empirical correlation for the compression index in which

$$C_c = 0.009(LL - 10) \quad (1.50)$$

where LL = liquid limit .

Besides Skempton, several other investigators also have proposed correlations for the compression index. Some of those are given here:

Rendon-Herrero (1983):

$$C_c = 0.141G_s^{1.2} \left( \frac{1 + e_o}{G_s} \right)^{2.38} \quad (1.51)$$

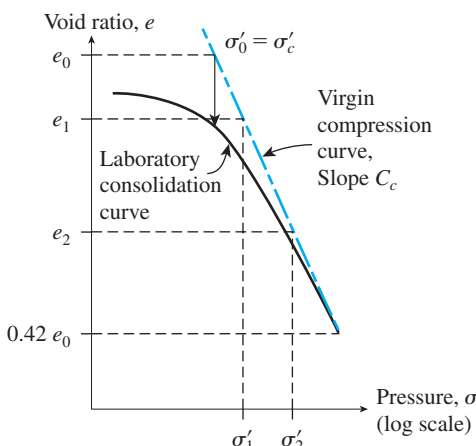


**Figure 1.16** Construction of virgin compression curve for normally consolidated clay

Nagaraj and Murty (1985):

$$C_c = 0.2343 \left[ \frac{\text{LL}(\%)}{100} \right] G_s \quad (1.52)$$

Park and Koumoto (2004):

$$C_c = \frac{n_o}{371.747 - 4.275n_o} \quad (1.53)$$

where  $n_o$  = *in situ* porosity of soil.

Wroth and Wood (1978):

$$C_c = 0.5G_s \left( \frac{\text{PI}(\%)}{100} \right) \quad (1.54)$$

If a typical value of  $G_s = 2.7$  is used in Eq. (1.54), we obtain (Kulhawy and Mayne, 1990)

$$C_c = \frac{\text{PI}(\%)}{74} \quad (1.55)$$

### **Swelling Index**

The *swelling index*,  $C_s$ , is the slope of the unloading portion of the  $e$ -log  $\sigma'$  curve. In Figure 1.15b, it is defined as

$$C_s = \frac{e_3 - e_4}{\log \left( \frac{\sigma'_4}{\sigma'_3} \right)} \quad (1.56)$$

In most cases, the value of the swelling index is  $\frac{1}{4}$  to  $\frac{1}{5}$  of the compression index. Following are some representative values of  $C_s/C_c$  for natural soil deposits:

Description of soil	$C_s/C_c$
Boston Blue clay	0.24–0.33
Chicago clay	0.15–0.3
New Orleans clay	0.15–0.28
St. Lawrence clay	0.05–0.1

The swelling index is also referred to as the *recompression index*.

The determination of the swelling index is important in the estimation of consolidation settlement of *overconsolidated clays*. In the field, depending on the pressure increase, an overconsolidated clay will follow an  $e$ -log  $\sigma'$  path  $abc$ , as shown in Figure 1.17. Note that point  $a$ , with coordinates  $\sigma'_o$  and  $e_o$ , corresponds to the field conditions before any increase in pressure. Point  $b$  corresponds to the preconsolidation pressure ( $\sigma'_c$ ) of the clay. Line  $ab$  is approximately parallel to the laboratory unloading curve  $cd$  (Schmertmann, 1953). Hence, if you know  $e_o$ ,  $\sigma'_o$ ,  $\sigma'_c$ ,  $C_c$ , and  $C_s$ , you can easily construct the field consolidation curve.

Using the modified Cam clay model and Eq. (1.54), Kulhawy and Mayne (1990) have shown that

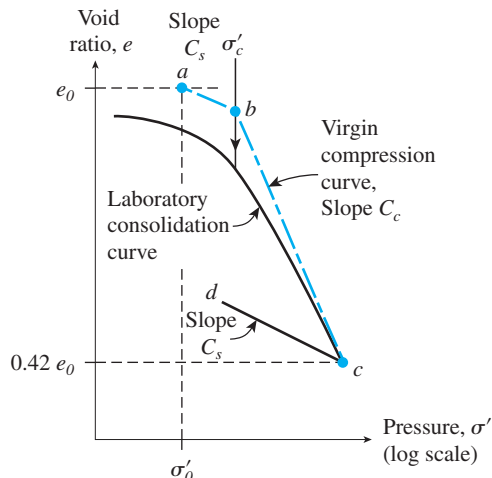


**Figure 1.17** Construction of field consolidation curve for overconsolidated clay

$$C_s = \frac{\text{PI}(\%)}{370} \quad (1.57)$$

Comparing Eqs. (1.55) and (1.57), we obtain

$$C_s \approx \frac{1}{5} C_c \quad (1.58)$$

## 1.14 Calculation of Primary Consolidation Settlement

The one-dimensional primary consolidation settlement (caused by an additional load) of a clay layer (Figure 1.18) having a thickness  $H_c$  may be calculated as

$$S_c = \frac{\Delta e}{1 + e_o} H_c \quad (1.59)$$

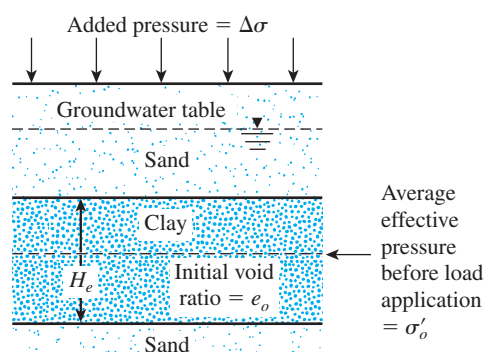


**Figure 1.18** One-dimensional settlement calculation

where

$S_c$  = primary consolidation settlement

$\Delta e$  = total change of void ratio caused by the additional load application

$e_o$  = void ratio of the clay before the application of load

For normally consolidated clay (that is,  $\sigma'_o = \sigma'_c$ )

$$\Delta e = C_c \log \frac{\sigma'_o + \Delta\sigma'}{\sigma'_o} \quad (1.60)$$

where

$\sigma'_o$  = average effective vertical stress on the clay layer

$\Delta\sigma'$  =  $\Delta\sigma$  (that is, added pressure)

Now, combining Eqs. (1.59) and (1.60) yields

$$S_c = \frac{C_c H_c}{1 + e_o} \log \frac{\sigma'_o + \Delta\sigma'}{\sigma'_o} \quad (1.61)$$

For overconsolidated clay with  $\sigma'_o + \Delta\sigma' \leq \sigma'_c$ ,

$$\Delta e = C_s \log \frac{\sigma'_o + \Delta\sigma'}{\sigma'_o} \quad (1.62)$$

Combining Eqs. (1.59) and (1.62) gives

$$S_c = \frac{C_s H_c}{1 + e_o} \log \frac{\sigma'_o + \Delta\sigma'}{\sigma'_o} \quad (1.63)$$

For overconsolidated clay, if  $\sigma'_o < \sigma'_c < \sigma'_o + \Delta\sigma'$ , then

$$\Delta e = \Delta e_1 + \Delta e_2 = C_s \log \frac{\sigma'_c}{\sigma'_o} + C_c \log \frac{\sigma'_o + \Delta\sigma'}{\sigma'_c} \quad (1.64)$$

Now, combining Eqs. (1.59) and (1.64) yields

$$S_c = \frac{C_s H_c}{1 + e_o} \log \frac{\sigma'_c}{\sigma'_o} + \frac{C_c H_c}{1 + e_o} \log \frac{\sigma'_o + \Delta\sigma'}{\sigma'_c} \quad (1.65)$$

## 1.15

### Time Rate of Consolidation

In Section 1.13 (see Figure 1.14), we showed that consolidation is the result of the gradual dissipation of the excess pore water pressure from a clay layer. The dissipation of pore water pressure, in turn, increases the effective stress, which induces settlement. Hence, to estimate the degree of consolidation of a clay layer at some time  $t$  after the load is applied, you need to know the rate of dissipation of the excess pore water pressure.

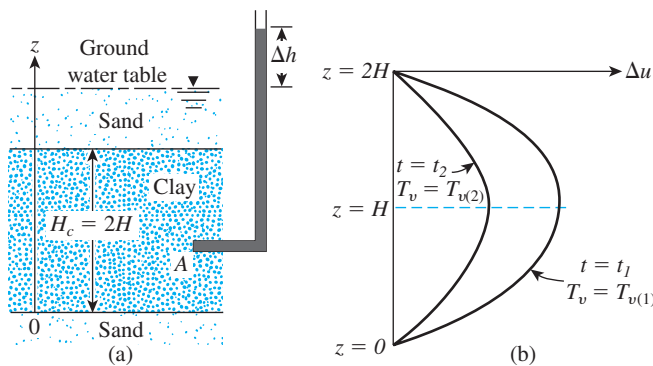


**Figure 1.19** (a) Derivation of Eq. (1.68); (b) nature of variation of  $\Delta u$  with time

Figure 1.19 shows a clay layer of thickness  $H_c$  that has highly permeable sand layers at its top and bottom. Here, the excess pore water pressure at any point  $A$  at any time  $t$  after the load is applied is  $\Delta u = (\Delta h)\gamma_w$ . For a vertical drainage condition (that is, in the direction of  $z$  only) from the clay layer, Terzaghi derived the differential equation

$$\frac{\partial(\Delta u)}{\partial t} = C_v \frac{\partial^2(\Delta u)}{\partial z^2} \quad (1.66)$$

where  $C_v$  = coefficient of consolidation, defined by

$$C_v = \frac{k}{m_v \gamma_w} = \frac{k}{\frac{\Delta e}{\Delta \sigma' (1 + e_{av})} \gamma_w} \quad (1.67)$$

in which

$k$  = hydraulic conductivity of the clay

$\Delta e$  = total change of void ratio caused by an effective stress increase of  $\Delta \sigma'$

$e_{av}$  = average void ratio during consolidation

$m_v$  = volume coefficient of compressibility =  $\Delta e / [\Delta \sigma' (1 + e_{av})]$

Equation (1.66) can be solved to obtain  $\Delta u$  as a function of time  $t$  with the following boundary conditions:

- Because highly permeable sand layers are located at  $z = 0$  and  $z = H_c$ , the excess pore water pressure developed in the clay at those points will be immediately dissipated. Hence,

$$\Delta u = 0 \quad \text{at } z = 0$$

and

$$\Delta u = 0 \quad \text{at } z = H_c = 2H$$

where  $H$  = length of maximum drainage path (due to two-way drainage condition—that is, at the top and bottom of the clay).

2. At time  $t = 0$ ,  $\Delta u = \Delta u_0$  = initial excess pore water pressure after the load is applied. With the preceding boundary conditions, Eq. (1.66) yields

$$\Delta u = \sum_{m=0}^{m=\infty} \left[ \frac{2(\Delta u_0)}{M} \sin\left(\frac{Mz}{H}\right) \right] e^{-M^2 T_v} \quad (1.68)$$

where

$$\begin{aligned} M &= [(2m + 1)\pi]/2 \\ m &= \text{an integer} = 1, 2, \dots \\ T_v &= \text{nondimensional time factor} = (C_v t)/H^2 \end{aligned} \quad (1.69)$$

The value of  $\Delta u$  for various depths (i.e.,  $z = 0$  to  $z = 2H$ ) at any given time  $t$  (and thus  $T_v$ ) can be calculated from Eq. (1.68). The nature of this variation of  $\Delta u$  is shown in Figures 1.20a and b. Figure 1.20c shows the variation of  $\Delta u/\Delta u_0$  with  $T_v$  and  $H/H_c$  using Eqs.(1.68) and (1.69).

The *average degree of consolidation* of the clay layer can be defined as

$$U = \frac{S_{c(t)}}{S_{c(\max)}} \quad (1.70)$$

where

$S_{c(t)}$  = settlement of a clay layer at time  $t$  after the load is applied  
 $S_{c(\max)}$  = maximum consolidation settlement that the clay will undergo under a given loading

If the initial pore water pressure ( $\Delta u_0$ ) distribution is constant with depth, as shown in Figure 1.20a, the average degree of consolidation also can be expressed as

$$U = \frac{S_{c(t)}}{S_{c(\max)}} = \frac{\int_0^{2H} (\Delta u_0) dz - \int_0^{2H} (\Delta u) dz}{\int_0^{2H} (\Delta u_0) dz} \quad (1.71)$$

or

$$U = \frac{(\Delta u_0)2H - \int_0^{2H} (\Delta u) dz}{(\Delta u_0)2H} = 1 - \frac{\int_0^{2H} (\Delta u) dz}{2H(\Delta u_0)} \quad (1.72)$$

Now, combining Eqs. (1.68) and (1.72), we obtain

$$U = \frac{S_{c(t)}}{S_{c(\max)}} = 1 - \sum_{m=0}^{m=\infty} \left( \frac{2}{M^2} \right) e^{-M^2 T_v} \quad (1.73)$$

The variation of  $U$  with  $T_v$  can be calculated from Eq. (1.73) and is plotted in Figure 1.21. Note that Eq. (1.73) and thus Figure 1.21 are also valid when an impermeable layer is located at the bottom of the clay layer (Figure 1.20). In that case, the dissipation of

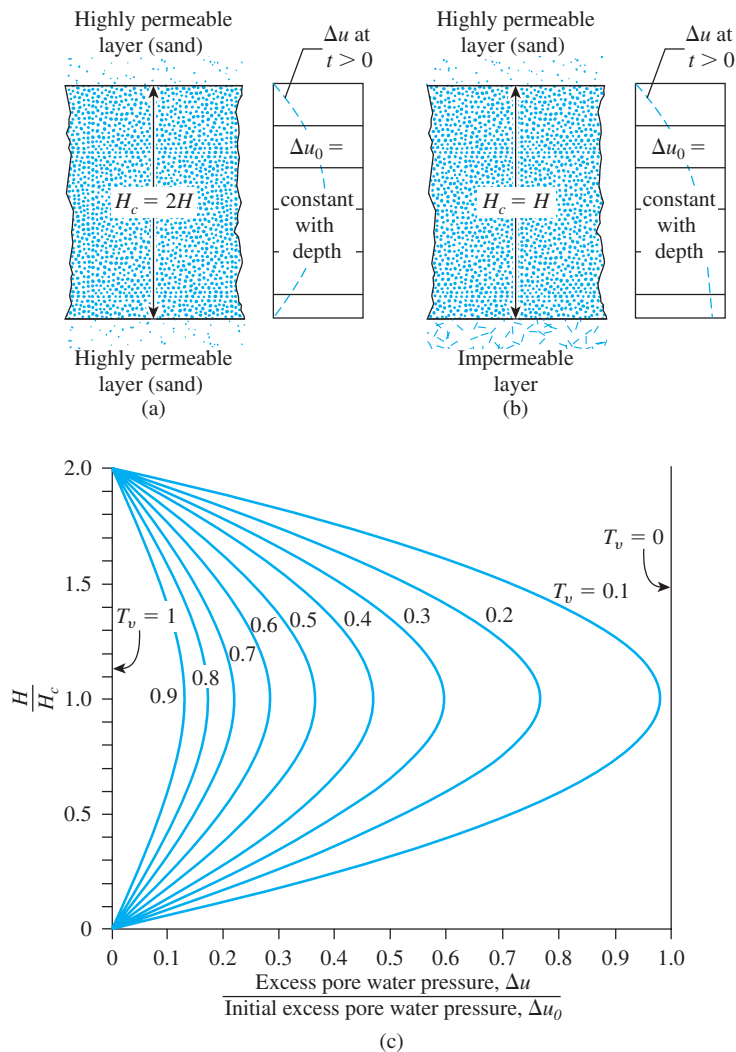


**Figure 1.20** Drainage condition for consolidation: (a) two-way drainage; (b) one-way drainage; (c) plot of  $\Delta u / \Delta u_0$  with  $T_v$  and  $H / H_c$

excess pore water pressure can take place in one direction only. The length of the *maximum drainage path* is then equal to  $H = H_c$ .

The variation of  $T_v$  with  $U$  shown in Figure 1.21 can also be approximated by

$$T_v = \frac{\pi}{4} \left( \frac{U\%}{100} \right)^2 \quad (\text{for } U = 0 \text{ to } 60\%) \quad (1.74)$$

and

$$T_v = 1.781 - 0.933 \log (100 - U\%) \quad (\text{for } U > 60\%) \quad (1.75)$$

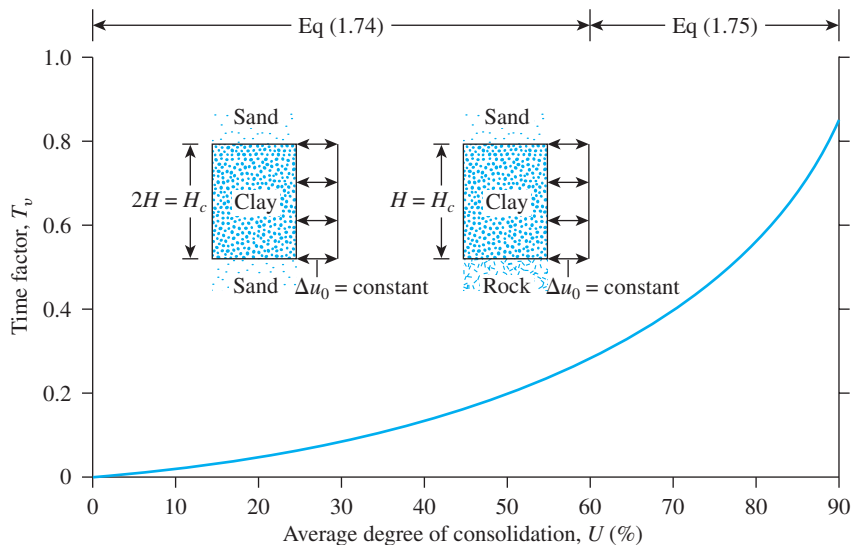


**Figure 1.21** Plot of time factor against average degree of consolidation ( $\Delta u_0 = \text{constant}$ )

Table 1.11 gives the variation of  $T_v$  with  $U$  on the basis of Eqs. (1.74) and (1.75)

Sivaram and Swamee (1977) gave the following equation for  $U$  varying from 0 to 100%:

$$\frac{U\%}{100} = \frac{(4T_v/\pi)^{0.5}}{[1 + (4T_v/\pi)^{2.8}]^{0.179}} \quad (1.76)$$

or

$$T_v = \frac{(\pi/4)(U\%/100)^2}{[1 - (U\%/100)^{5.6}]^{0.357}} \quad (1.77)$$

Equations (1.76) and (1.77) give an error in  $T_v$  of less than 1% for  $0\% < U < 90\%$  and less than 3% for  $90\% < U < 100\%$ .

**Table 1.11** Variation of  $T_v$  with  $U$

$U$ (%)	$T_v$	$U$ (%)	$T_v$	$U$ (%)	$T_v$	$U$ (%)	$T_v$
0	0	26	0.0531	52	0.212	78	0.529
1	0.00008	27	0.0572	53	0.221	79	0.547
2	0.0003	28	0.0615	54	0.230	80	0.567
3	0.00071	29	0.0660	55	0.239	81	0.588
4	0.00126	30	0.0707	56	0.248	82	0.610
5	0.00196	31	0.0754	57	0.257	83	0.633
6	0.00283	32	0.0803	58	0.267	84	0.658
7	0.00385	33	0.0855	59	0.276	85	0.684
8	0.00502	34	0.0907	60	0.286	86	0.712
9	0.00636	35	0.0962	61	0.297	87	0.742
10	0.00785	36	0.102	62	0.307	88	0.774

**Table 1.11** (Continued)

$U$ (%)	$T_v$	$U$ (%)	$T_v$	$U$ (%)	$T_v$	$U$ (%)	$T_v$
11	0.0095	37	0.107	63	0.318	89	0.809
12	0.0113	38	0.113	64	0.329	90	0.848
13	0.0133	39	0.119	65	0.304	91	0.891
14	0.0154	40	0.126	66	0.352	92	0.938
15	0.0177	41	0.132	67	0.364	93	0.993
16	0.0201	42	0.138	68	0.377	94	1.055
17	0.0227	43	0.145	69	0.390	95	1.129
18	0.0254	44	0.152	70	0.403	96	1.219
19	0.0283	45	0.159	71	0.417	97	1.336
20	0.0314	46	0.166	72	0.431	98	1.500
21	0.0346	47	0.173	73	0.446	99	1.781
22	0.0380	48	0.181	74	0.461	100	$\infty$
23	0.0415	49	0.188	75	0.477		
24	0.0452	50	0.197	76	0.493		
25	0.0491	51	0.204	77	0.511		

### Example 1.9

A laboratory consolidation test on a normally consolidated clay showed the following results:

Load, $\Delta\sigma'$ (kN/m <sup>2</sup> )	Void ratio at the end of consolidation, $e$
140	0.92
212	0.86

The specimen tested was 25.4 mm in thickness and drained on both sides. The time required for the specimen to reach 50% consolidation was 4.5 min.

A similar clay layer in the field 2.8 m thick and drained on both sides, is subjected to a similar increase in average effective pressure (i.e.,  $\sigma'_0 = 140$  kN/m<sup>2</sup> and  $\sigma'_0 + \Delta\sigma' = 212$  kN/m<sup>2</sup>). Determine

- a. the expected maximum primary consolidation settlement in the field.
- b. the length of time required for the total settlement in the field to reach 40 mm.  
(Assume a uniform initial increase in excess pore water pressure with depth.)

#### Solution

Part a

For normally consolidated clay [Eq. (1.49)],

$$C_c = \frac{e_1 - e_2}{\log\left(\frac{\sigma'_2}{\sigma'_1}\right)} = \frac{0.92 - 0.86}{\log\left(\frac{212}{140}\right)} = 0.333$$

From Eq. (1.61),

$$S_c = \frac{C_c H_c}{1 + e_0} \log \frac{\sigma'_0 + \Delta\sigma'}{\sigma'_0} = \frac{(0.333)(2.8)}{1 + 0.92} \log \frac{212}{140} = 0.0875 \text{ m} = \mathbf{87.5 \text{ mm}}$$

Part b

From Eq. (1.70), the average degree of consolidation is

$$U = \frac{S_{c(t)}}{S_{c(\max)}} = \frac{40}{87.5}(100) = 45.7\%$$

The coefficient of consolidation,  $C_v$ , can be calculated from the laboratory test. From Eq. (1.69),

$$T_v = \frac{C_v t}{H^2}$$

For 50% consolidation (Figure 1.21),  $T_v = 0.197$ ,  $t = 4.5$  min, and  $H = H_c/2 = 12.7$  mm, so

$$C_v = T_{50} \frac{H^2}{t} = \frac{(0.197)(12.7)^2}{4.5} = 7.061 \text{ mm}^2/\text{min}$$

Again, for field consolidation,  $U = 45.7\%$ . From Eq. (1.74)

$$T_v = \frac{\pi}{4} \left( \frac{U\%}{100} \right)^2 = \frac{\pi}{4} \left( \frac{45.7}{100} \right)^2 = 0.164$$

But

$$T_v = \frac{C_v t}{H^2}$$

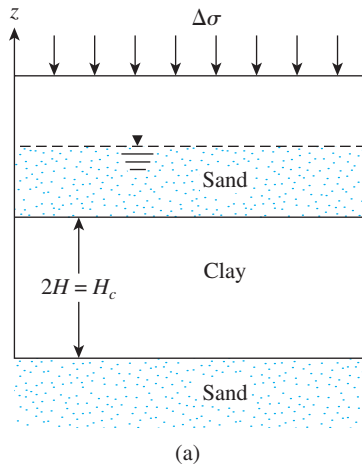
or

$$t = \frac{T_v H^2}{C_v} = \frac{0.164 \left( \frac{2.8 \times 1000}{2} \right)^2}{7.061} = 45,523 \text{ min} = \mathbf{31.6 \text{ days}} \quad \blacksquare$$

## 1.16

### Degree of Consolidation Under Ramp Loading

The relationships derived for the average degree of consolidation in Section 1.15 assume that the surcharge load per unit area ( $\Delta\sigma$ ) is applied instantly at time  $t = 0$ . However, in most practical situations,  $\Delta\sigma$  increases gradually with time to a maximum value and remains constant thereafter. Figure 1.22 shows  $\Delta\sigma$  increasing linearly with time ( $t$ ) up to a maximum at time  $t_c$  (a condition called ramp loading). For  $t \geq t_c$ , the magnitude of  $\Delta\sigma$



(a)

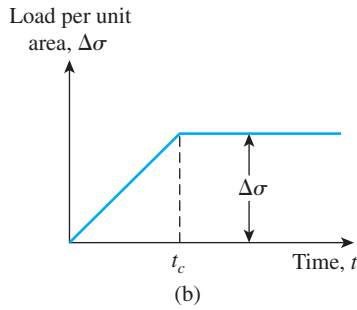


**Figure 1.22** One-dimensional consolidation due to single ramp loading

remains constant. Olson (1977) considered this phenomenon and presented the average degree of consolidation,  $U$ , in the following form:

For  $T_v \leq T_c$ ,

$$U = \frac{T_v}{T_c} \left\{ 1 - \frac{2}{T_v} \sum_{m=0}^{m=\infty} \frac{1}{M^4} [1 - \exp(-M^2 T_v)] \right\} \quad (1.78)$$

and for  $T_v \geq T_c$ ,

$$U = 1 - \frac{2}{T_c} \sum_{m=0}^{m=\infty} \frac{1}{M^4} [\exp(M^2 T_c) - 1] \exp(-M^2 T_c) \quad (1.79)$$

where  $m$ ,  $M$ , and  $T_c$  have the same definition as in Eq. (1.68) and where

$$T_c = \frac{C_v t_c}{H^2} \quad (1.80)$$

Figure 1.23 shows the variation of  $U$  with  $T_v$  for various values of  $T_c$ , based on the solution given by Eqs. (1.78) and (1.79).

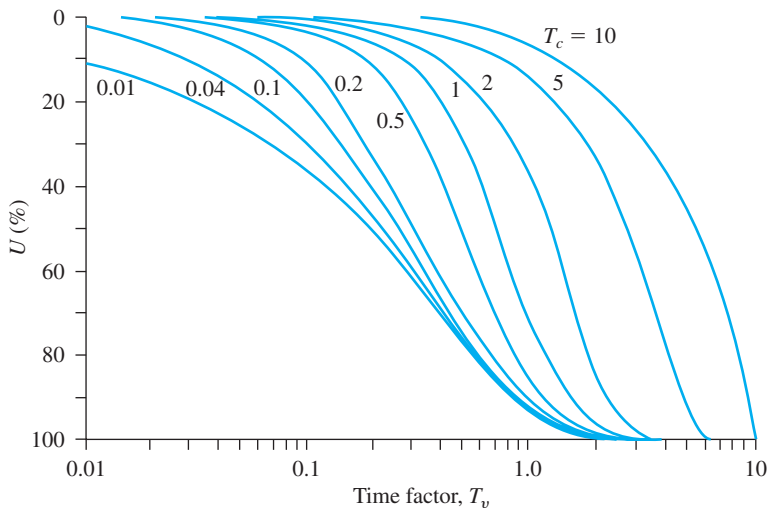


**Figure 1.23** Olson's ramp-loading solution: plot of  $U$  versus  $T_v$  (Eqs. 1.78 and 1.79)

### Example 1.10

In Example 1.9, Part (b), if the increase in  $\Delta\sigma$  would have been in the manner shown in Figure 1.24, calculate the settlement of the clay layer at time  $t = 31.6$  days after the beginning of the surcharge.

#### Solution

From Part (b) of Example 1.29,  $C_v = 7.061 \text{ mm}^2/\text{min}$ . From Eq. (1.80),

$$T_c = \frac{C_v t_c}{H^2} = \frac{(7.061 \text{ mm}^2/\text{min})(15 \times 24 \times 60 \text{ min})}{\left(\frac{2.8}{2} \times 1000 \text{ mm}\right)^2} = 0.0778$$

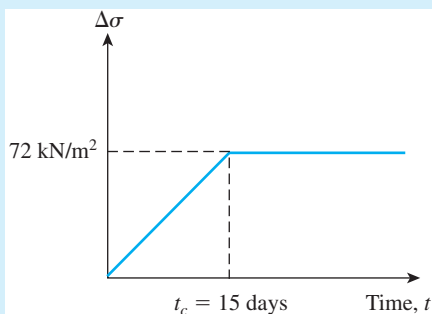


**Figure 1.24** Ramp loading

Also,

$$T_v = \frac{C_v t}{H^2} = \frac{(7.061 \text{ mm}^2/\text{min}) (31.6 \times 24 \times 60 \text{ min})}{\left(\frac{2.8}{2} \times 1000 \text{ mm}\right)^2} = 0.164$$

From Figure 1.23, for  $T_v = 0.164$  and  $T_c = 0.0778$ , the value of  $U$  is about 36%. Thus,

$$S_{c(t=31.6 \text{ days})} = S_{c(\max)}(0.36) = (87.5)(0.36) = 31.5 \text{ mm}$$

## 1.17 Shear Strength

The shear strength of a soil, defined in terms of effective stress, is

$$s = c' + \sigma' \tan \phi' \quad (1.81)$$

where

- $\sigma'$  = effective normal stress on plane of shearing
- $c'$  = cohesion, or apparent cohesion
- $\phi'$  = effective stress angle of friction

Equation (1.81) is referred to as the *Mohr–Coulomb failure criterion*. The value of  $c'$  for sands and normally consolidated clays is equal to zero. For overconsolidated clays,  $c' > 0$ .

For most day-to-day work, the shear strength parameters of a soil (i.e.,  $c'$  and  $\phi'$ ) are determined by two standard laboratory tests: the *direct shear test* and the *triaxial test*.

### Direct Shear Test

Dry sand can be conveniently tested by direct shear tests. The sand is placed in a shear box that is split into two halves (Figure 1.25a). First a normal load is applied to the specimen. Then a shear force is applied to the top half of the shear box to cause failure in the sand. The normal and shear stresses at failure are

$$\sigma' = \frac{N}{A}$$

and

$$s = \frac{R}{A}$$

where  $A$  = area of the failure plane in soil—that is, the cross-sectional area of the shear box.

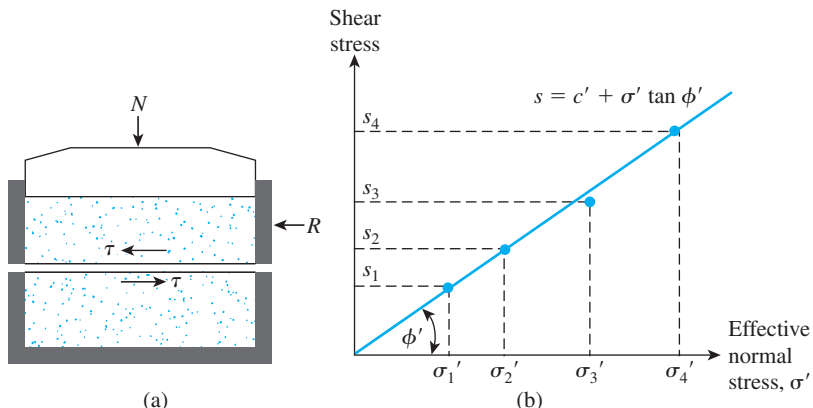


**Figure 1.25** Direct shear test in sand: (a) schematic diagram of test equipment; (b) plot of test results to obtain the friction angle  $\phi'$

Several tests of this type can be conducted by varying the normal load. The angle of friction of the sand can be determined by plotting a graph of  $s$  against  $\sigma'$  ( $= \sigma$  for dry sand), as shown in Figure 1.25b, or

$$\phi' = \tan^{-1}\left(\frac{s}{\sigma'}\right) \quad (1.82)$$

For sands, the angle of friction usually ranges from  $26^\circ$  to  $45^\circ$ , increasing with the relative density of compaction. A general range of the friction angle,  $\phi'$ , for sands is given in Table 1.12.

In 1970, Brinch Hansen (see Hansbo, 1975, and Thinh, 2001) gave the following correlation for  $\phi'$  of granular soils.

$$\phi' \text{ (deg)} = 26^\circ + 10D_r + 0.4C_u + 1.6 \log(D_{50}) \quad (1.83)$$

where

$D_r$  = relative density (fraction)

$C_u$  = uniformity coefficient

$D_{50}$  = mean grain size, in mm (i.e., the diameter through which 50% of the soil passes)

**Table 1.12** Relationship between Relative Density and Angle of Friction of Cohesionless Soils

State of packing	Relative density (%)	Angle of friction, $\phi'$ (deg.)
Very loose	<20	<30
Loose	20–40	30–35
Compact	40–60	35–40
Dense	60–80	40–45
Very dense	>80	>45

Teferra (1975) suggested the following empirical correlation based on a large data base.

$$\phi' \text{ (deg)} = \tan^{-1} \left( \frac{1}{ae+b} \right) \quad (1.84)$$

where

$$e = \text{void ratio}$$

$$a = 2.101 + 0.097 \left( \frac{D_{85}}{D_{15}} \right) \quad (1.85)$$

$$b = 0.845 - 0.398a \quad (1.86)$$

$D_{85}$  and  $D_{15}$  = diameters through which, respectively, 85% and 15% of soil passes

Thinh (2001) suggested that Eq. (1.84) provides as better correlation for  $\phi'$  compared to Eq. (1.83).

### Triaxial Tests

Triaxial compression tests can be conducted on sands and clays. Figure 1.26a shows a schematic diagram of the triaxial test arrangement. Essentially, the test consists of placing a soil specimen confined by a rubber membrane into a lucite chamber and then applying an all-around confining pressure ( $\sigma_3$ ) to the specimen by means of the chamber fluid (generally, water or glycerin). An added stress ( $\Delta\sigma$ ) can also be applied to the specimen in the axial direction to cause failure ( $\Delta\sigma = \Delta\sigma_f$  at failure). Drainage from the specimen can be allowed or stopped, depending on the condition being tested. For clays, three main types of tests can be conducted with triaxial equipment (see Figure 1.27):

1. Consolidated-drained test (CD test)
2. Consolidated-undrained test (CU test)
3. Unconsolidated-undrained test (UU test)

#### Consolidated-Drained Tests:

Step 1. Apply chamber pressure  $\sigma_3$ . Allow complete drainage, so that the pore water pressure ( $u = u_0$ ) developed is zero.

Step 2. Apply a deviator stress  $\Delta\sigma$  slowly. Allow drainage, so that the pore water pressure ( $u = u_d$ ) developed through the application of  $\Delta\sigma$  is zero. At failure,  $\Delta\sigma = \Delta\sigma_f$ ; the total pore water pressure  $u_f = u_0 + u_d = 0$ .

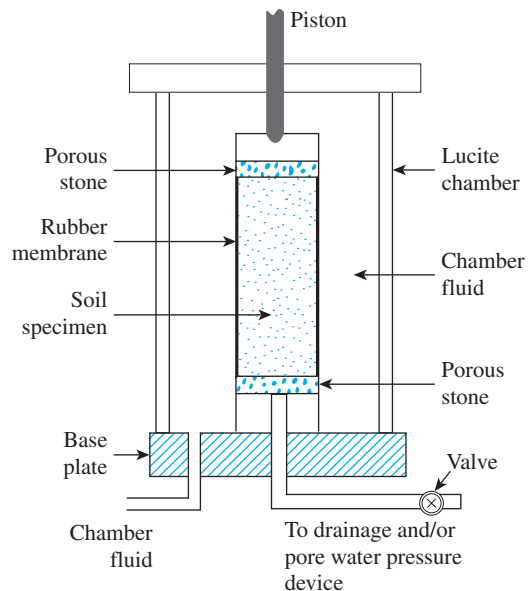
So for *consolidated-drained tests*, at failure,

Major principal effective stress =  $\sigma_3 + \Delta\sigma_f = \sigma_1 = \sigma'_1$

Minor principal effective stress =  $\sigma_3 = \sigma'_3$

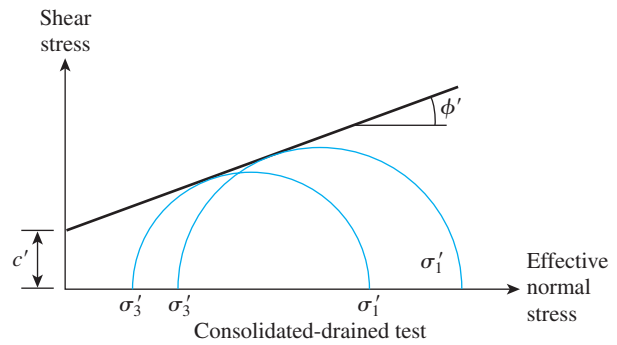
Changing  $\sigma_3$  allows several tests of this type to be conducted on various clay specimens. The shear strength parameters ( $c'$  and  $\phi'$ ) can now be determined by plotting Mohr's circle at failure, as shown in Figure 1.26b, and drawing a common tangent to the Mohr's circles. This is the *Mohr-Coulomb failure envelope*. (Note: For normally consolidated clay,  $c' \approx 0$ .) At failure,

$$\sigma'_1 = \sigma'_3 \tan^2 \left( 45 + \frac{\phi'}{2} \right) + 2c' \tan \left( 45 + \frac{\phi'}{2} \right) \quad (1.87)$$

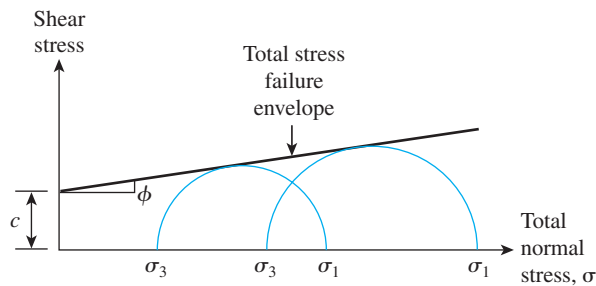


Schematic diagram of triaxial test equipment

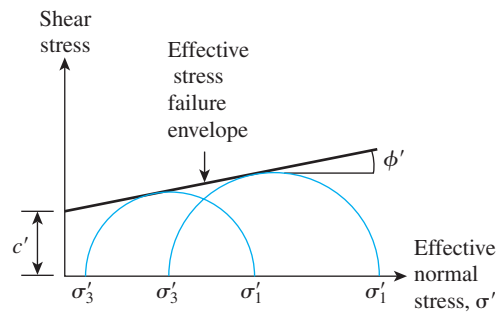
(a)



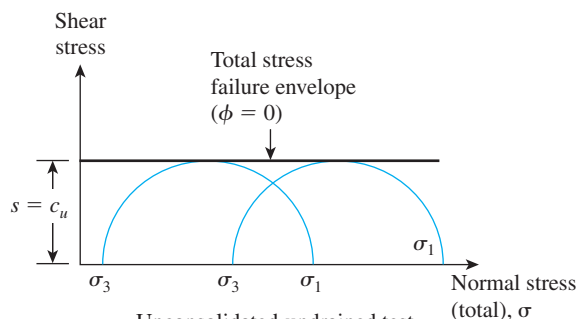
(b)



Consolidated-undrained test



(c)



Unconsolidated-undrained test

(d)

Figure 1.26 Triaxial test

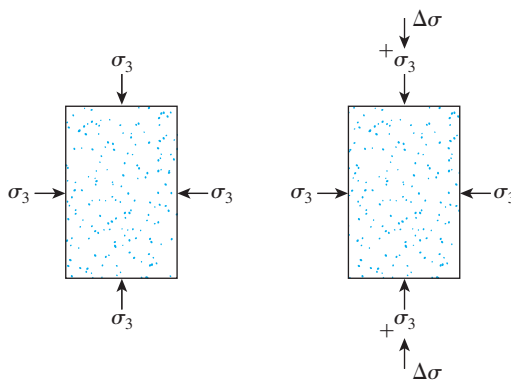


**Figure 1.27** Sequence of stress application in triaxial test

#### Consolidated-Undrained Tests:

- Step 1. Apply chamber pressure  $\sigma_3$ . Allow complete drainage, so that the pore water pressure ( $u = u_0$ ) developed is zero.
- Step 2. Apply a deviator stress  $\Delta\sigma$ . Do not allow drainage, so that the pore water pressure  $u = u_d \neq 0$ . At failure,  $\Delta\sigma = \Delta\sigma_f$ ; the pore water pressure  $u_f = u_0 + u_d = 0 + u_{d(f)}$ .

Hence, at failure,

$$\text{Major principal total stress} = \sigma_3 + \Delta\sigma_f = \sigma_1$$

$$\text{Minor principal total stress} = \sigma_3$$

$$\text{Major principal effective stress} = (\sigma_3 + \Delta\sigma_f) - u_f = \sigma'_1$$

$$\text{Minor principal effective stress} = \sigma_3 - u_f = \sigma'_3$$

Changing  $\sigma_3$  permits multiple tests of this type to be conducted on several soil specimens. The total stress Mohr's circles at failure can now be plotted, as shown in Figure 1.26c, and then a common tangent can be drawn to define the *failure envelope*. This *total stress failure envelope* is defined by the equation

$$s = c + \sigma \tan \phi \quad (1.88)$$

where  $c$  and  $\phi$  are the *consolidated-undrained cohesion* and *angle of friction*, respectively. (Note:  $c \approx 0$  for normally consolidated clays.)

Similarly, effective stress Mohr's circles at failure can be drawn to determine the *effective stress failure envelope* (Figure 1.26c), which satisfy the relation expressed in Eq. (1.81).

#### Unconsolidated-Undrained Tests:

- Step 1. Apply chamber pressure  $\sigma_3$ . Do not allow drainage, so that the pore water pressure ( $u = u_0$ ) developed through the application of  $\sigma_3$  is not zero.
- Step 2. Apply a deviator stress  $\Delta\sigma$ . Do not allow drainage ( $u = u_d \neq 0$ ). At failure,  $\Delta\sigma = \Delta\sigma_f$ ; the pore water pressure  $u_f = u_0 + u_{d(f)}$

For *unconsolidated-undrained* triaxial tests,

$$\text{Major principal total stress} = \sigma_3 + \Delta\sigma_f = \sigma_1$$

$$\text{Minor principal total stress} = \sigma_3$$

The total stress Mohr's circle at failure can now be drawn, as shown in Figure 1.26d. For saturated clays, the value of  $\sigma_1 - \sigma_3 = \Delta\sigma_f$  is a constant, irrespective of the chamber confining pressure  $\sigma_3$  (also shown in Figure 1.26d). The tangent to these Mohr's circles will be a horizontal line, called the  $\phi = 0$  condition. The shear strength for this condition is

$$s = c_u = \frac{\Delta\sigma_f}{2} \quad (1.89)$$

where  $c_u$  = undrained cohesion (or undrained shear strength).

The pore pressure developed in the soil specimen during the unconsolidated-undrained triaxial test is

$$u = u_0 + u_d \quad (1.90)$$

The pore pressure  $u_0$  is the contribution of the hydrostatic chamber pressure  $\sigma_3$ . Hence,

$$u_0 = B\sigma_3 \quad (1.91)$$

where  $B$  = Skempton's pore pressure parameter.

Similarly, the pore parameter  $u_d$  is the result of the added axial stress  $\Delta\sigma$ , so

$$u_d = A\Delta\sigma \quad (1.92)$$

where  $A$  = Skempton's pore pressure parameter.

However,

$$\Delta\sigma = \sigma_1 - \sigma_3 \quad (1.93)$$

Combining Eqs. (1.90), (1.91), (1.92), and (1.93) gives

$$u = u_0 + u_d = B\sigma_3 + A(\sigma_1 - \sigma_3) \quad (1.94)$$

The pore water pressure parameter  $B$  in soft saturated soils is approximately 1, so

$$u = \sigma_3 + A(\sigma_1 - \sigma_3) \quad (1.95)$$

The value of the pore water pressure parameter  $A$  at failure will vary with the type of soil. Following is a general range of the values of  $A$  at failure for various types of clayey soil encountered in nature:

Type of soil	$A$ at failure
Sandy clays	0.5–0.7
Normally consolidated clays	0.5–1
Overconsolidated clays	-0.5–0

## 1.18 Unconfined Compression Test

The *unconfined compression test* (Figure 1.28a) is a special type of unconsolidated-undrained triaxial test in which the confining pressure  $\sigma_3 = 0$ , as shown in Figure 1.28b. In this test, an axial stress  $\Delta\sigma$  is applied to the specimen to cause failure

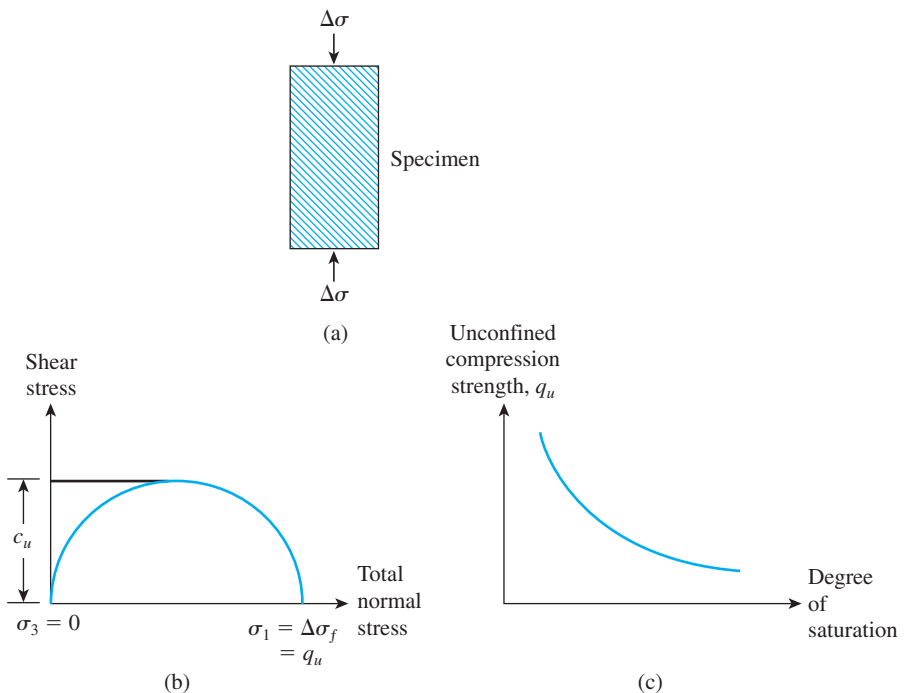


**Figure 1.28** Unconfined compression test: (a) soil specimen; (b) Mohr's circle for the test; (c) variation of  $q_u$  with the degree of saturation

(i.e.,  $\Delta\sigma = \Delta\sigma_f$ ). The corresponding Mohr's circle is shown in Figure 1.28b. Note that, for this case,

$$\begin{aligned} \text{Major principal total stress} &= \Delta\sigma_f = q_u \\ \text{Minor principal total stress} &= 0 \end{aligned}$$

The axial stress at failure,  $\Delta\sigma_f = q_u$ , is generally referred to as the *unconfined compression strength*. The shear strength of saturated clays under this condition ( $\phi = 0$ ), from Eq. (1.81), is

$$s = c_u = \frac{q_u}{2} \quad (1.96)$$

The unconfined compression strength can be used as an indicator of the consistency of clays.

Unconfined compression tests are sometimes conducted on unsaturated soils. With the void ratio of a soil specimen remaining constant, the unconfined compression strength rapidly decreases with the degree of saturation (Figure 1.28c).

## 1.19 Comments on Friction Angle, $\phi'$

### Effective Stress Friction Angle of Granular Soils

In general, the direct shear test yields a higher angle of friction compared with that obtained by the triaxial test. Also, note that the failure envelope for a given soil is actually curved. The Mohr–Coulomb failure criterion defined by Eq. (1.81) is only an approximation. Because of the curved nature of the failure envelope, a soil tested at higher normal stress will yield a lower value of  $\phi'$ . An example of this relationship is shown in Figure 1.29, which is a plot of  $\phi'$  versus the void ratio  $e$  for Chattahoochee River sand near Atlanta, Georgia (Vesic, 1963). The friction angles shown were obtained from triaxial tests. Note that, for a given value of  $e$ , the magnitude of  $\phi'$  is about  $4^\circ$  to  $5^\circ$  smaller when the confining pressure  $\sigma'_3$  is greater than about  $70 \text{ kN/m}^2$  ( $10 \text{ lb/in}^2$ ), compared with that when  $\sigma'_3 < 70 \text{ kN/m}^2$  ( $\approx 10 \text{ lb/in}^2$ ).

### Effective Stress Friction Angle of Cohesive Soils

Figure 1.30 shows the variation of effective stress friction angle,  $\phi'$ , for several normally consolidated clays (Bjerrum and Simons, 1960; Kenney, 1959). It can be seen from the figure that, in general, the friction angle  $\phi'$  decreases with the increase in plasticity index. The value of  $\phi'$  generally decreases from about  $37$  to  $38^\circ$  with a plasticity index of about  $10$  to about  $25^\circ$  or less with a plasticity index of about  $100$ . The consolidated undrained friction angle ( $\phi$ ) of normally consolidated saturated clays generally ranges from  $5$  to  $20^\circ$ .

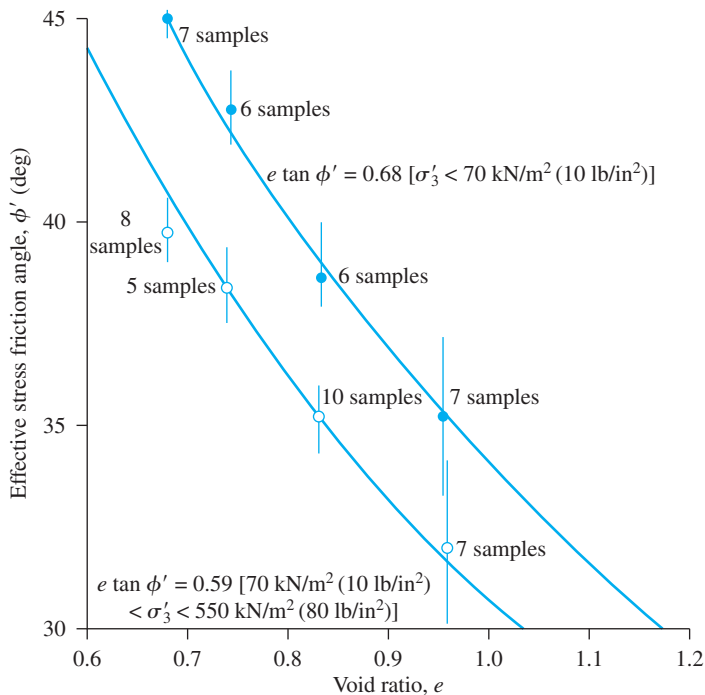


**Figure 1.29** Variation of friction angle  $\phi'$  with void ratio for Chattahoochee River sand (After Vesic, 1963) (From Vesic, A. B. Bearing Capacity of Deep Foundations in Sand. In Highway Research Record 39, Highway Research Board, National Research Council, Washington, D.C., 1963, Figure 11, p. 123. Reproduced with permission of the Transportation Research Board.)

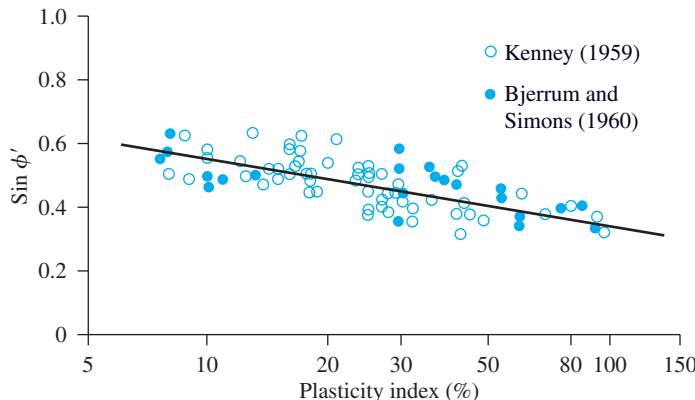


**Figure 1.30** Variation of  $\sin \phi'$  with plasticity index (PI) for several normally consolidated clays

The consolidated drained triaxial test was described in Section 1.17. Figure 1.31 shows a schematic diagram of a plot of  $\Delta\sigma$  versus axial strain in a drained triaxial test for a clay. At failure, for this test,  $\Delta\sigma = \Delta\sigma_f$ . However, at large axial strain (i.e., the ultimate strength condition), we have the following relationships:

Major principal stress:  $\sigma'_{1(\text{ult})} = \sigma_3 + \Delta\sigma_{\text{ult}}$

Minor principal stress:  $\sigma'_{3(\text{ult})} = \sigma_3$

At failure (i.e., peak strength), the relationship between  $\sigma'_1$  and  $\sigma'_3$  is given by Eq. (1.87). However, for ultimate strength, it can be shown that

$$\sigma'_{1(\text{ult})} = \sigma'_3 \tan^2 \left( 45 + \frac{\phi'_r}{2} \right) \quad (1.97)$$

where  $\phi'_r$  = residual effective stress friction angle.

Figure 1.32 shows the general nature of the failure envelopes at peak strength and ultimate strength (or *residual strength*). The residual shear strength of clays is important in the evaluation of the long-term stability of new and existing slopes and the design of remedial measures. The effective stress residual friction angles  $\phi'_r$  of clays may be substantially smaller than the effective stress peak friction angle  $\phi'$ . Past research has shown that the clay fraction (i.e., the percent finer than 2 microns) present in a given soil, CF, and

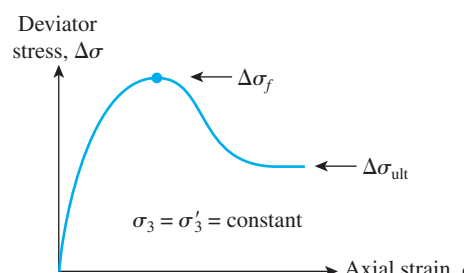


**Figure 1.31** Plot of deviator stress versus axial strain—drained triaxial test

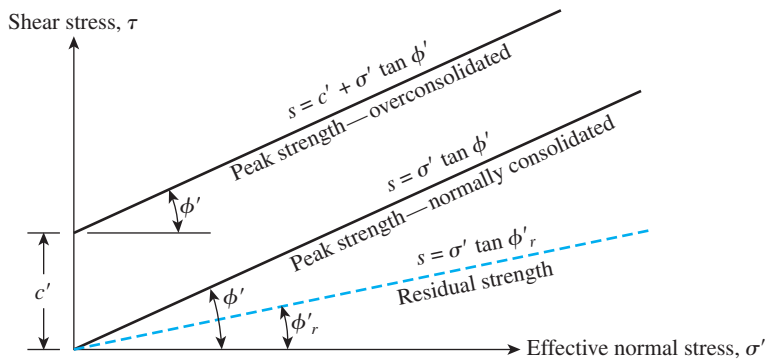


**Figure 1.32** Peak- and residual-strength envelopes for clay

the clay mineralogy are the two primary factors that control  $\phi'_r$ . The following is a summary of the effects of CF on  $\phi'_r$ .

1. If CF is less than about 15%, then  $\phi'_r$  is greater than about  $25^\circ$ .
2. For CF > about 50%,  $\phi'_r$  is entirely governed by the sliding of clay minerals and may be in the range of about  $10$  to  $15^\circ$ .
3. For kaolinite, illite, and montmorillonite,  $\phi'_r$  is about  $15^\circ$ ,  $10^\circ$ , and  $5^\circ$ , respectively.

Illustrating these facts, Figure 1.33 shows the variation of  $\phi'_r$  with CF for several soils (Skempton, 1985).

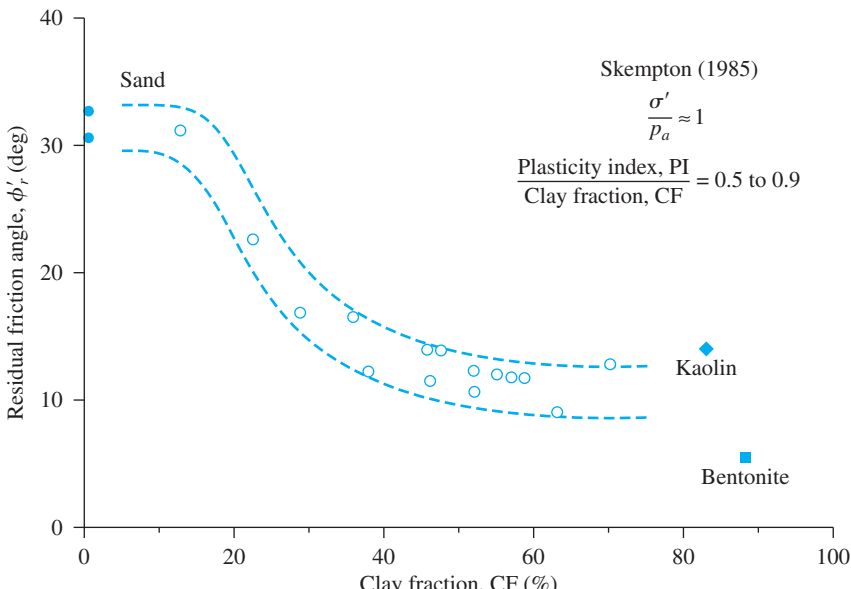


**Figure 1.33** Variation of  $\phi'_r$  with CF (Note:  $p_a$  = atmospheric pressure)

## 1.20 Correlations for Undrained Shear Strength, $C_u$

Several empirical relationships can be observed between  $c_u$  and the effective overburden pressure ( $\sigma'_0$ ) in the field. Some of these relationships are summarized in Table 1.13.

**Table 1.13** Empirical Equations Related to  $c_u$  and  $\sigma'_0$

Reference	Relationship	Remarks
Skempton (1957)	$\frac{c_{u(VST)}}{\sigma'_0} = 0.11 + 0.00037 \text{ (PI)}$ PI = plasticity index (%) $c_{u(VST)}$ = undrained shear strength from vane shear test	For normally consolidated clay
Chandler (1988)	$\frac{c_{u(VST)}}{\sigma'_c} = 0.11 + 0.0037 \text{ (PI)}$ $\sigma'_c$ = preconsolidation pressure	Can be used in overconsolidated soil; accuracy $\pm 25\%$ ; not valid for sensitive and fissured clays
Jamiolkowski, <i>et al.</i> (1985)	$\frac{c_u}{\sigma'_c} = 0.23 \pm 0.04$	For lightly overconsolidated clays
Mesri (1989)	$\frac{c_u}{\sigma'_0} = 0.22$	
Bjerrum and Simons (1960)	$\frac{c_u}{\sigma'_0} = 0.45 \left( \frac{\text{PI}\%}{100} \right)^{0.5}$ for PI > 50% $\frac{c_u}{\sigma'_0} = 0.118 (\text{LI})^{0.15}$ for LI = liquidity index > 0.5	Normally consolidated clay Normally consolidated clay
Ladd, <i>et al.</i> (1977)	$\frac{\left( \frac{c_u}{\sigma'_0} \right)_{\text{overconsolidated}}}{\left( \frac{c_u}{\sigma'_0} \right)_{\text{normally consolidated}}} = \text{OCR}^{0.8}$ OCR = overconsolidation ratio = $\sigma'_c/\sigma'_0$	

## 1.21 Sensitivity

For many naturally deposited clay soils, the unconfined compression strength is much less when the soils are tested after remolding without any change in the moisture content. This property of clay soil is called *sensitivity*. The degree of sensitivity is the ratio of the unconfined compression strength in an undisturbed state to that in a remolded state, or

$$S_t = \frac{q_{u(\text{undisturbed})}}{q_{u(\text{remolded})}} \quad (1.98)$$

The sensitivity ratio of most clays ranges from about 1 to 8; however, highly flocculent marine clay deposits may have sensitivity ratios ranging from about 10 to 80. Some clays turn to viscous liquids upon remolding, and these clays are referred to as “quick” clays. The loss of strength of clay soils from remolding is caused primarily by the destruction of the clay particle structure that was developed during the original process of sedimentation.

## Problems

- 1.1** A moist soil has a void ratio of 0.65. The moisture content of the soil is 14% and  $G_s = 2.7$ . Determine:
  - a. Porosity
  - b. Degree of saturation (%)
  - c. Dry unit weight ( $\text{kN}/\text{m}^3$ )
- 1.2** For the soil described in Problem 1.1:
  - a. What would be the saturated unit weight in  $\text{kN}/\text{m}^3$ ?
  - b. How much water, in  $\text{kN}/\text{m}^3$ , needs to be added to the soil for complete saturation?
  - c. What would be the moist unit weight in  $\text{kN}/\text{m}^3$  when the degree of saturation is 70%?
- 1.3** The moist unit weight of a soil is  $119.5 \text{ lb}/\text{ft}^3$ . For a moisture content of 12% and  $G_s = 2.65$ , calculate:
  - a. Void ratio
  - b. Porosity
  - c. Degree of saturation
  - d. Dry unit weight
- 1.4** A saturated soil specimen has  $w = 36\%$  and  $\gamma_d = 85.43 \text{ lb}/\text{ft}^3$ . Determine:
  - a. Void ratio
  - b. Porosity
  - c. Specific gravity of soil solids
  - d. Saturated unit weight (in  $\text{lb}/\text{ft}^3$ )
- 1.5** The laboratory test results of a sand are  $e_{\max} = 0.91$ ,  $e_{\min} = 0.48$ , and  $G_s = 2.67$ . What would be the dry and moist unit weights of this sand when compacted at a moisture content of 10% to a relative density of 65%?
- 1.6** The laboratory test results of six soils are given in the following table. Classify the soils by the AASHTO soil classification system and give the group indices.

Sieve Analysis—Percent Passing

Sieve No.	Soil A	Soil B	Soil C	Soil D	Soil E	Soil F
4	92	100	100	95	100	100
10	48	60	98	90	91	82
40	28	41	82	79	80	74
200	13	33	72	64	30	55
Liquid limit	31	38	56	35	43	35
Plastic limit	26	25	31	26	29	21

- 1.7** Classify the soils in Problem 1.6 using the Unified Soil Classification System. Give group symbols and group names.
- 1.8** The permeability of a sand was tested in the laboratory at a void ratio of 0.6 and was determined to be  $0.14 \text{ cm/sec}$ . Use Eq. (1.32) to estimate the hydraulic conductivity of this sand at a void ratio of 0.8.

- 1.9** A sand has the following:  $D_{10} = 0.08 \text{ mm}$ ;  $D_{60} = 0.37 \text{ mm}$ ; void ratio  $e = 0.6$ .
- Determine the hydraulic conductivity using Eq. (1.33).
  - Determine the hydraulic conductivity using Eq. (1.35).
- 1.10** The *in situ* hydraulic conductivity of a normally consolidated clay is  $5.4 \times 10^{-6} \text{ cm/sec}$  at a void ratio of 0.92. What would be its hydraulic conductivity at a void ratio of 0.72? Use Eq. (1.36) and  $n = 5.1$ .
- 1.11** Refer to the soil profile shown in Figure P1.11. Determine the total stress, pore water pressure, and effective stress at *A*, *B*, *C*, and *D*.
- 1.12** For a normally consolidated clay layer, the following are given:

Thickness = 3 m

Void ratio = 0.75

Liquid limit = 42

$G_s = 2.72$

Average effective stress on the clay layer =  $110 \text{ kN/m}^2$

How much consolidation settlement would the clay undergo if the average effective stress on the clay layer is increased to  $155 \text{ kN/m}^2$  as the result of the construction of a foundation? Use Eq. (1.51) to estimate the compression index.

- 1.13** Refer to Problem 1.12. Assume that the clay layer is preconsolidated,  $\sigma'_c = 130 \text{ kN/m}^2$ , and  $C_S = \frac{1}{5}C_c$ . Estimate the consolidation settlement.
- 1.14** A saturated clay deposit below the ground water table in the field has liquid limit = 61%, plastic limit = 21%, and moisture content = 38%. Estimate the preconsolidation pressure,  $\sigma'_c$  ( $\text{kN/m}^2$ ) using Eq. (1.46).
- 1.15** A normally consolidated clay layer in the field has a thickness of 3.2 m with an average effective stress of  $70 \text{ kN/m}^2$ . A laboratory consolidation test on the clay gave the following results.

Pressure ( $\text{kN/m}^2$ )	Void ratio
100	0.905
200	0.815

- a. Determine the compression index,  $C_c$ .
- b. If the average effective stress on the clay layer ( $\sigma'_o + \Delta\sigma$ ) is increased to  $115 \text{ kN/m}^2$ , what would be the total consolidation settlement?

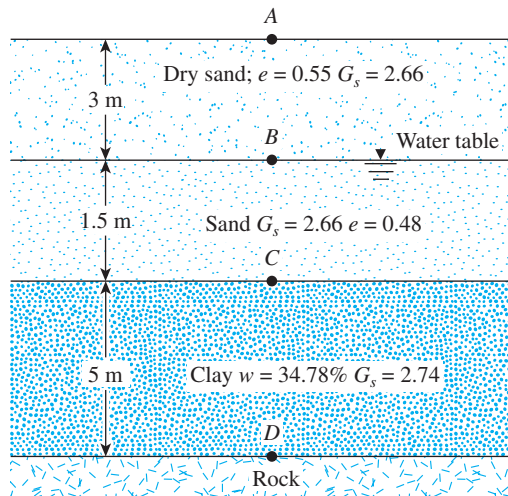


Figure P1.11

- 1.16** A clay soil specimen, 1 in. thick (drained on top and bottom), was tested in the laboratory. For a given load increment, the time for 50% consolidation was 5 min 20 sec. How long will it take for 50% consolidation of a similar clay layer in the field that is 8.2 ft thick and drained on one side only?
- 1.17** A clay soil specimen 1 in. thick (drained on top only) was tested in the laboratory. For a given load increment, the time for 60% consolidation was 6 min 20 sec. How long will it take for 50% consolidation for a similar clay layer in the field that is 10 ft thick and drained on both sides?
- 1.18** Refer to Figure P1.18. A total of 60-mm consolidation settlement is expected in the two clay layers due to a surcharge  $\Delta\sigma$ . Find the duration of surcharge application at which 30 mm of total settlement would take place.
- 1.19** The coefficient of consolidation of a clay for a given pressure range was obtained as  $8 \times 10^{-3} \text{ mm}^2/\text{sec}$  on the basis of one-dimensional consolidation test results. In the field, there is a 2-m thick layer of the same clay (Figure P1.19a). Based on the assumption that a uniform surcharge of  $70 \text{ kN/m}^2$  was to be applied instantaneously, the total consolidation settlement was estimated to be 150 mm.
- However, during construction, the loading was gradual; the resulting surcharge can be approximated as shown in Figure P1.19b. Estimate the settlement at  $t = 30$  days and  $t = 120$  days after the beginning of construction.
- 1.20** A direct shear test was conducted on a 2 in.  $\times$  2 in. specimen of dry sand had the following results.

Normal force (lb)	Shear force at failure (lb)
33	20.67
55.17	35.8
66.16	40.2

Draw a graph of shear stress at failure versus normal stress and determine the soil friction angle.

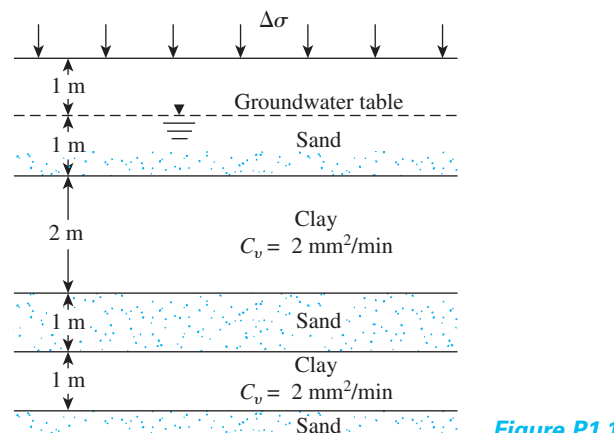


Figure P1.18

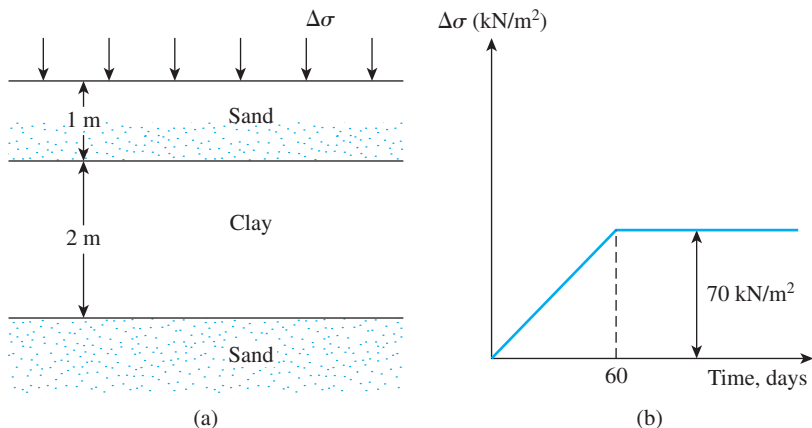


Figure P1.19

**1.21** For a sand, given:

$$D_{85} = 0.21 \text{ mm}$$

$$D_{50} = 0.13 \text{ mm}$$

$$D_{15} = 0.09 \text{ mm}$$

$$\text{Uniformity coefficient, } C_u = 2.1$$

$$\text{Void ratio, } e = 0.68$$

$$\text{Relative density} = 53\%$$

Estimate the soil friction angle using

a. Eq. (1.83)

b. Eq. (1.84)

**1.22** A consolidated-drained triaxial test on a normally consolidated clay yields the following results.

All around confining pressure,  $\sigma'_3 = 20 \text{ lb/in.}^2$

Added axial stress at failure,  $\Delta\sigma = 40 \text{ lb/in.}^2$

Determine the shear-strength parameters.

**1.23** The following are the results of two consolidated-drained triaxial tests on a clay.

Test I:  $\sigma'_3 = 82.8 \text{ kN/m}^2$ ;  $\sigma'_{1(\text{failure})} = 329.2 \text{ kN/m}^2$

Test II:  $\sigma'_3 = 165.6 \text{ kN/m}^2$ ;  $\sigma'_{1(\text{failure})} = 558.6 \text{ kN/m}^2$

Determine the shear-strength parameters—that is,  $c'$  and  $\phi'$ .

**1.24** A consolidated-undrained triaxial test was conducted on a saturated normally consolidated clay. The test results are

$$\sigma_3 = 13 \text{ lb/in.}^2$$

$$\sigma'_{1(\text{failure})} = 32 \text{ lb/in.}^2$$

Pore water pressure at failure =  $5.5 \text{ lb/in.}^2$

Determine  $c$ ,  $\phi$ ,  $c'$ , and  $\phi'$ .

**1.25** A normally consolidated clay soil has  $\phi = 20^\circ$  and  $\phi' = 28^\circ$ . If a consolidated-undrained test is conducted on this clay with an all around pressure of  $\sigma_3 = 21.5 \text{ lb/in.}^2$ , what would be the magnitude of the major principal stress,  $\sigma_1$ , and the pore water pressure,  $u$ , at failure?

## References

- AMER, A. M., and AWAD, A. A. (1974). "Permeability of Cohesionless Soils," *Journal of the Geotechnical Engineering Division*, American Society of Civil Engineers, Vol. 100, No. GT12, pp. 1309–1316.
- AMERICAN SOCIETY FOR TESTING AND MATERIALS (2009). *Annual Book of ASTM Standards*, Vol. 04.08, West Conshohocken, PA.
- BJERRUM, L., and SIMONS, N. E. (1960). "Comparison of Shear Strength Characteristics of Normally Consolidated Clay," *Proceedings, Research Conference on Shear Strength of Cohesive Soils*, ASCE, pp. 711–726.
- CARRIER III, W. D. (2003). "Goodbye, Hazen; Hello, Kozeny-Carman," *Journal of Geotechnical and Geoenvironmental Engineering*, ASCE, Vol. 129, No. 11, pp. 1054–1056.
- CASAGRANDE, A. (1936). "Determination of the Preconsolidation Load and Its Practical Significance," *Proceedings, First International Conference on Soil Mechanics and Foundation Engineering*, Cambridge, MA, Vol. 3, pp. 60–64.
- CHANDLER, R. J. (1988). "The *in situ* Measurement of the Undrained Shear Strength of Clays Using the Field Vane," *STP 1014, Vane Shear Strength Testing in Soils: Field and Laboratory Studies*, American Society for Testing and Materials, pp. 13–44.
- CHAPUIS, R. P. (2004). "Predicting the Saturated Hydraulic Conductivity of Sand and Gravel Using Effective Diameter and Void Ratio," *Canadian Geotechnical Journal*, Vol. 41, No. 5, pp. 787–795.
- DARCY, H. (1856). *Les Fontaines Publiques de la Ville de Dijon*, Paris.
- DAS, B. M. (2009). *Soil Mechanics Laboratory Manual*, 7th ed., Oxford University Press, New York.
- HANSBO, S. (1975). *Jordmateriallära*: 211, Stockholm, Awe/Gebers.
- HIGHWAY RESEARCH BOARD (1945). *Report of the Committee on Classification of Materials for Subgrades and Granular Type Roads*, Vol. 25, pp. 375–388.
- JAMILKOWSKI, M., LADD, C. C., GERMAINE, J. T., and LANCELOTTE, R. (1985). "New Developments in Field and Laboratory Testing of Soils," *Proceedings, XI International Conference on Soil Mechanics and Foundations Engineering*, San Francisco, Vol. 1, pp. 57–153.
- KENNEY, T. C. (1959). "Discussion," *Journal of the Soil Mechanics and Foundations Division*, American Society of Civil Engineers, Vol. 85, No. SM3, pp. 67–69.
- KULHAWY, F. H., and MAYNE, P. W. (1990). *Manual of Estimating Soil Properties for Foundation Design*, Electric Power Research Institute, Palo Alto, California.
- LADD, C. C., FOOTE, R., ISHIHARA, K., SCHLOSSER, F., and Poulos, H. G. (1977). "Stress Deformation and Strength Characteristics," *Proceedings, Ninth International Conference on Soil Mechanics and Foundation Engineering*, Tokyo, Vol. 2, pp. 421–494.
- MESRI, G. (1989). "A Re-evaluation of  $s_{u(\text{mob})} \approx 0.22\sigma_p$  Using Laboratory Shear Tests," *Canadian Geotechnical Journal*, Vol. 26, No. 1, pp. 162–164.
- MESRI, G., and OLSON, R. E. (1971). "Mechanism Controlling the Permeability of Clays," *Clay and Clay Minerals*, Vol. 19, pp. 151–158.
- NAGARAJ, T. S., and MURTHY, B. R. S. (1985). "Prediction of the Preconsolidation Pressure and Recompression Index of Soils," *Geotechnical Testing Journal*, American Society for Testing and Materials, Vol. 8, No. 4, pp. 199–202.
- OLSON, R. E. (1977). "Consolidation Under Time-Dependent Loading," *Journal of Geotechnical Engineering*, ASCE, Vol. 103, No. GT1, pp. 55–60.
- PARK, J. H., and KOUMOTO, T. (2004). "New Compression Index Equation," *Journal of Geotechnical and Geoenvironmental Engineering*, ASCE, Vol. 130, No. 2, pp. 223–226.
- RENDON-HERRERO, O. (1980). "Universal Compression Index Equation," *Journal of the Geotechnical Engineering Division*, American Society of Civil Engineers, Vol. 106, No. GT11, pp. 1178–1200.
- SAMARASINGHE, A. M., HUANG, Y. H., and DRNEVICH, V. P. (1982). "Permeability and Consolidation of Normally Consolidated Soils," *Journal of the Geotechnical Engineering Division*, ASCE, Vol. 108, No. GT6, pp. 835–850.

- SCHMERTMANN, J. H. (1953). "Undisturbed Consolidation Behavior of Clay," *Transactions, American Society of Civil Engineers*, Vol. 120, p. 1201.
- SIVARAM, B., and SWAMEE, A. (1977), "A Computational Method for Consolidation Coefficient," *Soils and Foundations*, Vol. 17, No. 2, pp. 48–52.
- SKEMPTON, A. W. (1944). "Notes on the Compressibility of Clays," *Quarterly Journal of Geological Society*, London, Vol. C, pp. 119–135.
- SKEMPTON, A. W. (1953). "The Colloidal Activity of Clays," *Proceedings, 3rd International Conference on Soil Mechanics and Foundation Engineering*, London, Vol. 1, pp. 57–61.
- SKEMPTON, A. W. (1957). "The Planning and Design of New Hong Kong Airport," *Proceedings, The Institute of Civil Engineers*, London, Vol. 7, pp. 305–307.
- SKEMPTON, A. W. (1985). "Residual Strength of Clays in Landslides, Folded Strata, and the Laboratory," *Geotechnique*, Vol. 35, No. 1, pp. 3–18.
- STAS, C. V., and KULHAWY, F. H. (1984). "Critical Evaluation of Design Methods for Foundations Under Axial Uplift and Compression Loading, REPORT EL-3771, Electric Power Research Institute, Palo Alto, California.
- TAVENAS, F., JEAN, P., LEBLOND, F. T. P., and LEROUEIL, S. (1983). "The Permeability of Natural Soft Clays. Part II: Permeability Characteristics," *Canadian Geotechnical Journal*, Vol. 20, No. 4, pp. 645–660.
- TAYLOR, D. W. (1948). *Fundamentals of Soil Mechanics*, Wiley, New York.
- TEFERRA, A. (1975). *Beziehungen zwischen Reibungswinkel, Lagerungsdichte und Sonderwiderständen nichtbindiger Böden mit verschiedener Kornverteilung*. Ph.D. Thesis, Technical University of Aachen Germany.
- TERZAGHI, K., and PECK, R. B. (1967). *Soil Mechanics in Engineering Practice*, Wiley, New York.
- THINH, K. D. (2001). "How Reliable is Your Angle of Internal Friction?" *Proceedings, XV International Conference on Soil Mechanics and Geotechnical Engineering*, Istanbul, Turkey, Vol. 1, pp. 73–76.
- VESIC, A. S. (1963). "Bearing Capacity of Deep Foundations in Sand," *Highway Research Record No. 39*, National Academy of Sciences, Washington, DC., pp. 112–154.
- WOOD, D. M. (1983). "Index Properties and Critical State Soil Mechanics," *Proceedings, Symposium on Recent Developments in Laboratory and Field Tests and Analysis of Geotechnical Problems*, Bangkok, p. 309.
- WROTH, C. P., and WOOD, D. M. (1978). "The Correlation of Index Properties with Some Basic Engineering Properties of Soils," *Canadian Geotechnical Journal*, Vol. 15, No. 2, pp. 137–145.

# Answers to Selected Problems

## Chapter 1

- 1.1**    a. 0.39  
          b. 58%  
          c. 16.05 kN/m<sup>3</sup>
- 1.3**    a. 0.55  
          b. 0.355  
          c. 57.8%  
          d. 106.7 lb/ft<sup>3</sup>
- 1.5**     $\gamma_d = 16.07 \text{ kN/m}^3$ ;  $\gamma = 17.68 \text{ kN/m}^3$
- 1.7**    Soil A: SM, silty sand  
          Soil B: SM, silty sand  
          Soil C: MH, elastic silt with sand  
          Soil D: ML, sandy silt  
          Soil E: SM, silty sand  
          Soil F: CL, sandy lean clay
- 1.9**    a. 0.01 cm/sec  
          b. 0.034 cm/sec

**1.11**

Point	kN/m <sup>2</sup>		
	$\sigma$	$u$	$\sigma'$
A	0	0	0
B	50.52	0	50.52
C	81.74	14.72	67.02
D	174.49	63.77	110.72

- 1.13** 25.56 mm
- 1.15** a. 0.299  
          b. 105.74 mm
- 1.17** 10.87 days
- 1.19**  $S_c = 7.5 \text{ mm } @ t = 30 \text{ days}$ ;  $S_c = 40.5 \text{ mm } @ t = 120 \text{ days}$
- 1.21** a. 30.7°  
          b. 33.67°

**1.23**  $\phi' = 28^\circ$

$c' = 30 \text{ kN/m}^2$

**1.25**  $\sigma_1 = 43.85 \text{ lb/in}^2$

$u = 8.87 \text{ lb/in}^2$

This page contains answers for this chapter only

# 2 Natural Soil Deposits and Subsoil Exploration

## 2.1 Introduction

To design a foundation that will support a structure, an engineer must understand the types of soil deposits that will support the foundation. Moreover, foundation engineers must remember that soil at any site frequently is nonhomogeneous; that is, the soil profile may vary. Soil mechanics theories involve idealized conditions, so the application of the theories to foundation engineering problems involves a judicious evaluation of site conditions and soil parameters. To do this requires some knowledge of the geological process by which the soil deposit at the site was formed, supplemented by subsurface exploration. Good professional judgment constitutes an essential part of geotechnical engineering—and it comes only with practice.

This chapter is divided into two parts. The first is a general overview of natural soil deposits generally encountered, and the second describes the general principles of subsoil exploration.

---

## Natural Soil Deposits

### 2.2 Soil Origin

Most of the soils that cover the earth are formed by the weathering of various rocks. There are two general types of weathering: (1) mechanical weathering and (2) chemical weathering.

*Mechanical weathering* is a process by which rocks are broken down into smaller and smaller pieces by physical forces without any change in the chemical composition. Changes in temperature result in *expansion and contraction of rock* due to gain and loss of heat. Continuous expansion and contraction will result in the development of cracks in rocks. Flakes and large fragments of rocks are split. *Frost action* is another source of mechanical weathering of rocks. Water can enter the pores, cracks, and other openings in the rock. When the temperature drops, the water freezes, thereby increasing the volume by about 9%. This results in an outward pressure from inside the rock. Continuous freezing and thawing will result in the breakup of a rock mass. *Exfoliation* is another mechanical

weathering process by which rock plates are peeled off from large rocks by physical forces. Mechanical weathering of rocks also takes place due to the action of *running water, glaciers, wind, ocean waves*, and so forth.

*Chemical weathering* is a process of decomposition or mineral alteration in which the original minerals are changed into something entirely different. For example, the common minerals in igneous rocks are quartz, feldspars, and ferromagnesian minerals. The decomposed products of these minerals due to chemical weathering are listed in Table 2.1.

**Table 2.1** Some Decomposed Products of Minerals in Igneous Rock

Mineral	Decomposed Product
Quartz	Quartz (sand grains)
Potassium feldspar ( $KAlSi_3O_8$ ) and Sodium feldspar ( $NaAlSi_3O_8$ )	Kaolinite (clay) Bauxite Illite (clay) Silica
Calcium feldspar ( $CaAl_2Si_2O_8$ )	Silica Calcite
Biotite	Clay Limonite Hematite Silica Calcite
Olivine ( $Mg, Fe)_2SiO_4$	Limonite Serpentine Hematite Silica

Most rock weathering is a combination of mechanical and chemical weathering. Soil produced by the weathering of rocks can be transported by physical processes to other places. The resulting soil deposits are called *transported soils*. In contrast, some soils stay where they were formed and cover the rock surface from which they derive. These soils are referred to as *residual soils*.

Transported soils can be subdivided into five major categories based on the *transporting agent*:

1. *Gravity transported soil*
2. *Lacustrine (lake) deposits*
3. *Alluvial or fluvial soil deposited by running water*
4. *Glacial deposited by glaciers*
5. *Aeolian deposited by the wind*

In addition to transported and residual soils, there are *peats* and *organic soils*, which derive from the decomposition of organic materials.

## 2.3 Residual Soil

Residual soils are found in areas where the rate of weathering is more than the rate at which the weathered materials are carried away by transporting agents. The rate of weathering is higher in warm and humid regions compared to cooler and drier regions and, depending on the climatic conditions, the effect of weathering may vary widely.

Residual soil deposits are common in the tropics, on islands such as the Hawaiian Islands, and in the southeastern United States. The nature of a residual soil deposit will generally depend on the parent rock. When hard rocks such as granite and gneiss undergo weathering, most of the materials are likely to remain in place. These soil deposits generally have a top layer of clayey or silty clay material, below which are silty or sandy soil layers. These layers in turn are generally underlain by a partially weathered rock and then sound bedrock. The depth of the sound bedrock may vary widely, even within a distance of a few meters. Figure 2.1 shows the boring log of a residual soil deposit derived from the weathering of granite.

In contrast to hard rocks, there are some chemical rocks, such as limestone, that are chiefly made up of calcite ( $\text{CaCO}_3$ ) mineral. Chalk and dolomite have large concentrations of dolomite minerals [ $\text{Ca Mg}(\text{CO}_3)_2$ ]. These rocks have large amounts of soluble materials,

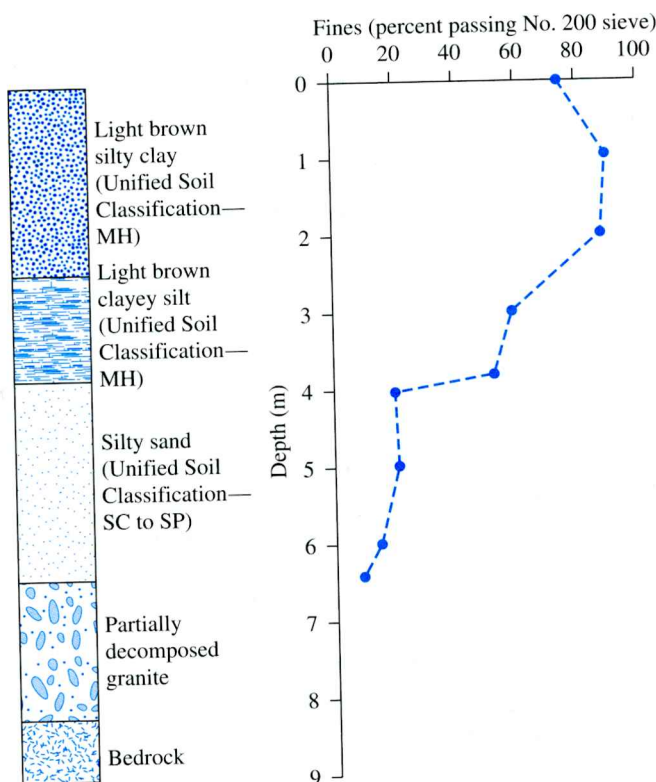


**Figure 2.1** Boring log for a residual soil derived from granite

some of which are removed by groundwater, leaving behind the insoluble fraction of the rock. Residual soils that derive from chemical rocks do not possess a gradual transition zone to the bedrock, as seen in Figure 2.1. The residual soils derived from the weathering of limestone-like rocks are mostly red in color. Although uniform in kind, the depth of weathering may vary greatly. The residual soils immediately above the bedrock may be normally consolidated. Large foundations with heavy loads may be susceptible to large consolidation settlements on these soils.

## 2.4

## Gravity Transported Soil

Residual soils on a natural slope can move downwards. Cruden and Varnes (1996) proposed a velocity scale for soil movement on a slope, which is summarized in Table 2.2. When residual soils move down a natural slope very slowly, the process is usually referred to as *creep*. When the downward movement of soil is sudden and rapid, it is called a *landslide*. The deposits formed by down-slope creep and landslides are *colluvium*.

**Table 2.2** Velocity Scale for Soil Movement on a Slope

Description	Velocity (mm/sec)
Very slow	$5 \times 10^{-5}$ to $5 \times 10^{-7}$
Slow	$5 \times 10^{-3}$ to $5 \times 10^{-5}$
Moderate	$5 \times 10^{-1}$ to $5 \times 10^{-3}$
Rapid	$5 \times 10^1$ to $5 \times 10^{-1}$

Colluvium is a heterogeneous mixture of soils and rock fragments ranging from clay-sized particles to rocks having diameters of one meter or more. *Mudflows* are one type of gravity-transported soil. Flows are downward movements of earth that resemble a viscous fluid (Figure 2.2) and come to rest in a more dense condition. The soil deposits derived from past mudflows are highly heterogeneous in composition.

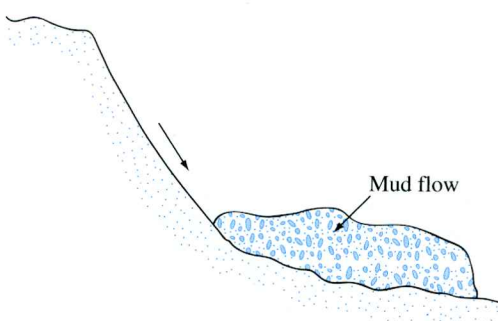


**Figure 2.2** Mudflow

## 2.5 Alluvial Deposits

Alluvial soil deposits derive from the action of streams and rivers and can be divided into two major categories: (1) *braided-stream deposits* and (2) deposits caused by the *meandering belt of streams*.

### Deposits from Braided Streams

Braided streams are high-gradient, rapidly flowing streams that are highly erosive and carry large amounts of sediment. Because of the high bed load, a minor change in the velocity of flow will cause sediments to deposit. By this process, these streams may build up a complex tangle of converging and diverging channels separated by sandbars and islands.

The deposits formed from braided streams are highly irregular in stratification and have a wide range of grain sizes. Figure 2.3 shows a cross section of such a deposit. These deposits share several characteristics:

1. The grain sizes usually range from gravel to silt. Clay-sized particles are generally *not* found in deposits from braided streams.
2. Although grain size varies widely, the soil in a given pocket or lens is rather uniform.
3. At any given depth, the void ratio and unit weight may vary over a wide range within a lateral distance of only a few meters. This variation can be observed during soil exploration for the construction of a foundation for a structure. The standard penetration resistance at a given depth obtained from various boreholes will be highly irregular and variable.

Alluvial deposits are present in several parts of the western United States, such as Southern California, Utah, and the basin and range sections of Nevada. Also, a large amount of sediment originally derived from the Rocky Mountain range was carried eastward to form the alluvial deposits of the Great Plains. On a smaller scale, this type of natural soil deposit, left by braided streams, can be encountered locally.

### Meander Belt Deposits

The term *meander* is derived from the Greek word *maiandros*, after the Maiandros (now Menderes) River in Asia, famous for its winding course. Mature streams in a valley curve back and forth. The valley floor in which a river meanders is referred to as the *meander*

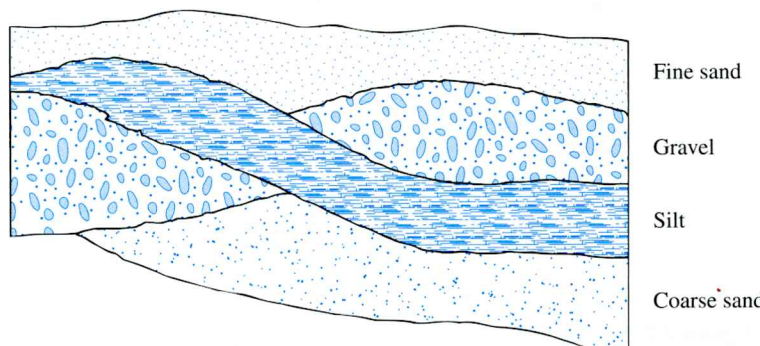


**Figure 2.3** Cross section of a braided-stream deposit

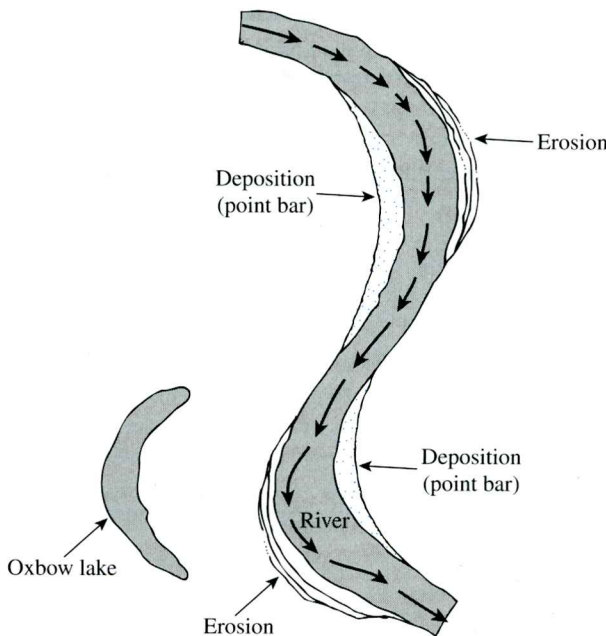


**Figure 2.4** Formation of point bar deposits and oxbow lake in a meandering stream

*belt.* In a meandering river, the soil from the bank is continually eroded from the points where it is concave in shape and is deposited at points where the bank is convex in shape, as shown in Figure 2.4. These deposits are called *point bar deposits*, and they usually consist of sand and silt-size particles. Sometimes, during the process of erosion and deposition, the river abandons a meander and cuts a shorter path. The abandoned meander, when filled with water, is called an *oxbow lake*. (See Figure 2.4.)

During floods, rivers overflow low-lying areas. The sand and silt-size particles carried by the river are deposited along the banks to form ridges known as *natural levees* (Figure 2.5).

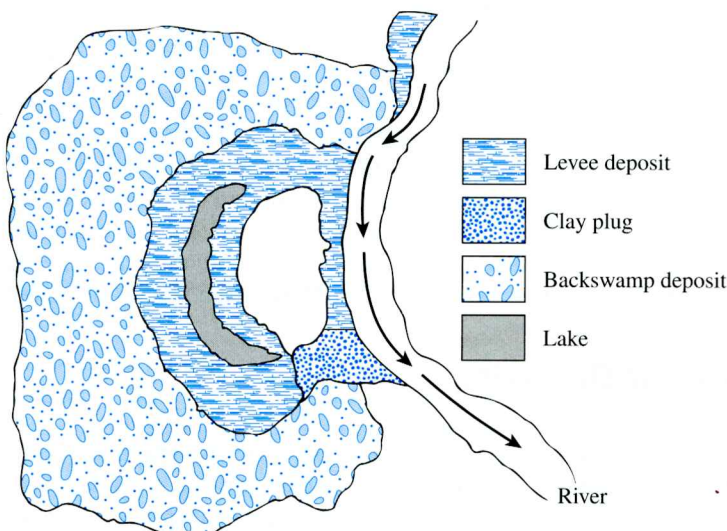


**Figure 2.5** Levee and backswamp deposit

**Table 2.3** Properties of Deposits within the Mississippi Alluvial Valley

Environment	Soil texture	Natural water content (%)	Liquid limit	Plasticity index
Natural levee	Clay (CL)	25–35	35–45	15–25
	Silt (ML)	15–35	NP–35	NP–5
Point bar	Silt (ML) and silty sand (SM)	25–45	30–55	10–25
Abandoned channel	Clay (CL, CH)	30–95	30–100	10–65
Backswamps	Clay (CH)	25–70	40–115	25–100
Swamp	Organic clay (OH)	100–265	135–300	100–165

(Note: NP—Nonplastic)

Finer soil particles consisting of silts and clays are carried by the water farther onto the flood-plains. These particles settle at different rates to form what is referred to as *backswamp deposits* (Figure 2.5), often highly plastic clays.

Table 2.3 gives some properties of soil deposits found in natural levees, point bars, abandoned channels, backswamps and swamps within the alluvial Mississippi Valley (Kolb and Shockley, 1959).

## 2.6

## Lacustrine Deposits

Water from rivers and springs flows into lakes. In arid regions, streams carry large amounts of suspended solids. Where the stream enters the lake, granular particles are deposited in the area forming a delta. Some coarser particles and the finer particles (that is, silt and clay) that are carried into the lake are deposited onto the lake bottom in alternate layers of coarse-grained and fine-grained particles. The deltas formed in humid regions usually have finer grained soil deposits compared to those in arid regions.

*Varved clays* are alternate layers of silt and silty clay with layer thicknesses rarely exceeding about 13 mm. ( $\frac{1}{2}$  in.). The silt and silty clay that constitute the layers were carried into fresh water lakes by melt water at the end of the Ice Age. The hydraulic conductivity (Section 1.10) of varved clays exhibits a high degree of anisotropy.

## 2.7

## Glacial Deposits

During the Pleistocene Ice Age, glaciers covered large areas of the earth. The glaciers advanced and retreated with time. During their advance, the glaciers carried large amounts of sand, silt, clay, gravel, and boulders. *Drift* is a general term usually applied to the deposits laid down by glaciers. The drifts can be broadly divided into two major categories: (a) unstratified drifts and (b) stratified drifts. A brief description of each category follows.

### Unstratified Drifts

The *unstratified drifts* laid down by melting glaciers are referred to as *till*. The physical characteristics of till may vary from glacier to glacier. Till is called *clay till* because of the presence of the large amount of clay-sized particles in it. In some areas, tills constitute large amounts of boulders, and they are referred to as *boulder till*. The range of grain sizes in a given till varies greatly. The amount of clay-sized fractions present and the plasticity indices of tills also vary widely. During the field exploration program, erratic values of standard penetration resistance (Section 2.13) also may be expected.

The land forms that developed from the till deposits are called *moraines*. A *terminal moraine* (Figure 2.6) is a ridge of till that marks the maximum limit of a glacier's advance. *Recreational moraines* are ridges of till developed behind the terminal moraine at varying distances apart. They are the result of temporary stabilization of the glacier during the recessional period. The till deposited by the glacier between the moraines is referred to as *ground moraine* (Figure 2.6). Ground moraines constitute large areas of the central United States and are called *till plains*.

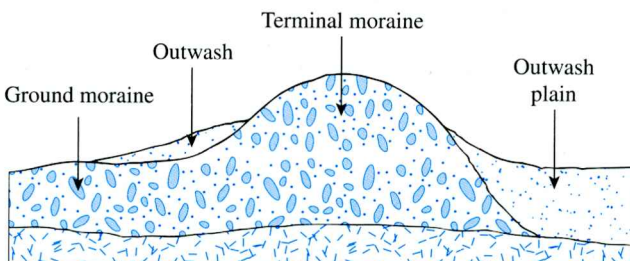


**Figure 2.6** Terminal moraine, ground moraine, and outwash plain

### Stratified Drifts

The sand, silt, and gravel that are carried by the melting water from the front of a glacier are called *outwash*. The melted water sorts out the particles by the grain size and forms stratified deposits. In a pattern similar to that of braided-stream deposits, the melted water also deposits the outwash, forming *outwash plains* (Figure 2.6), also called *glaciofluvial deposits*.

## 2.8

### Aeolian Soil Deposits

Wind is also a major transporting agent leading to the formation of soil deposits. When large areas of sand lie exposed, wind can blow the sand away and redeposit it elsewhere. Deposits of windblown sand generally take the shape of *dunes* (Figure 2.7). As dunes are formed, the sand is blown over the crest by the wind. Beyond the crest, the sand particles roll down the slope. The process tends to form a *compact sand deposit* on the *windward side*, and a rather *loose deposit* on the *leeward side*, of the dune.

Dunes exist along the southern and eastern shores of Lake Michigan, the Atlantic Coast, the southern coast of California, and at various places along the coasts of Oregon and

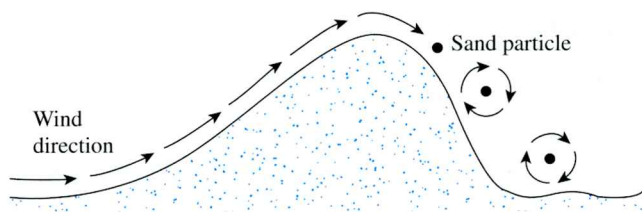


Figure 2.7 Sand dune

Washington. Sand dunes can also be found in the alluvial and rocky plains of the western United States. Following are some of the typical properties of *dune sand*:

1. The grain-size distribution of the sand at any particular location is surprisingly uniform. This uniformity can be attributed to the sorting action of the wind.
2. The general grain size decreases with distance from the source, because the wind carries the small particles farther than the large ones.
3. The relative density of sand deposited on the windward side of dunes may be as high as 50 to 65%, decreasing to about 0 to 15% on the leeward side.

Figure 2.8 shows a sand dune from the Thar Desert, which is a large arid region located in the northwestern part of India which covers an area of about 200,000 square kilometers.

*Loess* is an aeolian deposit consisting of silt and silt-sized particles. The grain-size distribution of loess is rather uniform. The cohesion of loess is generally derived from a clay coating over the silt-sized particles, which contributes to a stable soil structure in



Figure 2.8 A sand dune from the Thar Desert, India (Courtesy of A. S. Wayal, K. J. Somaia Polytechnic, Mumbai, India)

an unsaturated state. The cohesion may also be the result of the precipitation of chemicals leached by rainwater. Loess is a *collapsing soil*, because when the soil becomes saturated, it loses its binding strength between particles. Special precautions need to be taken for the construction of foundations over loessial deposits. There are extensive deposits of loess in the United States, mostly in the midwestern states of Iowa, Missouri, Illinois, and Nebraska and for some distance along the Mississippi River in Tennessee and Mississippi.

Volcanic ash (with grain sizes between 0.25 to 4 mm) and volcanic dust (with grain sizes less than 0.25 mm) may be classified as wind-transported soil. Volcanic ash is a lightweight sand or sandy gravel. Decomposition of volcanic ash results in highly plastic and compressible clays.

## 2.9

### Organic Soil

Organic soils are usually found in low-lying areas where the water table is near or above the ground surface. The presence of a high water table helps in the growth of aquatic plants that, when decomposed, form organic soil. This type of soil deposit is usually encountered in coastal areas and in glaciated regions. Organic soils show the following characteristics:

1. Their natural moisture content may range from 200 to 300%.
2. They are highly compressible.
3. Laboratory tests have shown that, under loads, a large amount of settlement is derived from secondary consolidation.

## 2.10

### Some Local Terms for Soils

Soils are sometimes referred to by local terms. The following are a few of these terms with a brief description of each.

1. *Caliche*: a Spanish word derived from the Latin word *calix*, meaning *lime*. It is mostly found in the desert southwest of the United States. It is a mixture of sand, silt, and gravel bonded together by *calcareous deposits*. The calcareous deposits are brought to the surface by a net upward migration of water. The water evaporates in the high local temperature. Because of the sparse rainfall, the carbonates are not washed out of the top layer of soil.
2. *Gumbo*: a highly plastic, clayey soil.
3. *Adobe*: a highly plastic, clayey soil found in the southwestern United States.
4. *Terra Rossa*: residual soil deposits that are red in color and derive from limestone and dolomite.
5. *Muck*: organic soil with a very high moisture content.
6. *Muskeg*: organic soil deposit.
7. *Saprolite*: residual soil deposit derived from mostly insoluble rock.
8. *Loam*: a mixture of soil grains of various sizes, such as sand, silt, and clay.
9. *Laterite*: characterized by the accumulation of iron oxide ( $\text{Fe}_2\text{O}_3$ ) and aluminum oxide ( $\text{Al}_2\text{O}_3$ ) near the surface, and the leaching of silica. Lateritic soils in Central America contain about 80 to 90% of clay and silt-size particles. In the United States, lateritic soils can be found in the southeastern states, such as Alabama, Georgia, and the Carolinas.

## Subsurface Exploration

### 2.11 Purpose of Subsurface Exploration

The process of identifying the layers of deposits that underlie a proposed structure and their physical characteristics is generally referred to as *subsurface exploration*. The purpose of subsurface exploration is to obtain information that will aid the geotechnical engineer in

1. Selecting the type and depth of foundation suitable for a given structure.
2. Evaluating the load-bearing capacity of the foundation.
3. Estimating the probable settlement of a structure.
4. Determining potential foundation problems (e.g., expansive soil, collapsible soil, sanitary landfill, and so on).
5. Determining the location of the water table.
6. Predicting the lateral earth pressure for structures such as retaining walls, sheet pile bulkheads, and braced cuts.
7. Establishing construction methods for changing subsoil conditions.

Subsurface exploration may also be necessary when additions and alterations to existing structures are contemplated.

### 2.12 Subsurface Exploration Program

Subsurface exploration comprises several steps, including the collection of preliminary information, reconnaissance, and site investigation.

#### Collection of Preliminary Information

This step involves obtaining information regarding the type of structure to be built and its general use. For the construction of buildings, the approximate column loads and their spacing and the local building-code and basement requirements should be known. The construction of bridges requires determining the lengths of their spans and the loading on piers and abutments.

A general idea of the topography and the type of soil to be encountered near and around the proposed site can be obtained from the following sources:

1. United States Geological Survey maps.
2. State government geological survey maps.
3. United States Department of Agriculture's Soil Conservation Service county soil reports.
4. Agronomy maps published by the agriculture departments of various states.
5. Hydrological information published by the United States Corps of Engineers, including records of stream flow, information on high flood levels, tidal records, and so on.
6. Highway department soil manuals published by several states.

The information collected from these sources can be extremely helpful in planning a site investigation. In some cases, substantial savings may be realized by anticipating problems that may be encountered later in the exploration program.

### **Reconnaissance**

The engineer should always make a visual inspection of the site to obtain information about

1. The general topography of the site, the possible existence of drainage ditches, abandoned dumps of debris, and other materials present at the site. Also, evidence of creep of slopes and deep, wide shrinkage cracks at regularly spaced intervals may be indicative of expansive soils.
2. Soil stratification from deep cuts, such as those made for the construction of nearby highways and railroads.
3. The type of vegetation at the site, which may indicate the nature of the soil. For example, a mesquite cover in central Texas may indicate the existence of expansive clays that can cause foundation problems.
4. High-water marks on nearby buildings and bridge abutments.
5. Groundwater levels, which can be determined by checking nearby wells.
6. The types of construction nearby and the existence of any cracks in walls or other problems.

The nature of the stratification and physical properties of the soil nearby also can be obtained from any available soil-exploration reports on existing structures.

### **Site Investigation**

The site investigation phase of the exploration program consists of planning, making test boreholes, and collecting soil samples at desired intervals for subsequent observation and laboratory tests. The approximate required minimum depth of the borings should be predetermined. The depth can be changed during the drilling operation, depending on the subsoil encountered. To determine the approximate minimum depth of boring, engineers may use the rules established by the American Society of Civil Engineers (1972):

1. Determine the net increase in the effective stress,  $\Delta\sigma'$ , under a foundation with depth as shown in Figure 2.9. (The general equations for estimating increases in stress are given in Chapter 5.)
2. Estimate the variation of the vertical effective stress,  $\sigma'_o$ , with depth.

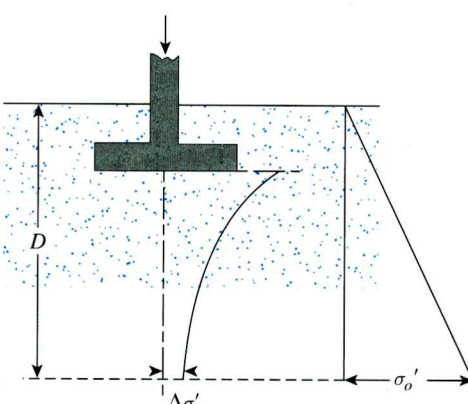


**Figure 2.9** Determination of the minimum depth of boring

3. Determine the depth,  $D = D_1$ , at which the effective stress increase  $\Delta\sigma'$  is equal to  $(\frac{1}{10})q$  ( $q$  = estimated net stress on the foundation).
4. Determine the depth,  $D = D_2$ , at which  $\Delta\sigma'/\sigma'_o = 0.05$ .
5. Choose the smaller of the two depths,  $D_1$  and  $D_2$ , just determined as the approximate minimum depth of boring required, unless bedrock is encountered.

If the preceding rules are used, the depths of boring for a building with a width of 30 m (100 ft) will be approximately the following, according to Sowers and Sowers (1970):

No. of stories	Boring depth
1	3.5 m (11 ft)
2	6 m (20 ft)
3	10 m (33 ft)
4	16 m (53 ft)
5	24 m (79 ft)

To determine the boring depth for hospitals and office buildings, Sowers and Sowers (1970) also used the following rules.

- For light steel or narrow concrete buildings,

$$\frac{D_b}{S^{0.7}} = a \quad (2.1)$$

where

$D_b$  = depth of boring

$S$  = number of stories

$$a = \begin{cases} \approx 3 & \text{if } D_b \text{ is in meters} \\ \approx 10 & \text{if } D_b \text{ is in feet} \end{cases}$$

- For heavy steel or wide concrete buildings,

$$\frac{D_b}{S^{0.7}} = b \quad (2.2)$$

where

$$b = \begin{cases} \approx 6 & \text{if } D_b \text{ is in meters} \\ \approx 20 & \text{if } D_b \text{ is in feet} \end{cases}$$

When deep excavations are anticipated, the depth of boring should be at least 1.5 times the depth of excavation.

Sometimes, subsoil conditions require that the foundation load be transmitted to bedrock. The minimum depth of core boring into the bedrock is about 3 m (10 ft). If the bedrock is irregular or weathered, the core borings may have to be deeper.

There are no hard-and-fast rules for borehole spacing. Table 2.4 gives some general guidelines. Spacing can be increased or decreased, depending on the condition of the subsoil. If various soil strata are more or less uniform and predictable, fewer boreholes are needed than in nonhomogeneous soil strata.

**Table 2.4** Approximate Spacing of Boreholes

Type of project	Spacing	
	(m)	(ft)
Multistory building	10–30	30–100
One-story industrial plants	20–60	60–200
Highways	250–500	800–1600
Residential subdivision	250–500	800–1600
Dams and dikes	40–80	130–260

The engineer should also take into account the ultimate cost of the structure when making decisions regarding the extent of field exploration. The exploration cost generally should be 0.1 to 0.5% of the cost of the structure. Soil borings can be made by several methods, including auger boring, wash boring, percussion drilling, and rotary drilling.

## 2.13

### Exploratory Borings in the Field

*Auger boring* is the simplest method of making exploratory boreholes. Figure 2.10 shows two types of hand auger: the *posthole auger* and the *helical auger*. Hand augers cannot be used for advancing holes to depths exceeding 3 to 5 m (10 to 16 ft). However, they can be used for soil exploration work on some highways and small structures. *Portable power-driven helical augers* (76 mm to 305 mm in diameter) are available for making deeper boreholes. The soil samples obtained from such borings are highly disturbed. In some non-cohesive soils or soils having low cohesion, the walls of the boreholes will not stand unsupported. In such circumstances, a metal pipe is used as a *casing* to prevent the soil from caving in.

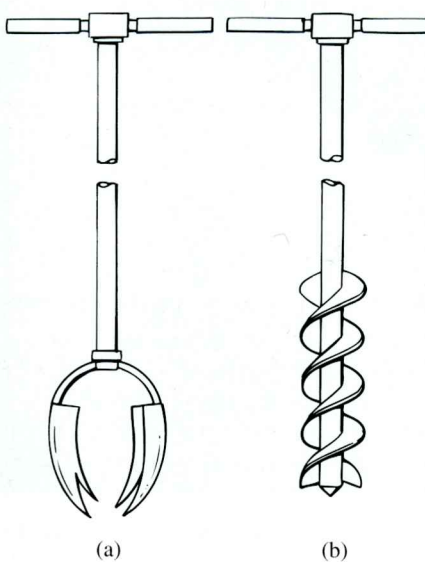


**Figure 2.10** Hand tools: (a) posthole auger; (b) helical auger

When power is available, *continuous-flight augers* are probably the most common method used for advancing a borehole. The power for drilling is delivered by truck- or tractor-mounted drilling rigs. Boreholes up to about 60 to 70 m (200 to 230 ft) can easily be made by this method. Continuous-flight augers are available in sections of about 1 to 2 m (3 to 6 ft) with either a solid or hollow stem. Some of the commonly used solid-stem augers have outside diameters of 66.68 mm ( $2\frac{5}{8}$  in.), 82.55 mm ( $3\frac{1}{4}$  in.), 101.6 mm (4 in.), and 114.3 mm ( $4\frac{1}{2}$  in.). Common commercially available hollow-stem augers have dimensions of 63.5 mm ID and 158.75 mm OD (2.5 in.  $\times$  6.25 in.), 69.85 mm ID and 177.8 OD (2.75 in.  $\times$  7 in.), 76.2 mm ID and 203.2 OD (3 in.  $\times$  8 in.), and 82.55 mm ID and 228.6 mm OD (3.25 in.  $\times$  9 in.).

The tip of the auger is attached to a cutter head (Figure 2.11). During the drilling operation (Figure 2.12), section after section of auger can be added and the hole extended downward. The flights of the augers bring the loose soil from the bottom of the hole to the surface. The driller can detect changes in the type of soil by noting changes in the speed and sound of drilling. When solid-stem augers are used, the auger must be withdrawn at regular intervals to obtain soil samples and also to conduct other operations such as standard penetration tests. Hollow-stem augers have a distinct advantage over solid-stem augers in that they do not have to be removed frequently for sampling

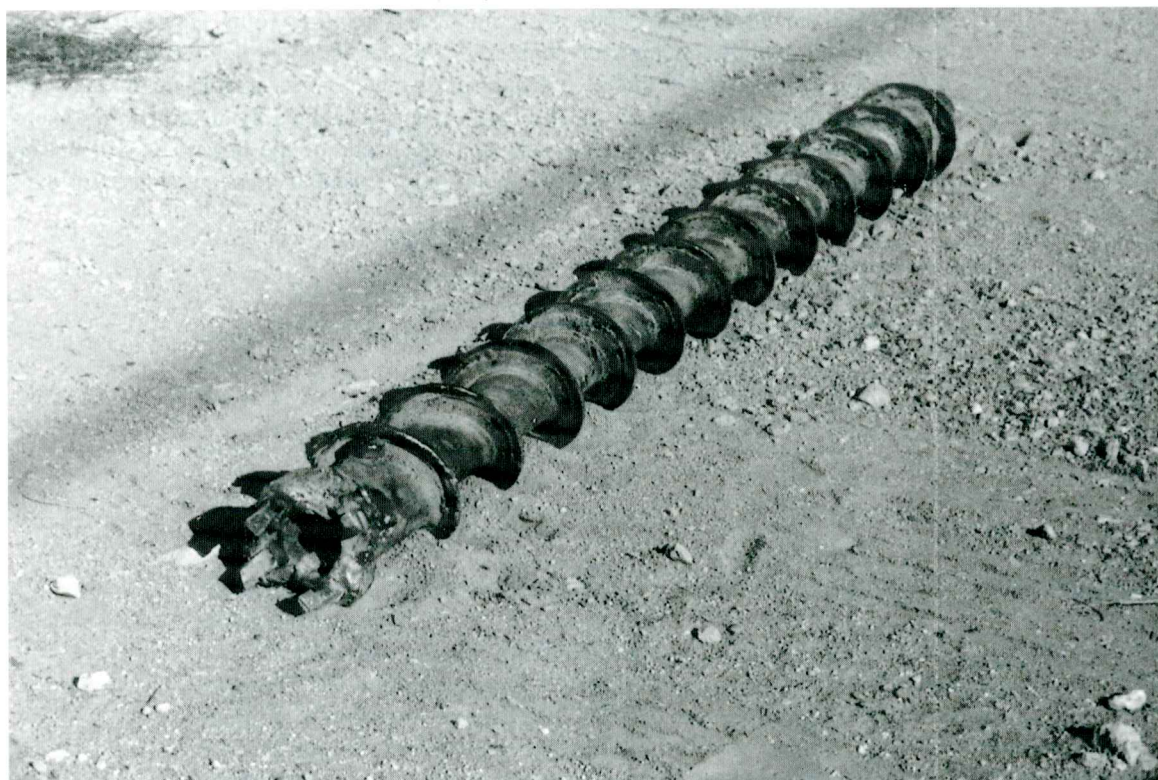


**Figure 2.11** Carbide-tipped cutting head on auger flight (Courtesy of Braja M. Das, Henderson, NV)

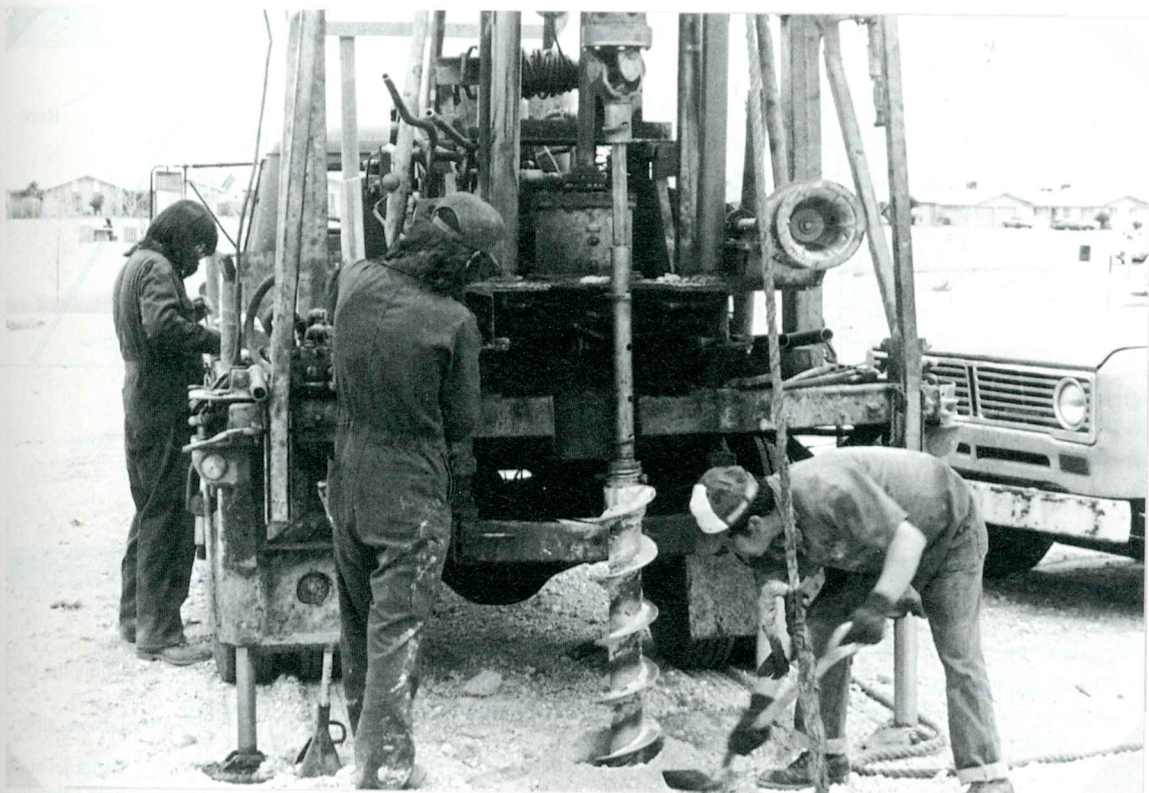


**Figure 2.12** Drilling with continuous-flight augers (Danny R. Anderson, PE of Professional Service Industries, Inc., El Paso, Texas.)

or other tests. As shown schematically in Figure 2.13, the outside of the hollow-stem auger acts as a casing.

The hollow-stem auger system includes the following components:

*Outer component:* (a) hollow auger sections, (b) hollow auger cap, and  
(c) drive cap

*Inner component:* (a) pilot assembly, (b) center rod column, and  
(c) rod-to-cap adapter

The auger head contains replaceable carbide teeth. During drilling, if soil samples are to be collected at a certain depth, the pilot assembly and the center rod are removed. The soil sampler is then inserted through the hollow stem of the auger column.

*Wash boring* is another method of advancing boreholes. In this method, a casing about 2 to 3 m (6 to 10 ft) long is driven into the ground. The soil inside the casing is then removed by means of a chopping bit attached to a drilling rod. Water is forced through the drilling rod and exits at a very high velocity through the holes at the bottom of the chopping bit (Figure 2.14). The water and the chopped soil particles rise in the drill hole and overflow at the top of the casing through a T connection. The washwater

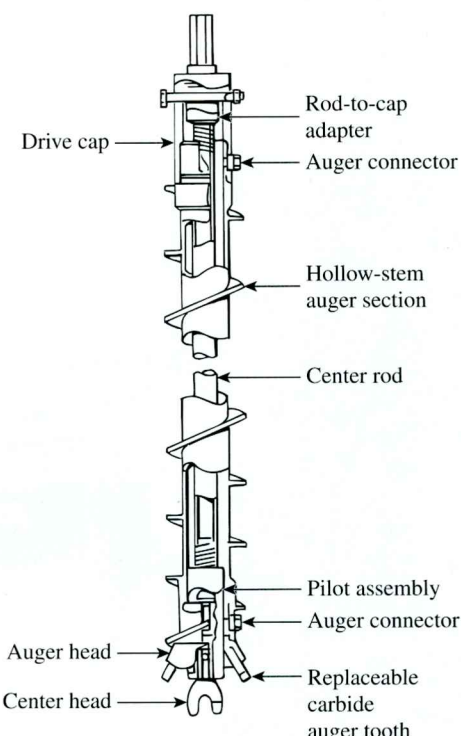


**Figure 2.13** Hollow-stem auger components  
 (After ASTM, 2001) (ASTM D4700-91: Standard Guide for Soil Sampling from the Vadose Zone. Copyright ASTM INTERNATIONAL. Reprinted with permission.)

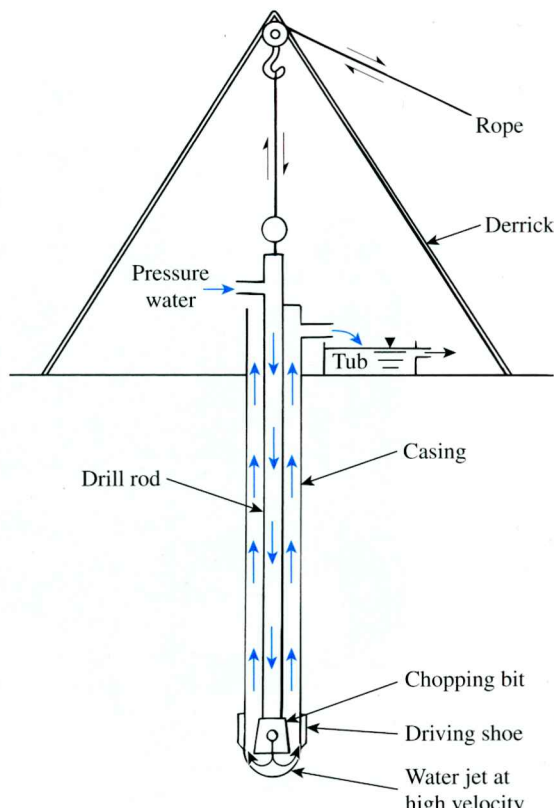


**Figure 2.14** Wash boring

is collected in a container. The casing can be extended with additional pieces as the borehole progresses; however, that is not required if the borehole will stay open and not cave in. Wash borings are rarely used now in the United States and other developed countries.

*Rotary drilling* is a procedure by which rapidly rotating drilling bits attached to the bottom of drilling rods cut and grind the soil and advance the borehole. There are several types of drilling bit. Rotary drilling can be used in sand, clay, and rocks (unless they are badly fissured). Water or *drilling mud* is forced down the drilling rods to the bits, and the return flow forces the cuttings to the surface. Boreholes with diameters of 50 to 203 mm (2 to 8 in.) can easily be made by this technique. The drilling mud is a slurry of water and bentonite. Generally, it is used when the soil that is encountered is likely to cave in. When soil samples are needed, the drilling rod is raised and the drilling bit is replaced by a sampler. With the environmental drilling applications, rotary drilling with air is becoming more common.

*Percussion drilling* is an alternative method of advancing a borehole, particularly through hard soil and rock. A heavy drilling bit is raised and lowered to chop the hard soil. The chopped soil particles are brought up by the circulation of water. Percussion drilling may require casing.

**2.14****Procedures for Sampling Soil**

Two types of soil samples can be obtained during subsurface exploration: *disturbed* and *undisturbed*. Disturbed, but representative, samples can generally be used for the following types of laboratory test:

1. Grain-size analysis
2. Determination of liquid and plastic limits
3. Specific gravity of soil solids
4. Determination of organic content
5. Classification of soil

Disturbed soil samples, however, cannot be used for consolidation, hydraulic conductivity, or shear strength tests. Undisturbed soil samples must be obtained for these types of laboratory tests. Sections 2.15 through 2.18 describe some procedures for obtaining soil samples during field exploration.

**2.15****Split-Spoon Sampling**

Split-spoon samplers can be used in the field to obtain soil samples that are generally disturbed, but still representative. A section of a *standard split-spoon sampler* is shown in Figure 2.15a. The tool consists of a steel driving shoe, a steel tube that is split longitudinally

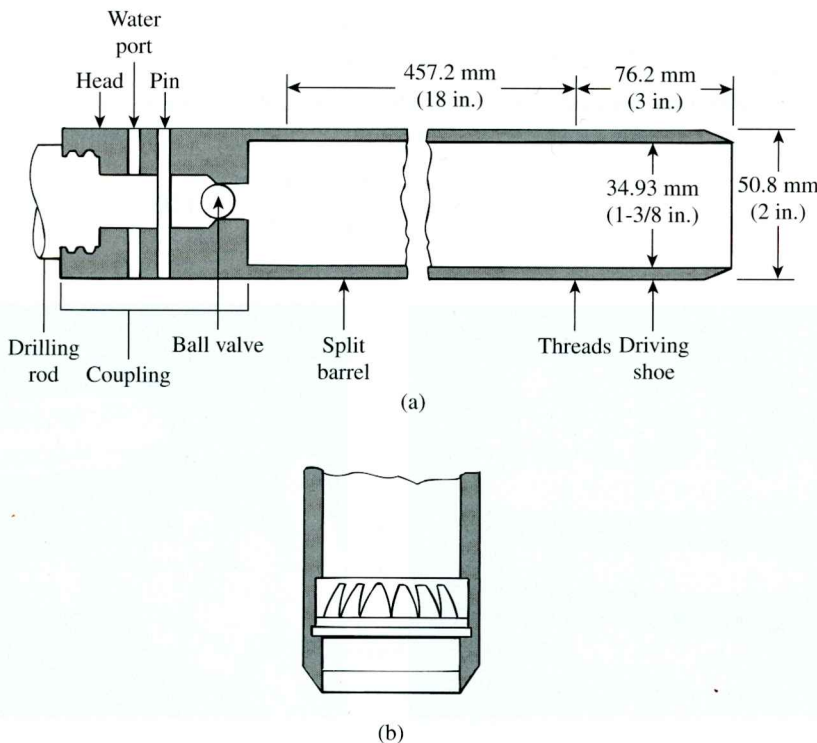


**Figure 2.15** (a) Standard split-spoon sampler; (b) spring core catcher

in half, and a coupling at the top. The coupling connects the sampler to the drill rod. The standard split tube has an inside diameter of 34.93 mm ( $1\frac{3}{8}$  in.) and an outside diameter of 50.8 mm (2 in.); however, samplers having inside and outside diameters up to 63.5 mm ( $2\frac{1}{2}$  in.) and 76.2 mm (3 in.), respectively, are also available. When a borehole is extended to a predetermined depth, the drill tools are removed and the sampler is lowered to the bottom of the hole. The sampler is driven into the soil by hammer blows to the top of the drill rod. The standard weight of the hammer is 622.72 N (140 lb), and for each blow, the hammer drops a distance of 0.762 m (30 in.). The number of blows required for a spoon penetration of three 152.4-mm (6-in.) intervals are recorded. The number of blows required for the last two intervals are added to give the *standard penetration number*,  $N$ , at that depth. This number is generally referred to as the  $N$  value (American Society for Testing and Materials, 2001, Designation D-1586-99). The sampler is then withdrawn, and the shoe and coupling are removed. Finally, the soil sample recovered from the tube is placed in a glass bottle and transported to the laboratory. This field test is called the standard penetration test (SPT). Figure 2.16a and b show a split-spoon sampler unassembled before and after sampling.

The degree of disturbance for a soil sample is usually expressed as

$$A_R(\%) = \frac{D_o^2 - D_i^2}{D_i^2} (100) \quad (2.3)$$

where

$A_R$  = area ratio (ratio of disturbed area to total area of soil)

$D_o$  = outside diameter of the sampling tube

$D_i$  = inside diameter of the sampling tube

When the area ratio is 10% or less, the sample generally is considered to be undisturbed. For a standard split-spoon sampler,

$$A_R(\%) = \frac{(50.8)^2 - (34.93)^2}{(34.93)^2} (100) = 111.5\%$$



Figure 2.16 (a) Unassembled split-spoon sampler; (b) after sampling (Courtesy of Professional Service Industries, Inc. (PSI), Waukesha, Wisconsin)

Hence, these samples are highly disturbed. Split-spoon samples generally are taken at intervals of about 1.5 m (5 ft). When the material encountered in the field is sand (particularly fine sand below the water table), recovery of the sample by a split-spoon sampler may be difficult. In that case, a device such as a *spring core catcher* may have to be placed inside the split spoon (Figure 2.15b).

At this juncture, it is important to point out that several factors contribute to the variation of the standard penetration number  $N$  at a given depth for similar soil profiles. Among these factors are the SPT hammer efficiency, borehole diameter, sampling method, and rod length (Skempton, 1986; Seed, et al., 1985). The SPT hammer energy efficiency can be expressed as

$$E_r(\%) = \frac{\text{actual hammer energy to the sampler}}{\text{input energy}} \times 100 \quad (2.4)$$

$$\text{Theoretical input energy} = Wh \quad (2.5)$$

where

$W$  = weight of the hammer  $\approx 0.623$  kN (140 lb)

$h$  = height of drop  $\approx 0.76$  mm (30 in.)

So,

$$Wh = (0.623)(0.76) = 0.474 \text{ kN-m (4200 in.-lb)}$$

In the field, the magnitude of  $E_r$  can vary from 30 to 90%. The standard practice now in the U.S. is to express the  $N$ -value to an average energy ratio of 60% ( $\approx N_{60}$ ). Thus, correcting for field procedures and on the basis of field observations, it appears reasonable to standardize the field penetration number as a function of the input driving energy and its dissipation around the sampler into the surrounding soil, or

$$N_{60} = \frac{N \eta_H \eta_B \eta_S \eta_R}{60} \quad (2.6)$$

where

$N_{60}$  = standard penetration number, corrected for field conditions

$N$  = measured penetration number

$\eta_H$  = hammer efficiency (%)

$\eta_B$  = correction for borehole diameter

$\eta_S$  = sampler correction

$\eta_R$  = correction for rod length

Variations of  $\eta_H$ ,  $\eta_B$ ,  $\eta_S$ , and  $\eta_R$ , based on recommendations by Seed et al. (1985) and Skempton (1986), are summarized in Table 2.5.

### Correlations for $N_{60}$ in Cohesive Soil

Besides compelling the geotechnical engineer to obtain soil samples, standard penetration tests provide several useful correlations. For example, the consistency of clay soils can be estimated from the standard penetration number,  $N_{60}$ . In order to achieve that, Szechy and Vargi (1978) calculated the *consistency index* (CI) as

**Table 2.5** Variations of  $\eta_H$ ,  $\eta_B$ ,  $\eta_S$ , and  $\eta_R$  [Eq. (2.6)]**1. Variation of  $\eta_H$** 

Country	Hammer type	Hammer release	$\eta_H$ (%)
Japan	Donut	Free fall	78
	Donut	Rope and pulley	67
United States	Safety	Rope and pulley	60
	Donut	Rope and pulley	45
Argentina	Donut	Rope and pulley	45
China	Donut	Free fall	60
	Donut	Rope and pulley	50

**3. Variation of  $\eta_S$** 

Variable	$\eta_S$
Standard sampler	1.0
With liner for dense sand and clay	0.8
With liner for loose sand	0.9

**2. Variation of  $\eta_B$** 

Diameter		
mm	in.	$\eta_B$
60–120	2.4–4.7	1
150	6	1.05
200	8	1.15

**4. Variation of  $\eta_R$** 

Rod length		
m	ft	$\eta_R$
>10	>30	1.0
6–10	20–30	0.95
4–6	12–20	0.85
0–4	0–12	0.75

$$CI = \frac{LL - w}{LL - PL} \quad (2.7)$$

where

$w$  = natural moisture content

LL = liquid limit

PL = plastic limit

The approximate correlation between CI,  $N_{60}$ , and the unconfined compression strength ( $q_u$ ) is given in Table 2.6.

Hara, et al. (1971) also suggested the following correlation between the undrained shear strength of clay ( $c_u$ ) and  $N_{60}$ .

$$\frac{c_u}{p_a} = 0.29 N_{60}^{0.72} \quad (2.8)$$

where  $p_a$  = atmospheric pressure ( $\approx 100 \text{ kN/m}^2$ ;  $\approx 2000 \text{ lb/in}^2$ ).

**Table 2.6** Approximate Correlation between CI,  $N_{60}$ , and  $q_u$ 

Standard penetration number, $N_{60}$	Consistency	CI	Unconfined compression strength, $q_u$	
			(kN/m <sup>2</sup> )	(lb/ft <sup>2</sup> )
<2	Very soft	<0.5	<25	500
2–8	Soft to medium	0.5–0.75	25–80	500–1700
8–15	Stiff	0.75–1.0	80–150	1700–3100
15–30	Very stiff	1.0–1.5	150–400	3100–8400
>30	Hard	>1.5	>400	8400

The overconsolidation ratio, OCR, of a natural clay deposit can also be correlated with the standard penetration number. On the basis of the regression analysis of 110 data points, Mayne and Kemper (1988) obtained the relationship

$$\text{OCR} = 0.193 \left( \frac{N_{60}}{\sigma'_o} \right)^{0.689} \quad (2.9)$$

where  $\sigma'_o$  = effective vertical stress in MN/m<sup>2</sup>.

It is important to point out that any correlation between  $c_u$ , OCR, and  $N_{60}$  is only approximate.

### **Correction for $N_{60}$ in Granular Soil**

In granular soils, the value of  $N$  is affected by the effective overburden pressure,  $\sigma'_o$ . For that reason, the value of  $N_{60}$  obtained from field exploration under different effective overburden pressures should be changed to correspond to a standard value of  $\sigma'_o$ . That is,

$$(N_1)_{60} = C_N N_{60} \quad (2.10)$$

where

$(N_1)_{60}$  = value of  $N_{60}$  corrected to a standard value of  $\sigma'_o$  [100 kN/m<sup>2</sup> (2000 lb/ft<sup>2</sup>)]

$C_N$  = correction factor

$N_{60}$  = value of  $N$  obtained from field exploration [Eq. (2.6)]

In the past, a number of empirical relations were proposed for  $C_N$ . Some of the relationships are given next. The most commonly cited relationships are those of Liao and Whitman (1986) and Skempton (1986).

In the following relationships for  $C_N$ , note that  $\sigma'_o$  is the effective overburden pressure and  $p_a$  = atmospheric pressure ( $\approx 100$  kN/m<sup>2</sup>, or  $\approx 2000$  lb/ft<sup>2</sup>)

Liao and Whitman's relationship (1986):

$$C_N = \left[ \frac{1}{\left( \frac{\sigma'_o}{p_a} \right)} \right]^{0.5} \quad (2.11)$$

Skempton's relationship (1986):

$$C_N = \frac{2}{1 + \left( \frac{\sigma'_o}{p_a} \right)} \quad (\text{for normally consolidated fine sand}) \quad (2.12)$$

$$C_N = \frac{3}{2 + \left( \frac{\sigma'_o}{p_a} \right)} \quad (\text{for normally consolidated coarse sand}) \quad (2.13)$$

$$C_N = \frac{1.7}{0.7 + \left( \frac{\sigma'_o}{p_a} \right)} \quad (\text{for overconsolidated sand}) \quad (2.14)$$

Seed et al.'s relationship (1975):

$$C_N = 1 - 1.25 \log \left( \frac{\sigma'_o}{p_a} \right) \quad (2.15)$$

Peck et al.'s relationship (1974):

$$C_N = 0.77 \log \left[ \frac{20}{\left( \frac{\sigma'_o}{p_a} \right)} \right] \left( \text{for } \frac{\sigma'_o}{p_a} \geq 0.25 \right) \quad (2.16)$$

Bazaraa (1967):

$$C_N = \frac{4}{1 + 4 \left( \frac{\sigma'_o}{p_a} \right)} \left( \text{for } \frac{\sigma'_o}{p_a} \leq 0.75 \right) \quad (2.17)$$

$$C_N = \frac{4}{3.25 + \left( \frac{\sigma'_o}{p_a} \right)} \left( \text{for } \frac{\sigma'_o}{p_a} > 0.75 \right) \quad (2.18)$$

Table 2.7 shows the comparison of  $C_N$  derived using various relationships cited above. It can be seen that the magnitude of the correction factor estimated by using any one of the relationships is approximately the same, considering the uncertainties involved in conducting the standard penetration tests. Hence, it is recommended that Eq. (2.11) may be used for all calculations.

**Table 2.7** Variation of  $C_N$

$\frac{\sigma'_o}{p_a}$	$C_N$							Eqs. (2.17) and (2.18)
	Eq. (2.11)	Eq. (2.12)	Eq. (2.13)	Eq. (2.14)	Eq. (2.15)	Eq. (2.16)		
0.25	2.00	1.60	1.33	1.78	1.75	1.47		2.00
0.50	1.41	1.33	1.20	1.17	1.38	1.23		1.33
0.75	1.15	1.14	1.09	1.17	1.15	1.10		1.00
1.00	1.00	1.00	1.00	1.00	1.00	1.00		0.94
1.50	0.82	0.80	0.86	0.77	0.78	0.87		0.84
2.00	0.71	0.67	0.75	0.63	0.62	0.77		0.76
3.00	0.58	0.50	0.60	0.46	0.40	0.63		0.65
4.00	0.50	0.40	0.60	0.36	0.25	0.54		0.55

### Correlation between $N_{60}$ and Relative Density of Granular Soil

An approximate relationship between the corrected standard penetration number and the relative density of sand is given in Table 2.8. The values are approximate primarily because the effective overburden pressure and the stress history of the soil significantly influence the  $N_{60}$  values of sand. Kulhawy and Mayne (1990) modified an empirical relationship for relative density that was given by Marcuson and Biegansky (1977), which can be expressed as

$$D_r(\%) = 12.2 + 0.75 \left[ 222N_{60} + 2311 - 711\text{OCR} - 779 \left( \frac{\sigma'_o}{p_a} \right) - 50C_u^2 \right]^{0.5} \quad (2.19)$$

where

$D_r$  = relative density

$\sigma'_o$  = effective overburden pressure

$C_u$  = uniformity coefficient of sand

$$\text{OCR} = \frac{\text{preconsolidation pressure, } \sigma'_c}{\text{effective overburden pressure, } \sigma'_o}$$

$p_a$  = atmospheric pressure

Meyerhof (1957) developed a correlation between  $D_r$  and  $N_{60}$  as

$$N_{60} = \left[ 17 + 24 \left( \frac{\sigma'_o}{p_a} \right) \right] D_r^2$$

or

$$D_r = \left\{ \frac{N_{60}}{\left[ 17 + 24 \left( \frac{\sigma'_o}{p_a} \right) \right]} \right\}^{0.5} \quad (2.20)$$

Equation (2.20) provides a reasonable estimate only for clean, medium fine sand.

Cubrinovski and Ishihara (1999) also proposed a correlation between  $N_{60}$  and the relative density of sand ( $D_r$ ) that can be expressed as

$$D_r(\%) = \left[ \frac{N_{60} \left( 0.23 + \frac{0.06}{D_{50}} \right)^{1.7}}{9} \left( \frac{1}{\frac{\sigma'_o}{p_a}} \right) \right]^{0.5} \quad (2.21)$$

**Table 2.8** Relation between the Corrected  $(N_1)_{60}$  Values and the Relative Density in Sands

Standard penetration number, $(N_1)_{60}$	Approximate relative density, $D_r$ (%)
0–5	0–5
5–10	5–30
10–30	30–60
30–50	60–95

where

$p_a$  = atmospheric pressure ( $\approx 100 \text{ kN/m}^2$ , or  $\approx 2000 \text{ lb/ft}^2$ )  
 $D_{50}$  = sieve size through which 50% of the soil will pass (mm)

Kulhawy and Mayne (1990) correlated the corrected standard penetration number and the relative density of sand in the form

$$D_r(\%) = \left[ \frac{(N_1)_{60}}{C_p C_A C_{OCR}} \right]^{0.5} \quad (2.22)$$

where

$$C_p = \text{grain-size correlations factor} = 60 + 25 \log D_{50} \quad (2.23)$$

$$C_A = \text{correlation factor for aging} = 1.2 + 0.05 \log \left( \frac{t}{100} \right) \quad (2.24)$$

$$C_{OCR} = \text{correlation factor for overconsolidation} = OCR^{0.18} \quad (2.25)$$

$$D_{50} = \text{diameter through which 50% soil will pass through (mm)}$$

$$t = \text{age of soil since deposition (years)}$$

$$OCR = \text{overconsolidation ratio}$$

### Correlation between Angle of Friction and Standard Penetration Number

The peak friction angle,  $\phi'$ , of granular soil has also been correlated with  $N_{60}$  or  $(N_1)_{60}$  by several investigators. Some of these correlations are as follows:

1. Peck, Hanson, and Thornburn (1974) give a correlation between  $N_{60}$  and  $\phi'$  in a graphical form, which can be approximated as (Wolff, 1989)

$$\phi'(\text{deg}) = 27.1 + 0.3N_{60} - 0.00054[N_{60}]^2 \quad (2.26)$$

2. Schmertmann (1975) provided the correlation between  $N_{60}$ ,  $\sigma'_o$ , and  $\phi'$ . Mathematically, the correlation can be approximated as (Kulhawy and Mayne, 1990)

$$\phi' = \tan^{-1} \left[ \frac{N_{60}}{12.2 + 20.3 \left( \frac{\sigma'_o}{p_a} \right)} \right]^{0.34} \quad (2.27)$$

where

$$N_{60} = \text{field standard penetration number}$$

$$\sigma'_o = \text{effective overburden pressure}$$

$$p_a = \text{atmospheric pressure in the same unit as } \sigma'_o$$

$$\phi' = \text{soil friction angle}$$

3. Hatanaka and Uchida (1996) provided a simple correlation between  $\phi'$  and  $(N_1)_{60}$  that can be expressed as

$$\phi' = \sqrt{20(N_1)_{60}} + 20 \quad (2.28)$$

The following qualifications should be noted when standard penetration resistance values are used in the preceding correlations to estimate soil parameters:

1. The equations are approximate.
2. Because the soil is not homogeneous, the values of  $N_{60}$  obtained from a given borehole vary widely.
3. In soil deposits that contain large boulders and gravel, standard penetration numbers may be erratic and unreliable.

Although approximate, with correct interpretation the standard penetration test provides a good evaluation of soil properties. The primary sources of error in standard penetration tests are inadequate cleaning of the borehole, careless measurement of the blow count, eccentric hammer strikes on the drill rod, and inadequate maintenance of water head in the borehole.

### **Correlation between Modulus of Elasticity and Standard Penetration Number**

The modulus of elasticity of granular soils ( $E_s$ ) is an important parameter in estimating the elastic settlement of foundations. A first order estimation for  $E_s$  was given by Kulhawy and Mayne (1990) as

$$\frac{E_s}{p_a} = \alpha N_{60} \quad (2.29)$$

where

$p_a$  = atmospheric pressure (same unit as  $E_s$ )

$$\alpha = \begin{cases} 5 & \text{for sands with fines} \\ 10 & \text{for clean normally consolidated sand} \\ 15 & \text{for clean overconsolidated sand} \end{cases}$$

## 2.16

### **Sampling with a Scraper Bucket**

When the soil deposits are sand mixed with pebbles, obtaining samples by split spoon with a spring core catcher may not be possible because the pebbles may prevent the springs from closing. In such cases, a scraper bucket may be used to obtain disturbed representative samples (Figure 2.17). The scraper bucket has a driving point and can be attached to a drilling rod. The sampler is driven down into the soil and rotated, and the scrapings from the side fall into the bucket.

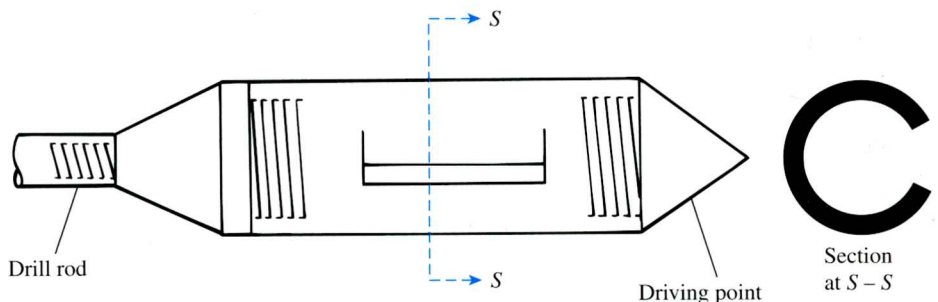


**Figure 2.17** Scraper bucket

## 2.17

### **Sampling with a Thin-Walled Tube**

Thin-walled tubes are sometimes referred to as *Shelby tubes*. They are made of seamless steel and are frequently used to obtain undisturbed clayey soils. The most common thin-walled tube samplers have outside diameters of 50.8 mm (2 in.) and 76.2 mm (3 in.). The bottom end of the tube is sharpened. The tubes can be attached to drill rods (Figure 2.18). The drill rod with the sampler attached is lowered to the bottom of the borehole, and the sampler is pushed into the soil. The soil sample inside the tube is then pulled out. The two ends are sealed, and the sampler is sent to the laboratory for testing. Figure 2.19 shows the sequence of sampling with a thin-walled tube in the field.

Samples obtained in this manner may be used for consolidation or shear tests. A thin-walled tube with a 50.8-mm (2-in.) outside diameter has an inside diameter of about 47.63 mm ( $1\frac{7}{8}$  in.). The area ratio is

$$A_R(\%) = \frac{D_o^2 - D_i^2}{D_i^2} (100) = \frac{(50.8)^2 - (47.63)^2}{(47.63)^2} (100) = 13.75\%$$

Increasing the diameters of samples increases the cost of obtaining them.

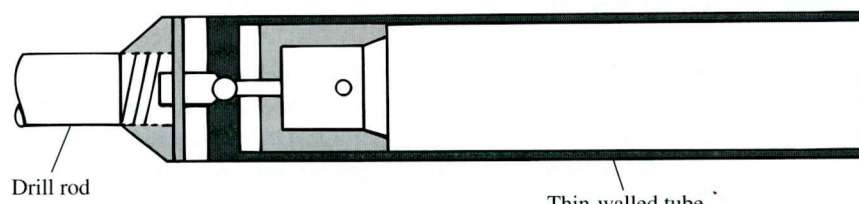


**Figure 2.18** Thin-walled tube



(a)



(b)

**Figure 2.19** Sampling with a thin-walled tube: (a) tube being attached to drill rod; (b) tube sampler pushed into soil (*Courtesy of Khaled Sobhan, Florida Atlantic University, Boca Raton, Florida*)



(c)

**Figure 2.19** (continued) (c) recovery of soil sample (*Courtesy of Khaled Sobhan, Florida Atlantic University, Boca Raton, Florida*)

## 2.18

### ***Sampling with a Piston Sampler***

When undisturbed soil samples are very soft or larger than 76.2 mm (3 in.) in diameter, they tend to fall out of the sampler. Piston samplers are particularly useful under such conditions. There are several types of piston sampler; however, the sampler proposed by Osterberg (1952) is the most useful. (see Figures 2.20a and 2.20b). It consists of a thin-walled tube with a piston. Initially, the piston closes the end of the tube. The sampler is lowered to the bottom of the borehole (Figure 2.20a), and the tube is pushed into the soil hydraulically, past the piston. Then the pressure is released through a hole in the piston rod (Figure 2.20b). To a large extent, the presence of the piston prevents distortion in the sample by not letting the soil squeeze into the sampling tube very fast and by not admitting excess soil. Consequently, samples obtained in this manner are less disturbed than those obtained by Shelby tubes.

## 2.19

### ***Observation of Water Tables***

The presence of a water table near a foundation significantly affects the foundation's load-bearing capacity and settlement, among other things. The water level will change seasonally. In many cases, establishing the highest and lowest possible levels of water during the life of a project may become necessary.

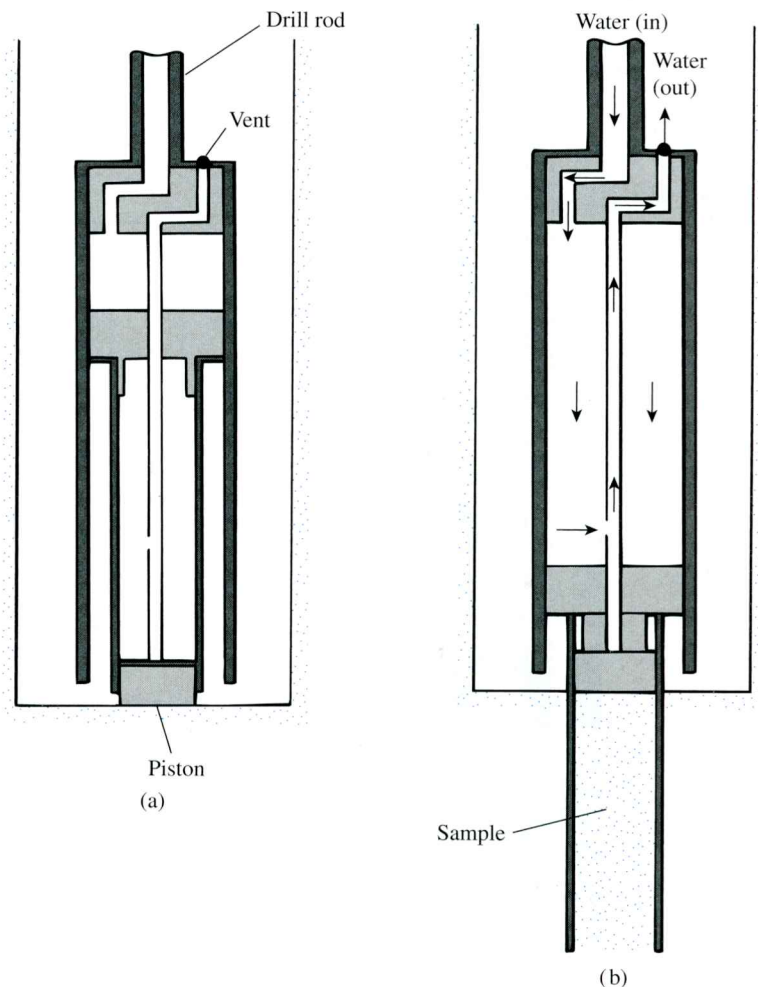


**Figure 2.20** Piston sampler: (a) sampler at the bottom of borehole; (b) tube pushed into the soil hydraulically

If water is encountered in a borehole during a field exploration, that fact should be recorded. In soils with high hydraulic conductivity, the level of water in a borehole will stabilize about 24 hours after completion of the boring. The depth of the water table can then be recorded by lowering a chain or tape into the borehole.

In highly impermeable layers, the water level in a borehole may not stabilize for several weeks. In such cases, if accurate water-level measurements are required, a *piezometer* can be used. A piezometer basically consists of a porous stone or a perforated pipe with a plastic standpipe attached to it. Figure 2.21 shows the general placement of a piezometer in a borehole. This procedure will allow periodic checking until the water level stabilizes.

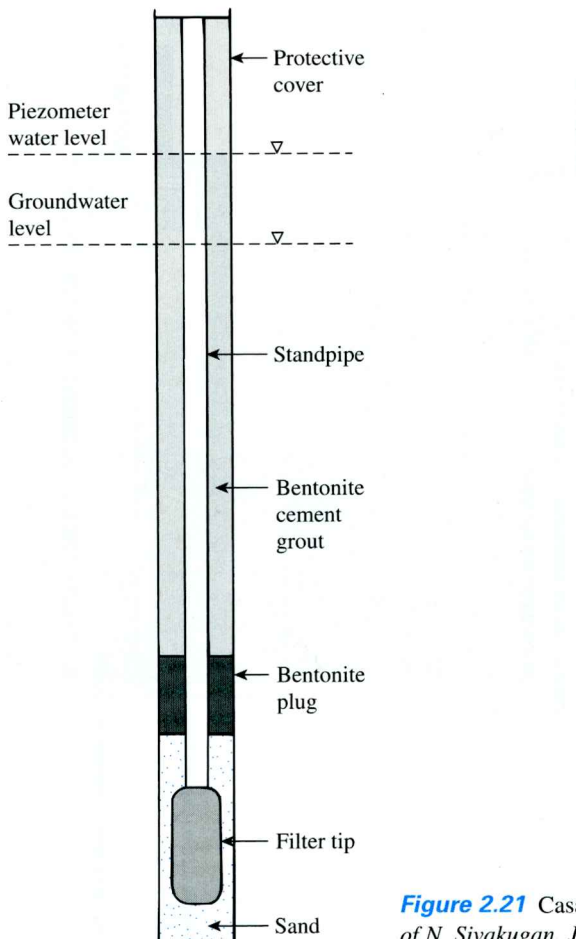


**Figure 2.21** Casagrande-type piezometer (Courtesy of N. Sivakugan, James Cook University, Australia.)

## 2.20 Vane Shear Test

The *vane shear test* (ASTM D-2573) may be used during the drilling operation to determine the *in situ* undrained shear strength ( $c_u$ ) of clay soils—particularly soft clays. The vane shear apparatus consists of four blades on the end of a rod, as shown in Figure 2.22. The height,  $H$ , of the vane is twice the diameter,  $D$ . The vane can be either rectangular or tapered (see Figure 2.22). The dimensions of vanes used in the field are given in Table 2.9. The vanes of the apparatus are pushed into the soil at the bottom of a borehole without disturbing the soil appreciably. Torque is applied at the top of the rod to rotate the vanes at a standard rate of  $0.1^\circ/\text{sec}$ . This rotation will induce failure in a soil of cylindrical shape surrounding the vanes. The maximum torque,  $T$ , applied to cause failure is measured. Note that

$$T = f(c_u, H, \text{ and } D) \quad (2.30)$$

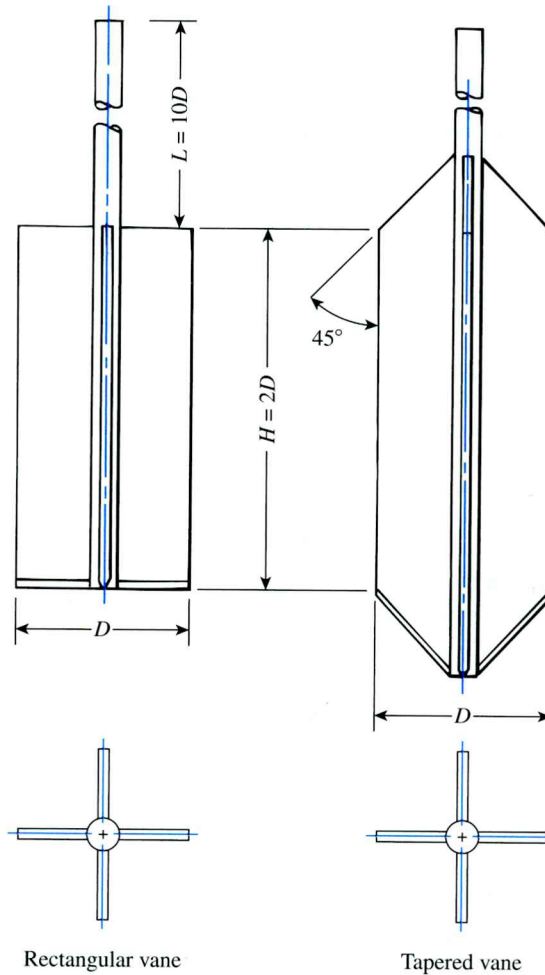


**Figure 2.22** Geometry of field vane (After ASTM, 2001)  
(Annual Book of ASTM Standards, Vol. 04.08. Copyright ASTM INTERNATIONAL. Reprinted with permission.)

or

$$c_u = \frac{T}{K} \quad (2.31)$$

where

$T$  is in  $\text{N}\cdot\text{m}$ ,  $c_u$  is in  $\text{kN}/\text{m}^2$ , and

$K$  = a constant with a magnitude depending on the dimension and shape of the vane

The constant

$$K = \left( \frac{\pi}{10^6} \right) \left( \frac{D^2 H}{2} \right) \left( 1 + \frac{D}{3H} \right) \quad (2.32a)$$

**Table 2.9** ASTM Recommended Dimensions of Field Vanes<sup>a</sup> (Annual Book of ASTM Standards, Vol. 04.08. Copyright ASTM INTERNATIONAL. Reprinted with permission.)

Casing size	Diameter, $D$ mm (in.)	Height, $H$ mm (in.)	Thickness of blade mm (in.)	Diameter of rod mm (in.)
AX	38.1 (1½)	76.2 (3)	1.6 (¹/₁₆)	12.7 (¹/₂)
BX	50.8 (2)	101.6 (4)	1.6 (¹/₁₆)	12.7 (¹/₂)
NX	63.5 (2¹/₂)	127.0 (5)	3.2 (¹/₈)	12.7 (¹/₂)
101.6 mm (4 in.) <sup>b</sup>	92.1 (3⁵/₈)	184.1 (7¹/₄)	3.2 (¹/₈)	12.7 (¹/₂)

<sup>a</sup>The selection of a vane size is directly related to the consistency of the soil being tested; that is, the softer the soil, the larger the vane diameter should be.

<sup>b</sup>Inside diameter.

where

$D$  = diameter of vane in cm

$H$  = measured height of vane in cm

If  $H/D = 2$ , Eq. (2.32a) yields

$$K = 366 \times 10^{-8} D^3 \quad (2.32b)$$

↑  
(cm)

In English units, if  $c_u$  and  $T$  in Eq. (2.31) are expressed in lb/ft<sup>2</sup> and lb-ft, respectively, then

$$K = \left( \frac{\pi}{1728} \right) \left( \frac{D^2 H}{2} \right) \left( 1 + \frac{D}{3H} \right) \quad (2.33a)$$

If  $H/D = 2$ , Eq. (2.33a) yields

$$K = 0.0021 D^3 \quad (2.33b)$$

↑  
(in.)

Field vane shear tests are moderately rapid and economical and are used extensively in field soil-exploration programs. The test gives good results in soft and medium-stiff clays and gives excellent results in determining the properties of sensitive clays.

Sources of significant error in the field vane shear test are poor calibration of torque measurement and damaged vanes. Other errors may be introduced if the rate of rotation of the vane is not properly controlled.

For actual design purposes, the undrained shear strength values obtained from field vane shear tests [ $c_{u(VST)}$ ] are too high, and it is recommended that they be corrected according to the equation

$$c_{u(\text{corrected})} = \lambda c_{u(VST)} \quad (2.34)$$

where  $\lambda$  = correction factor.

Several correlations have been given previously for the correction factor  $\lambda$ . The most commonly used correlation for  $\lambda$  is that given by Bjerrum (1972), which can be expressed as

$$\lambda = 1.7 - 0.54 \log[\text{PI}(\%)] \quad (2.35a)$$

Morris and Williams (1994) provided the following correlations:

$$\lambda = 1.18e^{-0.08(\text{PI})} + 0.57 \quad (\text{for PI} > 5) \quad (2.35b)$$

$$\lambda = 7.01e^{-0.08(\text{LL})} + 0.57 \quad (\text{where LL is in \%}) \quad (2.35c)$$

The field vane shear strength can be correlated with the preconsolidation pressure and the overconsolidation ratio of the clay. Using 343 data points, Mayne and Mitchell (1988) derived the following empirical relationship for estimating the preconsolidation pressure of a natural clay deposit:

$$\sigma'_c = 7.04[c_{u(\text{field})}]^{0.83} \quad (2.36)$$

Here,

$\sigma'_c$  = preconsolidation pressure ( $\text{kN}/\text{m}^2$ )

$c_{u(\text{field})}$  = field vane shear strength ( $\text{kN}/\text{m}^2$ )

The overconsolidation ratio, OCR, also can be correlated to  $c_{u(\text{field})}$  according to the equation

$$\text{OCR} = \beta \frac{c_{u(\text{field})}}{\sigma'_o} \quad (2.37)$$

where  $\sigma'_o$  = effective overburden pressure.

The magnitudes of  $\beta$  developed by various investigators are given below.

- Mayne and Mitchell (1988):

$$\beta = 22[\text{PI}(\%)]^{-0.48} \quad (2.38)$$

- Hansbo (1957):

$$\beta = \frac{222}{w(\%)} \quad (2.39)$$

- Larsson (1980):

$$\beta = \frac{1}{0.08 + 0.0055(\text{PI})} \quad (2.40)$$

## 2.21

**Cone Penetration Test**

The cone penetration test (CPT), originally known as the Dutch cone penetration test, is a versatile sounding method that can be used to determine the materials in a soil profile and estimate their engineering properties. The test is also called the *static penetration test*, and no boreholes are necessary to perform it. In the original version, a  $60^\circ$  cone with a base area of  $10 \text{ cm}^2$  ( $1.55 \text{ in.}^2$ ) was pushed into the ground at a steady rate of about  $20 \text{ mm/sec}$  ( $\approx 0.8 \text{ in./sec}$ ), and the resistance to penetration (called the point resistance) was measured.

The cone penetrometers in use at present measure (a) the *cone resistance* ( $q_c$ ) to penetration developed by the cone, which is equal to the vertical force applied to the cone, divided by its horizontally projected area; and (b) the *frictional resistance* ( $f_c$ ), which is the resistance measured by a sleeve located above the cone with the local soil surrounding it. The frictional resistance is equal to the vertical force applied to the sleeve, divided by its surface area—actually, the sum of friction and adhesion.

Generally, two types of penetrometers are used to measure  $q_c$  and  $f_c$ :

1. *Mechanical friction-cone penetrometer* (Figure 2.23). The tip of this penetrometer is connected to an inner set of rods. The tip is first advanced about 40 mm, giving the

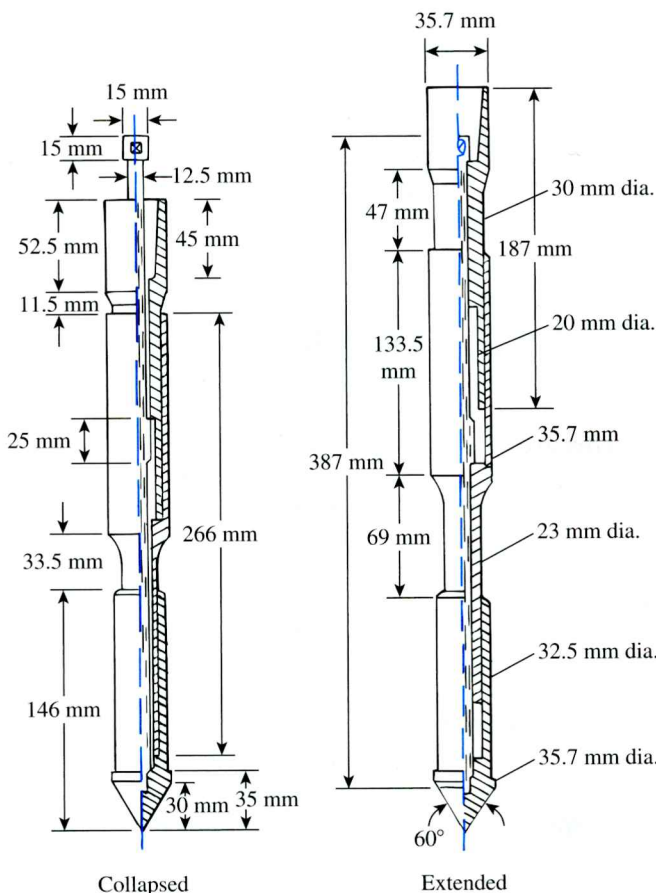


**Figure 2.23** Mechanical friction-cone penetrometer (After ASTM, 2001) (Annual Book of ASTM Standards, Vol. 04.08. Copyright ASTM INTERNATIONAL. Reprinted with permission.)

cone resistance. With further thrusting, the tip engages the friction sleeve. As the inner rod advances, the rod force is equal to the sum of the vertical force on the cone and sleeve. Subtracting the force on the cone gives the side resistance.

2. *Electric friction-cone penetrometer* (Figure 2.24). The tip of this penetrometer is attached to a string of steel rods. The tip is pushed into the ground at the rate of 20 mm/sec. Wires from the transducers are threaded through the center of the rods and continuously measure the cone and side resistances. Figure 2.25 shows a photograph of an electric friction-cone penetrometer.

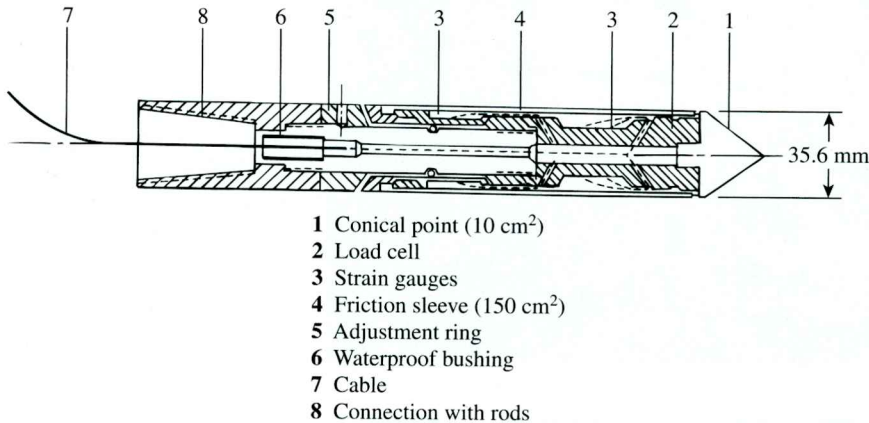


**Figure 2.24** Electric friction-cone penetrometer (After ASTM, 2001) (Annual Book of ASTM Standards, Vol. 04.08. Copyright ASTM INTERNATIONAL. Reprinted with permission.)

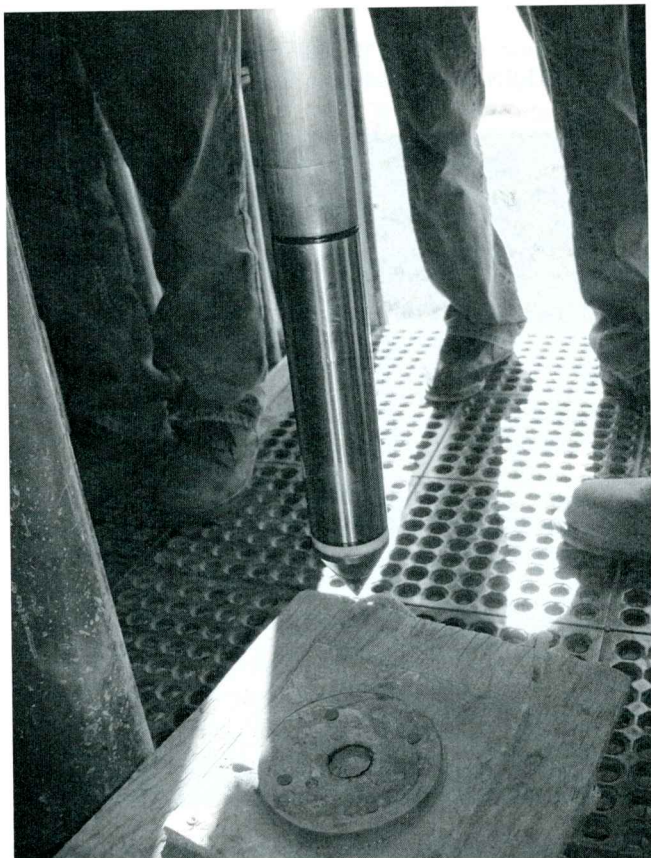


**Figure 2.25** Photograph of an electric friction-cone penetrometer (Courtesy of Sanjeev Kumar, Southern Illinois University, Carbondale, Illinois)

Figure 2.26 shows the sequence of a cone penetration test in the field. A truck-mounted CPT rig is shown in Figure 2.26a. A hydraulic ram located inside the truck pushes the cone into the ground. Figure 2.26b shows the cone penetrometer in the truck being put in the proper location. Figure 2.26c shows the progress of the CPT.



(a)



(a)

**Figure 2.26** Cone penetration test in field:  
(a) mounted CPT rig; (b) cone penetrometer being set in proper location (*Courtesy of Sanjeev Kumar, Southern Illinois University, Carbondale, Illinois*)

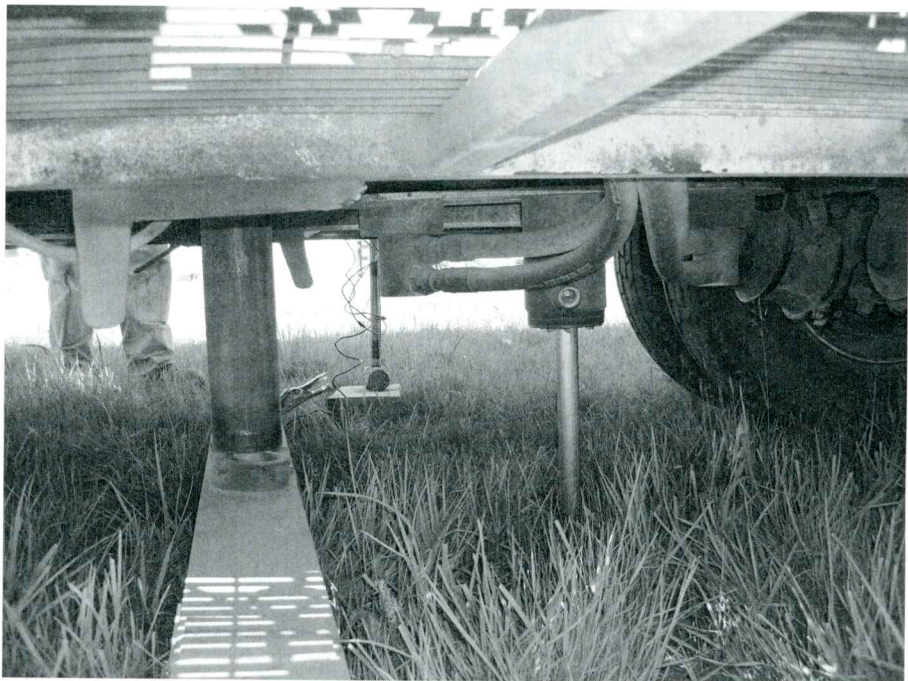


**Figure 2.26 (continued) (c)** test in progress (*Courtesy of Sanjeev Kumar, Southern Illinois University, Carbondale, Illinois*)

Figure 2.27 shows the results of penetrometer test in a soil profile with friction measurement by an electric friction-cone penetrometer.

Several correlations that are useful in estimating the properties of soils encountered during an exploration program have been developed for the point resistance ( $q_c$ ) and the friction ratio ( $F_r$ ) obtained from the cone penetration tests. The friction ratio is defined as

$$F_r = \frac{\text{frictional resistance}}{\text{cone resistance}} = \frac{f_c}{q_c} \quad (2.41)$$

In a more recent study on several soils in Greece, Anagnostopoulos et al. (2003) expressed  $F_r$  as

$$F_r(\%) = 1.45 - 1.36 \log D_{50} \text{ (electric cone)} \quad (2.42)$$

and

$$F_r(\%) = 0.7811 - 1.611 \log D_{50} \text{ (mechanical cone)} \quad (2.43)$$

where  $D_{50}$  = size through which 50% of soil will pass through (mm).

The  $D_{50}$  for soils based on which Eqs. (2.42) and (2.43) have been developed ranged from 0.001 mm to about 10 mm.

As in the case of standard penetration tests, several correlations have been developed between  $q_c$  and other soil properties. Some of these correlations are presented next.

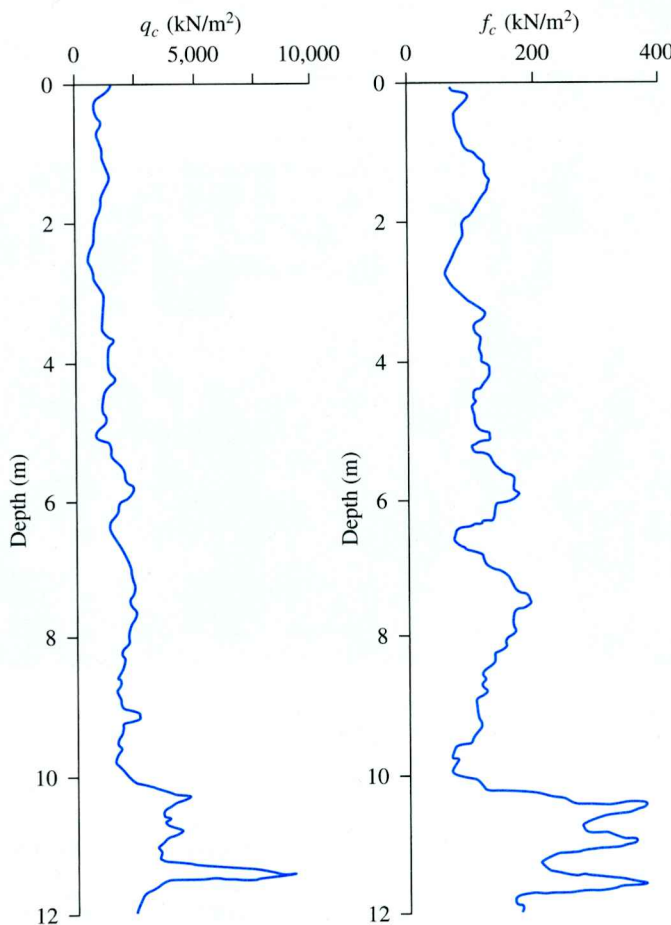


**Figure 2.27** Cone penetrometer test with friction measurement

### Correlation between Relative Density ( $D_r$ ) and $q_c$ for Sand

Lancellotta (1983) and Jamiolkowski et al. (1985) showed that the relative density of normally consolidated sand,  $D_r$ , and  $q_c$  can be correlated according to the formula (Figure 2.28).

$$D_r(\%) = A + B \log_{10} \left( \frac{q_c}{\sqrt{\sigma'_o}} \right) \quad (2.44)$$

The preceding relationship can be rewritten as (Kulhawy and Mayne, 1990)

$$D_r(\%) = 68 \left[ \log \left( \frac{q_c}{\sqrt{p_a \cdot \sigma'_0}} \right) - 1 \right] \quad (2.45)$$

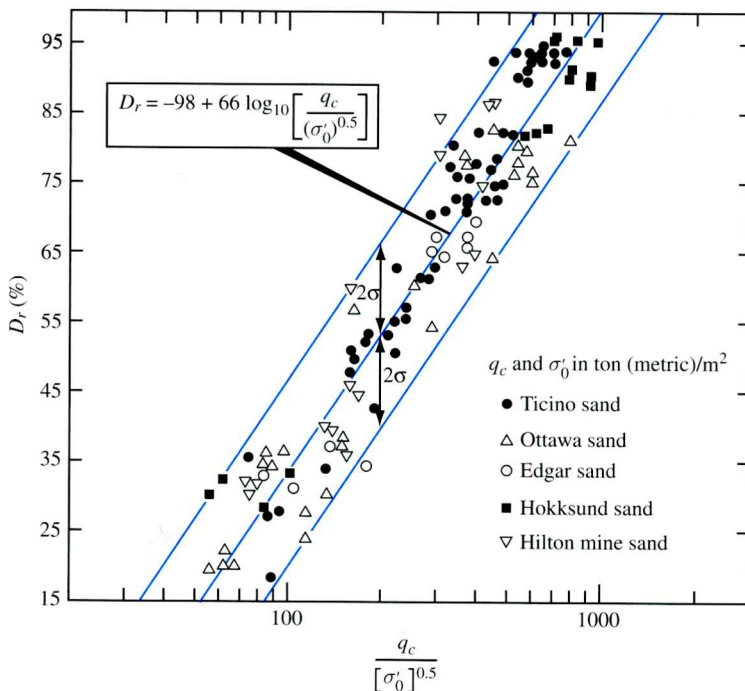


**Figure 2.28** Relationship between  $D_r$  and  $q_c$  (Based on Lancellotta, 1983, and Jamiolski et al., 1985)

where

$p_a$  = atmospheric pressure ( $\approx 100$  kN/m<sup>2</sup>)

$\sigma'_o$  = vertical effective stress

Baldi et al. (1982), and Robertson and Campanella (1983) recommended the empirical relationship shown in Figure 2.29 between vertical effective stress ( $\sigma'_o$ ), relative density ( $D_r$ ), and  $q_c$  for *normally consolidated sand*.

Kulhawy and Mayne (1990) proposed the following relationship to correlate  $D_r$ ,  $q_c$ , and the vertical effective stress  $\sigma'_o$ :

$$D_r = \sqrt{\left[ \frac{1}{305Q_c \text{OCR}^{1.8}} \right] \left[ \frac{\frac{q_c}{p_a}}{\left( \frac{\sigma'_o}{p_a} \right)^{0.5}} \right]} \quad (2.46)$$

In this equation,

OCR = overconsolidation ratio

$p_a$  = atmospheric pressure

$Q_c$  = compressibility factor

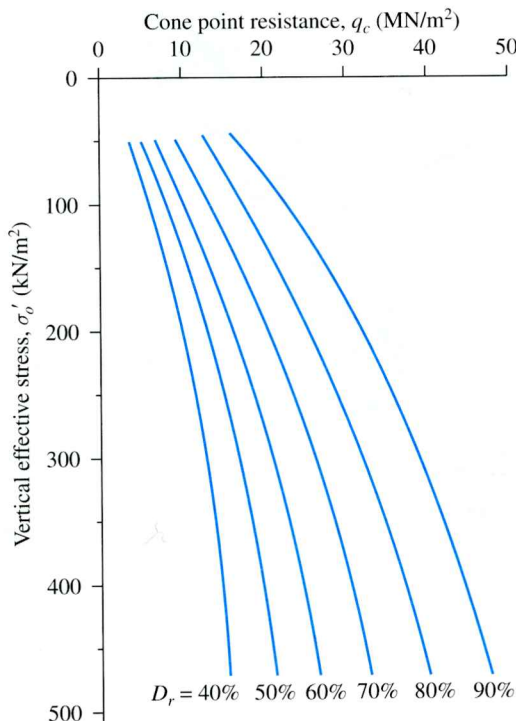


**Figure 2.29** Variation of  $q_c$ ,  $\sigma'_v$ , and  $D_r$  for normally consolidated quartz sand (Based on Baldi et al., 1982, and Robertson and Campanella, 1983)

The recommended values of  $Q_c$  are as follows:

Highly compressible sand = 0.91

Moderately compressible sand = 1.0

Low compressible sand = 1.09

### Correlation between $q_c$ and Drained Friction Angle ( $\phi'$ ) for Sand

On the basis of experimental results, Robertson and Campanella (1983) suggested the variation of  $D_r$ ,  $\sigma'_v$ , and  $\phi'$  for normally consolidated quartz sand. This relationship can be expressed as (Kulhawy and Mayne, 1990)

$$\phi' = \tan^{-1} \left[ 0.1 + 0.38 \log \left( \frac{q_c}{\sigma'_v} \right) \right] \quad (2.47)$$

Based on the cone penetration tests on the soils in the Venice Lagoon (Italy), Ricceri et al. (2002) proposed a similar relationship for soil with classifications of ML and SP-SM as

$$\phi' = \tan^{-1} \left[ 0.38 + 0.27 \log \left( \frac{q_c}{\sigma'_v} \right) \right] \quad (2.48)$$

In a more recent study, Lee et al. (2004) developed a correlation between  $\phi'$ ,  $q_c$ , and the horizontal effective stress ( $\sigma'_h$ ) in the form

$$\phi' = 15.575 \left( \frac{q_c}{\sigma'_h} \right)^{0.1714} \quad (2.49)$$

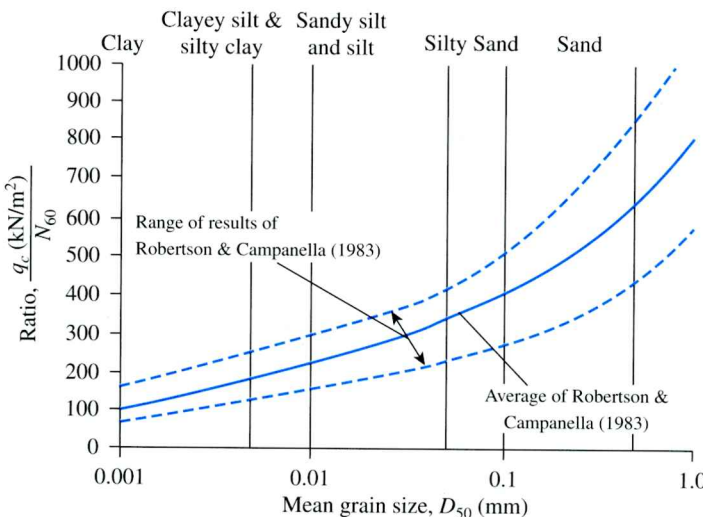


**Figure 2.30** General range of variation of  $q_c/N_{60}$  for various types of soil

### Correlation between $q_c$ and $N_{60}$

Figure 2.30 shows a plot of  $q_c$  ( $\text{kN}/\text{m}^2$ )/ $N_{60}$  ( $N_{60}$  = standard penetration resistance) against the mean grain size ( $D_{50}$  in mm) for various types of soil. This was developed from field test results by Robertson and Campanella (1983).

Anagnostopoulos et al. (2003) provided a similar relationship correlating  $q_c$ ,  $N_{60}$ , and  $D_{50}$ . Or

$$\frac{\left(\frac{q_c}{p_a}\right)}{N_{60}} = 7.6429 D_{50}^{0.26} \quad (2.50)$$

where  $p_a$  = atmospheric pressure (same unit as  $q_c$ ).

### Correlations of Soil Types

Robertson and Campanella (1983) provided the correlations shown in Figure 2.31 between  $q_c$  and the friction ratio [Eq. (2.41)] to identify various types of soil encountered in the field.

### Correlations for Undrained Shear Strength ( $c_u$ ), Preconsolidation Pressure ( $\sigma'_o$ ), and Overconsolidation Ratio (OCR) for Clays

The undrained shear strength,  $c_u$ , can be expressed as

$$c_u = \frac{q_c - \sigma_o}{N_K} \quad (2.51)$$

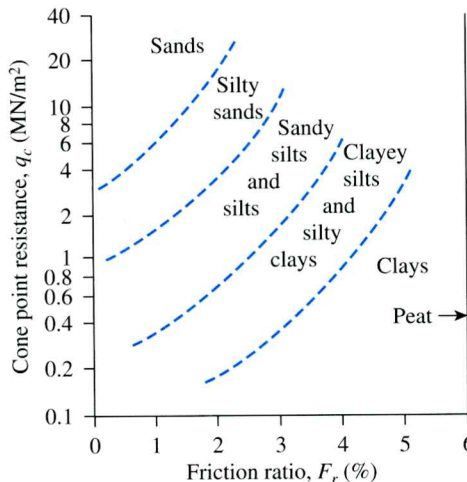


**Figure 2.31** Robertson and Campanella's correlation (1983) between  $q_c$ ,  $F_r$ , and the type of soil (Robertson and Campanella, 1983)

where

$\sigma_o$  = total vertical stress

$N_K$  = bearing capacity factor

The bearing capacity factor,  $N_K$ , may vary from 11 to 19 for normally consolidated clays and may approach 25 for overconsolidated clay. According to Mayne and Kemper (1988)

$$N_K = 15 \text{ (for electric cone)}$$

and

$$N_K = 20 \text{ (for mechanical cone)}$$

Based on tests in Greece, Anagnostopoulos et al. (2003) determined

$$N_K = 17.2 \text{ (for electric cone)}$$

and

$$N_K = 18.9 \text{ (for mechanical cone)}$$

These field tests also showed that

$$c_u = \frac{f_c}{1.26} \text{ (for mechanical cones)} \quad (2.52)$$

and

$$c_u = f_c \text{ (for electrical cones)} \quad (2.53)$$

Mayne and Kemper (1988) provided correlations for preconsolidation pressure ( $\sigma'_c$ ) and overconsolidation ratio (OCR) as

$$\sigma'_c = 0.243(q_c)^{0.96} \quad (2.54)$$

$\uparrow \qquad \uparrow$   
 $\text{MN/m}^2 \qquad \text{MN/m}^2$

and

$$\text{OCR} = 0.37 \left( \frac{q_c - \sigma'_o}{\sigma'_o} \right)^{1.01} \quad (2.55)$$

where  $\sigma_o$  and  $\sigma'_o$  = total and effective stress, respectively.

## 2.22 Pressuremeter Test (PMT)

The pressuremeter test is an *in situ* test conducted in a borehole. It was originally developed by Menard (1956) to measure the strength and deformability of soil. It has also been adopted by ASTM as Test Designation 4719. The Menard-type PMT consists essentially of a probe with three cells. The top and bottom ones are *guard cells* and the middle one is the *measuring cell*, as shown schematically in Figure 2.32a. The test is conducted in a prebored hole with a diameter that is between 1.03 and 1.2 times the nominal diameter of the probe. The probe that is most commonly used has a diameter of 58 mm and a length of 420 mm. The probe cells can be expanded by either liquid or gas. The guard cells are expanded to reduce the end-condition effect on the measuring cell, which has a volume ( $V_o$ ) of 535 cm<sup>3</sup>. Following are the dimensions for the probe diameter and the diameter of the borehole, as recommended by ASTM:

Probe diameter (mm)	Borehole diameter	
	Nominal (mm)	Maximum (mm)
44	45	53
58	60	70
74	76	89

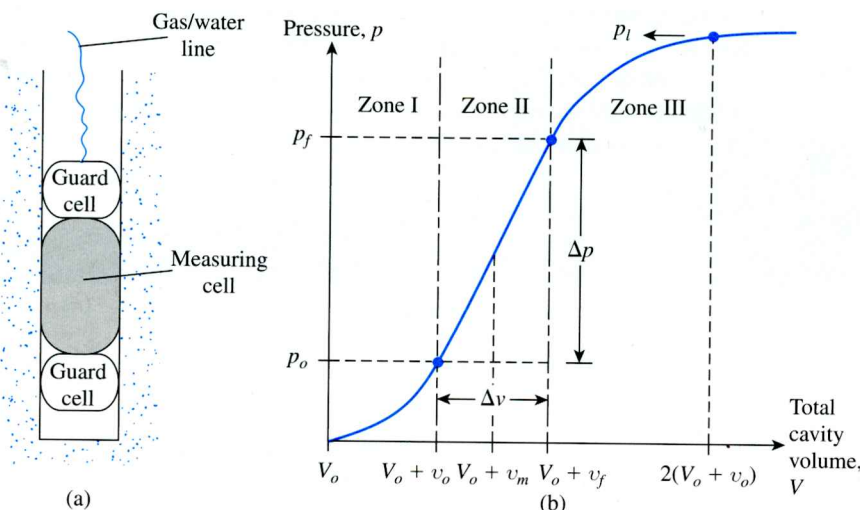


Figure 2.32 (a) Pressuremeter; (b) plot of pressure versus total cavity volume

In order to conduct a test, the measuring cell volume,  $V_o$ , is measured and the probe is inserted into the borehole. Pressure is applied in increments and the new volume of the cell is measured. The process is continued until the soil fails or until the pressure limit of the device is reached. The soil is considered to have failed when the total volume of the expanded cavity ( $V$ ) is about twice the volume of the original cavity. After the completion of the test, the probe is deflated and advanced for testing at another depth.

The results of the pressuremeter test are expressed in the graphical form of pressure versus volume, as shown in Figure 2.32b. In the figure, Zone I represents the reloading portion during which the soil around the borehole is pushed back into the initial state (i.e., the state it was in before drilling). The pressure  $p_o$  represents the *in situ* total horizontal stress. Zone II represents a pseudoelastic zone in which the cell volume versus cell pressure is practically linear. The pressure  $p_f$  represents the creep, or yield, pressure. The zone marked III is the plastic zone. The pressure  $p_l$  represents the limit pressure. Figure 2.33 shows some photographs for a pressuremeter test in the field.

The pressuremeter modulus,  $E_p$ , of the soil is determined with the use of the theory of expansion of an infinitely thick cylinder. Thus,

$$E_p = 2(1 + \mu_s)(V_o + v_m) \left( \frac{\Delta p}{\Delta v} \right) \quad (2.56)$$

where

$$v_m = \frac{v_o + v_f}{2}$$

$$\Delta p = p_f - p_o$$

$$\Delta v = v_f - v_o$$

$\mu_s$  = Poisson's ratio (which may be assumed to be 0.33)

The limit pressure  $p_l$  is usually obtained by extrapolation and not by direct measurement.

In order to overcome the difficulty of preparing the borehole to the proper size, self-boring pressuremeters (SBPMTs) have also been developed. The details concerning SBPMTs can be found in the work of Baguelin et al. (1978).

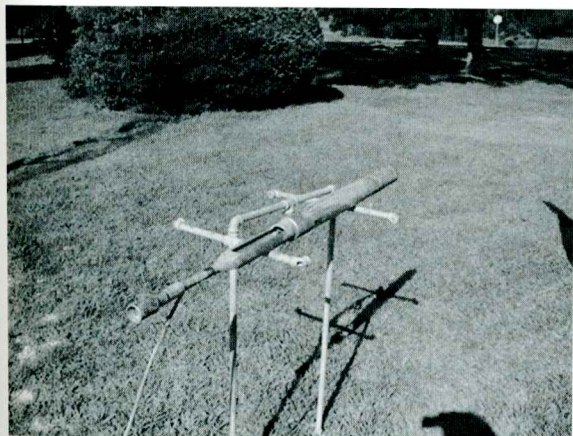
Correlations between various soil parameters and the results obtained from the pressuremeter tests have been developed by various investigators. Kulhawy and Mayne (1990) proposed that, for clays,

$$\sigma'_c = 0.45p_l \quad (2.57)$$

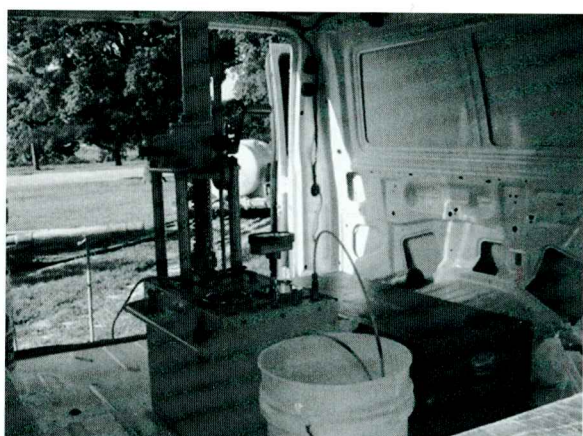
where  $\sigma'_c$  = preconsolidation pressure.

On the basis of the cavity expansion theory, Baguelin et al. (1978) proposed that

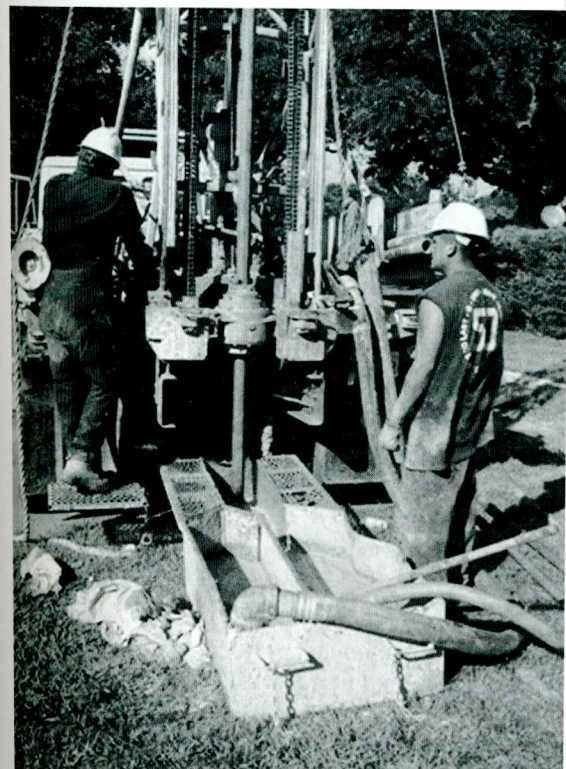
$$c_u = \frac{(p_l - p_o)}{N_p} \quad (2.58)$$



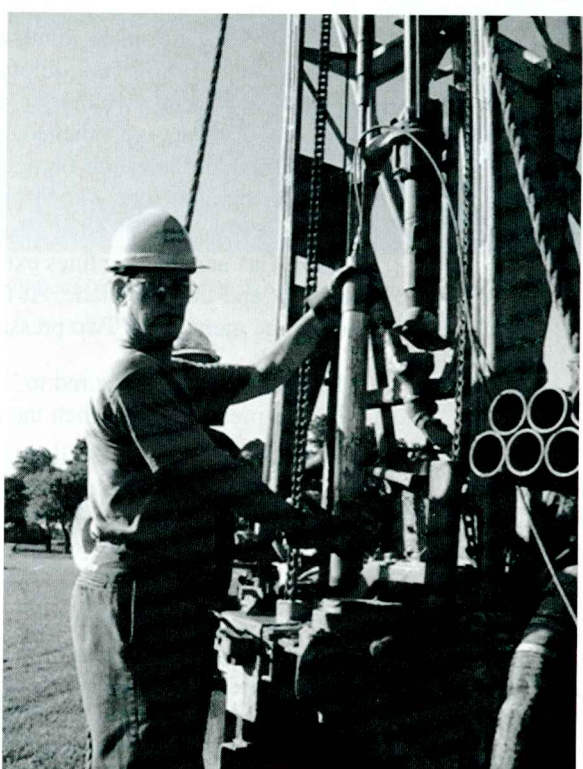
(a)



(c)



(b)



(d)

**Figure 2.33** Pressuremeter test in the field: (a) the pressuremeter probe; (b) drilling the bore hole by wet rotary method; (c) pressuremeter control unit with probe in the background; (d) getting ready to insert the pressuremeter probe into the bore hole (*Courtesy of Jean-Louis Briaud, Texas A&M University, College Station, Texas*)

where

$c_u$  = undrained shear strength of a clay

$$N_p = 1 + \ln\left(\frac{E_p}{3c_u}\right)$$

Typical values of  $N_p$  vary between 5 and 12, with an average of about 8.5. Ohya et al. (1982) (see also Kulhawy and Mayne, 1990) correlated  $E_p$  with field standard penetration numbers ( $N_{60}$ ) for sand and clay as follows:

$$\text{Clay: } E_p (\text{kN/m}^2) = 1930 N_{60}^{0.63} \quad (2.59)$$

$$\text{Sand: } E_p (\text{kN/m}^2) = 908 N_{60}^{0.66} \quad (2.60)$$

## 2.23 Dilatometer Test

The use of the flat-plate dilatometer test (DMT) is relatively recent (Marchetti, 1980; Schmertmann, 1986). The equipment essentially consists of a flat plate measuring 220 mm (length)  $\times$  95 mm (width)  $\times$  14 mm (thickness) (8.66 in.  $\times$  3.74 in.  $\times$  0.55 in.). A thin, flat, circular, expandable steel membrane having a diameter of 60 mm (2.36 in.) is located flush at the center on one side of the plate (Figure 2.34a). Figure 2.35 shows two flat-plate dilatometers with other instruments for conducting a test in the field. The dilatometer probe is inserted into the ground with a cone penetrometer testing rig (Figure 2.34b). Gas and electric lines extend from the surface control box, through the penetrometer rod, and into the blade. At the required depth, high-pressure nitrogen gas is used to inflate the membrane. Two pressure readings are taken:

1. The pressure  $A$  required to “lift off” the membrane.
2. The pressure  $B$  at which the membrane expands 1.1 mm (0.4 in.) into the surrounding soil

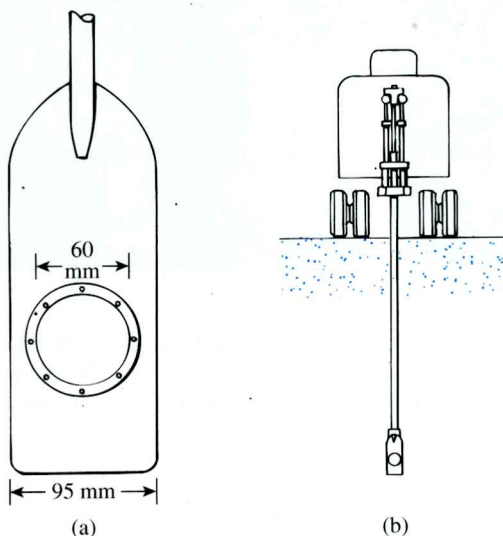


**Figure 2.34** (a) Schematic diagram of a flat-plate dilatometer; (b) dilatometer probe inserted into ground



**Figure 2.35** Dilatometer and other equipment (Courtesy of N. Sivakugan, James Cook University, Australia)

The A and B readings are corrected as follows (Schmertmann, 1986):

$$\text{Contact stress, } p_o = 1.05(A + \Delta A - Z_m) - 0.05(B - \Delta B - Z_m) \quad (2.61)$$

$$\text{Expansion stress, } p_1 = B - Z_m - \Delta B \quad (2.62)$$

where

$\Delta A$  = vacuum pressure required to keep the membrane in contact with its seating

$\Delta B$  = air pressure required inside the membrane to deflect it outward to a center expansion of 1.1 mm

$Z_m$  = gauge pressure deviation from zero when vented to atmospheric pressure

The test is normally conducted at depths 200 to 300 mm apart. The result of a given test is used to determine three parameters:

1. Material index,  $I_D = \frac{p_1 - p_o}{p_o - u_o}$

2. Horizontal stress index,  $K_D = \frac{p_o - u_o}{\sigma'_o}$

3. Dilatometer modulus,  $E_D(\text{kN/m}^2) = 34.7(p_1 \text{ kN/m}^2 - p_o \text{ kN/m}^2)$

where

$u_o$  = pore water pressure

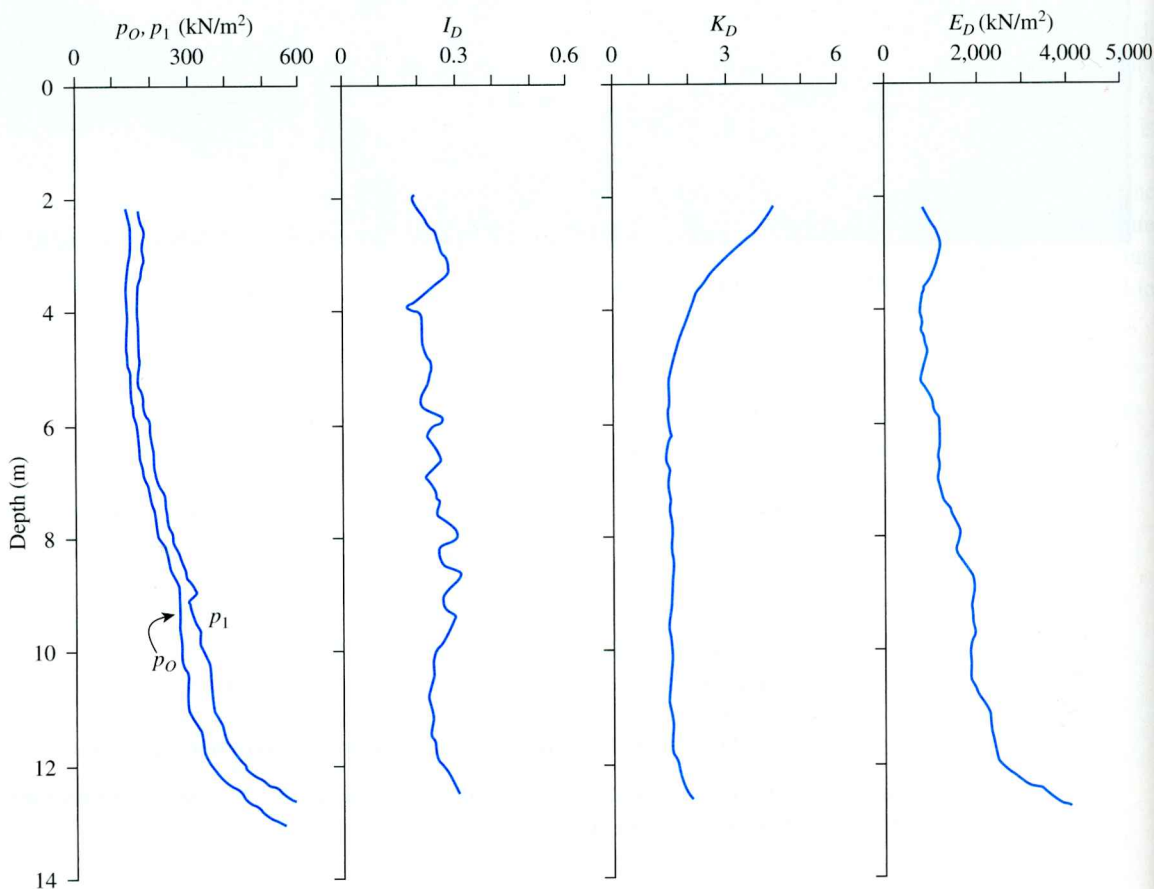
$\sigma'_o$  = *in situ* vertical effective stress

Figure 2.36 shows the results of a dilatometer test conducted in Bangkok soft clay and reported by Shibuya and Hanh (2001). Based on his initial tests, Marchetti (1980) provided the following correlations.

$$K_o = \left( \frac{K_D}{1.5} \right)^{0.47} - 0.6 \quad (2.63)$$

$$\text{OCR} = (0.5K_D)^{1.56} \quad (2.64)$$

$$\frac{c_u}{\sigma'_o} = 0.22 \quad (\text{for normally consolidated clay}) \quad (2.65)$$



**Figure 2.36** A dilatometer test result conducted on soft Bangkok clay (Redrawn from Shibuya and Hanh, 2001)

$$\left(\frac{c_u}{\sigma'_o}\right)_{OC} = \left(\frac{c_u}{\sigma'_o}\right)_{NC} (0.5K_D)^{1.25} \quad (2.66)$$

$$E_s = (1 - \mu_s^2) E_D \quad (2.67)$$

where

$K_o$  = coefficient of at-rest earth pressure

OCR = overconsolidation ratio

OC = overconsolidated soil

NC = normally consolidated soil

$E_s$  = modulus of elasticity

Other relevant correlations using the results of dilatometer tests are as follows:

- For undrained cohesion in clay (Kamei and Iwasaki, 1995):

$$c_u = 0.35 \sigma'_0 (0.47K_D)^{1.14} \quad (2.68)$$

- For soil friction angle (ML and SP-SM soils) (Ricceri et al., 2002):

$$\phi' = 31 + \frac{K_D}{0.236 + 0.066K_D} \quad (2.69a)$$

$$\phi'_{ult} = 28 + 14.6 \log K_D - 2.1 (\log K_D)^2 \quad (2.69b)$$

Schmertmann (1986) also provided a correlation between the material index ( $I_D$ ) and the dilatometer modulus ( $E_D$ ) for a determination of the nature of the soil and its unit weight ( $\gamma$ ). This relationship is shown in Figure 2.37.

## 2.24

## Coring of Rocks

When a rock layer is encountered during a drilling operation, rock coring may be necessary. To core rocks, a *core barrel* is attached to a drilling rod. A *coring bit* is attached to the bottom of the barrel (Fig. 2.38). The cutting elements may be diamond, tungsten, carbide, and so on. Table 2.10 summarizes the various types of core barrel and their sizes, as well as the compatible drill rods commonly used for exploring foundations. The coring is advanced by rotary drilling. Water is circulated through the drilling rod during coring, and the cutting is washed out.

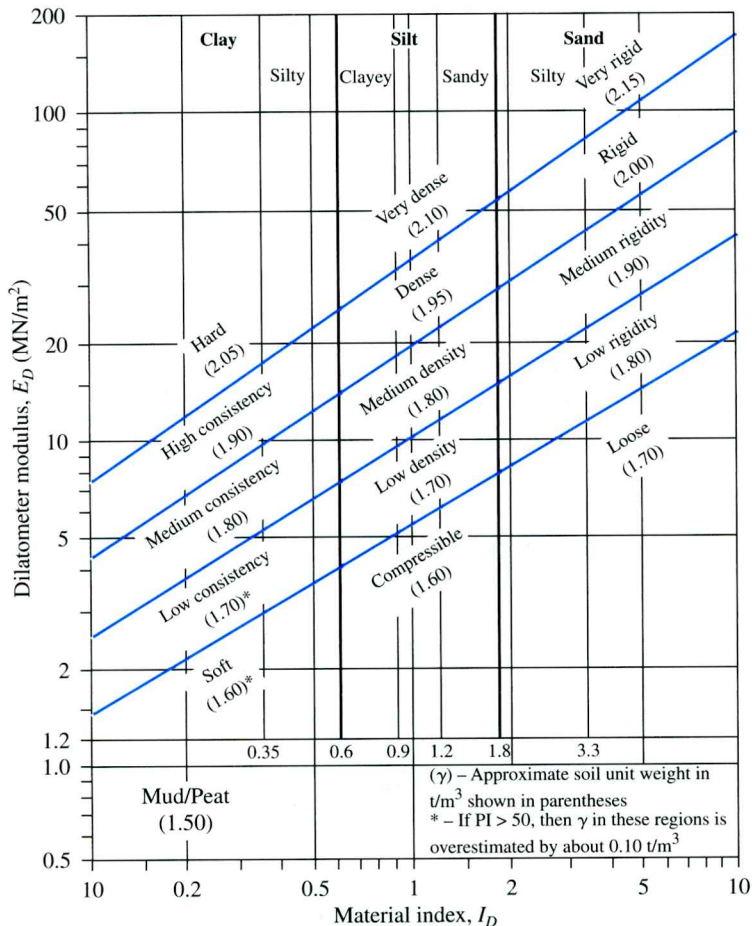


**Figure 2.37** Chart for determination of soil description and unit weight  
 (After Schmertmann, 1986)  
 (Note:  $1 \text{ t/m}^3 = 9.81 \text{ kN/m}^3$ )  
 (Schmertmann, J. H. (1986). "Suggested method for performing the flat dilatometer test," Geotechnical Testing Journal, ASTM, Vol. 9, No. 2, pp. 93-101, Fig. 2. Copyright ASTM INTERNATIONAL. Reprinted with permission.)

**Table 2.10** Standard Size and Designation of Casing, Core Barrel, and Compatible Drill Rod

Casing and core barrel designation	Outside diameter of core barrel bit		Drill rod designation	Outside diameter of drill rod		Diameter of borehole		Diameter of core sample	
	(mm)	(in.)		(mm)	(in.)	(mm)	(in.)	(mm)	(in.)
EX	36.51	$1\frac{7}{16}$	E	33.34	$1\frac{5}{16}$	38.1	$1\frac{1}{2}$	22.23	$\frac{7}{8}$
AX	47.63	$1\frac{7}{8}$	A	41.28	$1\frac{5}{8}$	50.8	2	28.58	$1\frac{1}{8}$
BX	58.74	$2\frac{5}{16}$	B	47.63	$1\frac{7}{8}$	63.5	$2\frac{1}{2}$	41.28	$1\frac{5}{8}$
NX	74.61	$2\frac{15}{16}$	N	60.33	$2\frac{3}{8}$	76.2	3	53.98	$2\frac{1}{8}$

Two types of core barrel are available: the *single-tube core barrel* (Figure 2.38a) and the *double-tube core barrel* (Figure 2.38b). Rock cores obtained by single-tube core barrels can be highly disturbed and fractured because of torsion. Rock cores smaller than the BX size tend to fracture during the coring process. Figure 2.39 shows

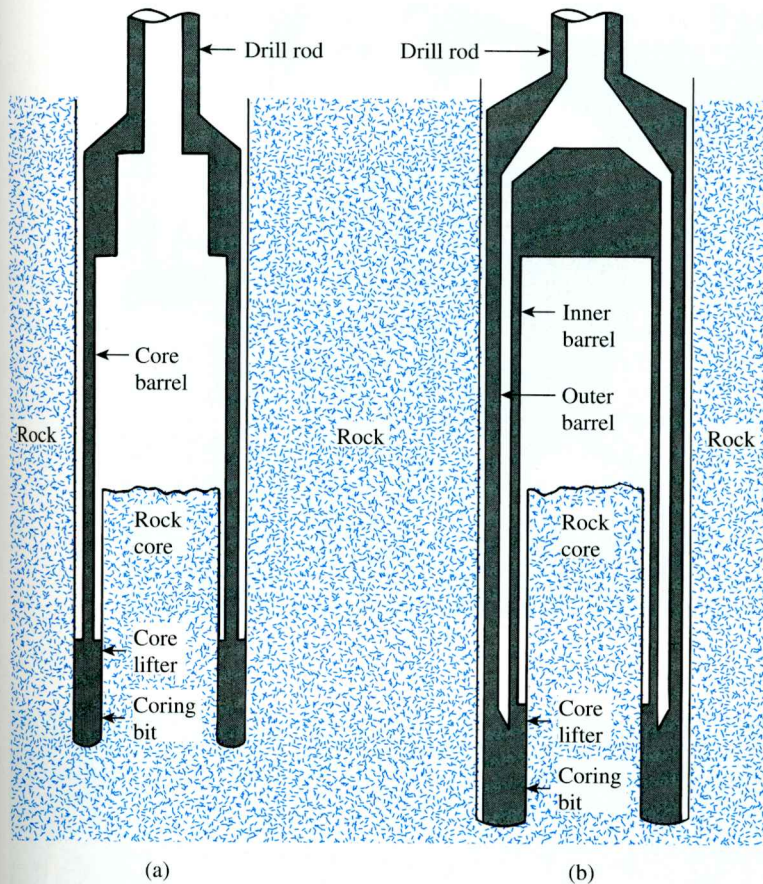
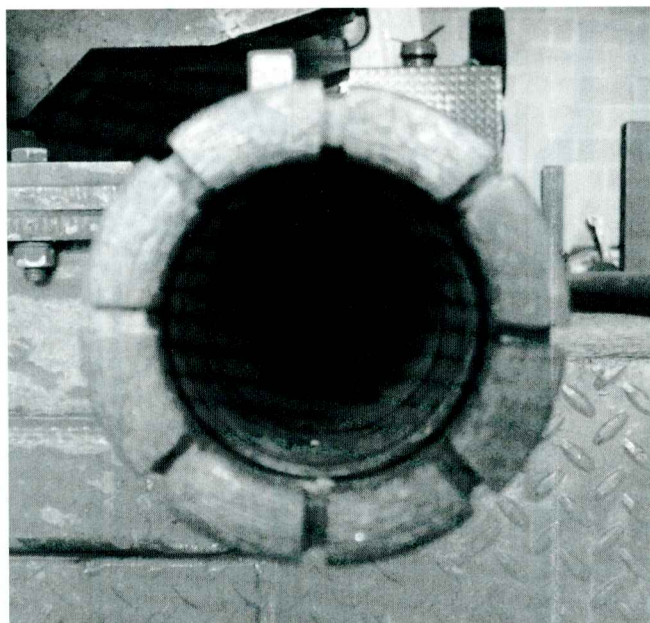


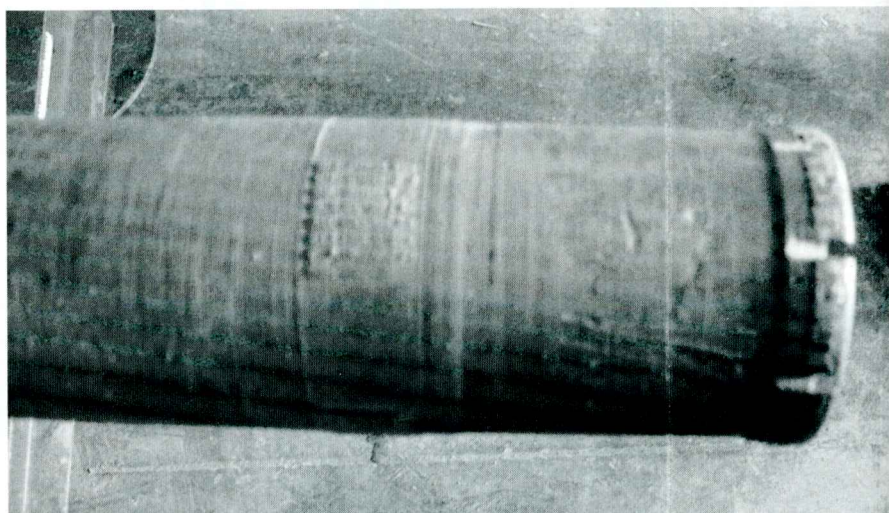
**Figure 2.38** Rock coring: (a) single-tube core barrel; (b) double-tube core barrel



**Figure 2.39** Diamond coring bit  
(Courtesy of Braja M. Das,  
Henderson, NV)



(a)



(b)

**Figure 2.40** Diamond coring bit attached to a double-tube core barrel: (a) end view; (b) side view (*Courtesy of Professional Service Industries, Inc. (PSI), Waukesha, Wisconsin*)

the photograph of a diamond coring bit. Figure 2.40 shows the end and side views of a diamond coring bit attached to a double-tube core barrel.

When the core samples are recovered, the depth of recovery should be properly recorded for further evaluation in the laboratory. Based on the length of the rock core

recovered from each run, the following quantities may be calculated for a general evaluation of the rock quality encountered:

$$\text{Recovery ratio} = \frac{\text{length of core recovered}}{\text{theoretical length of rock cored}} \quad (2.70)$$

#### Rock quality designation (RQD)

$$= \frac{\sum \text{length of recovered pieces equal to or larger than } 101.6 \text{ mm (4 in.)}}{\text{theoretical length of rock cored}} \quad (2.71)$$

A recovery ratio of unity indicates the presence of intact rock; for highly fractured rocks, the recovery ratio may be 0.5 or smaller. Table 2.11 presents the general relationship (Deere, 1963) between the RQD and the *in situ* rock quality.

**Table 2.11** Relation between *in situ* Rock Quality and RQD

RQD	Rock quality
0–0.25	Very poor
0.25–0.5	Poor
0.5–0.75	Fair
0.75–0.9	Good
0.9–1	Excellent

## 2.25

### Preparation of Boring Logs

The detailed information gathered from each borehole is presented in a graphical form called the *boring log*. As a borehole is advanced downward, the driller generally should record the following information in a standard log:

1. Name and address of the drilling company
2. Driller's name
3. Job description and number
4. Number, type, and location of boring
5. Date of boring
6. Subsurface stratification, which can be obtained by visual observation of the soil brought out by auger, split-spoon sampler, and thin-walled Shelby tube sampler
7. Elevation of water table and date observed, use of casing and mud losses, and so on
8. Standard penetration resistance and the depth of SPT
9. Number, type, and depth of soil sample collected
10. In case of rock coring, type of core barrel used and, for each run, the actual length of coring, length of core recovery, and RQD

This information should never be left to memory, because doing so often results in erroneous boring logs.

## Boring Log

Name of the Project <u>Two-story apartment building</u>					
Location <u>Johnson &amp; Olive St.</u> Date of Boring <u>March 2, 2005</u>					
Boring No. <u>3</u>	Type of <u>Hollow-stem auger</u>	Ground Boring	<u>60.8 m</u>	Elevation	
Soil description	Depth (m)	Soil sample type and number	$N_{60}$	$w_n$ (%)	Comments
Light brown clay (fill)					
Silty sand (SM)	1				
	2	SS-1	9	8.2	
<sup>°</sup> G.W.T. — <u>3.5 m</u> —	3	SS-2	12	17.6	LL = 38 PI = 11
Light gray clayey silt (ML)	4				
	5	ST-1		20.4	LL = 36 $q_u = 112 \text{ kN/m}^2$
Sand with some gravel (SP)	6	SS-3	11	20.6	
End of boring @ 8 m	7				
	8	SS-4	27	9	
$N_{60}$ = standard penetration number $w_n$ = natural moisture content LL = liquid limit; PI = plasticity index $q_u$ = unconfined compression strength SS = split-spoon sample; ST = Shelby tube sample			Groundwater table observed after one week of drilling		

Figure 2.41 A typical boring log

After completion of the necessary laboratory tests, the geotechnical engineer prepares a finished log that includes notes from the driller's field log and the results of tests conducted in the laboratory. Figure 2.41 shows a typical boring log. These logs have to be attached to the final soil-exploration report submitted to the client. The figure also lists the classifications of the soils in the left-hand column, along with the description of each soil (based on the Unified Soil Classification System).

## 2.26

## Geophysical Exploration

Several types of geophysical exploration techniques permit a rapid evaluation of subsoil characteristics. These methods also allow rapid coverage of large areas and are less expensive than conventional exploration by drilling. However, in many cases, definitive interpretation of the results is difficult. For that reason, such techniques should be used for preliminary work only. Here, we discuss three types of geophysical exploration technique: the seismic refraction survey, cross-hole seismic survey, and resistivity survey.

## Seismic Refraction Survey

Seismic refraction surveys are useful in obtaining preliminary information about the thickness of the layering of various soils and the depth to rock or hard soil at a site.

Refraction surveys are conducted by impacting the surface, such as at point A in Figure 2.42a, and observing the first arrival of the disturbance (stress waves) at several other points (e.g., B, C, D, . . .). The impact can be created by a hammer blow or by a small explosive charge. The first arrival of disturbance waves at various points can be recorded by geophones.

The impact on the ground surface creates two types of *stress wave*: *P waves* (or *plane waves*) and *S waves* (or *shear waves*). *P* waves travel faster than *S* waves; hence, the first arrival of disturbance waves will be related to the velocities of the *P* waves in various layers. The velocity of *P* waves in a medium is

$$v = \sqrt{\frac{E_s}{\left(\frac{\gamma}{g}\right)}} \frac{(1 - \mu_s)}{(1 - 2\mu_s)(1 + \mu_s)} \quad (2.72)$$

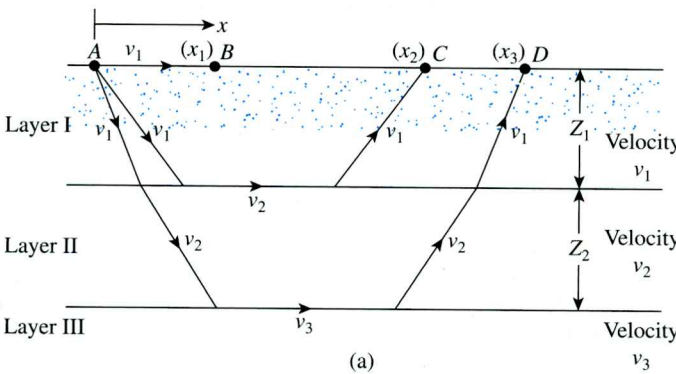
where

$E_s$  = modulus of elasticity of the medium

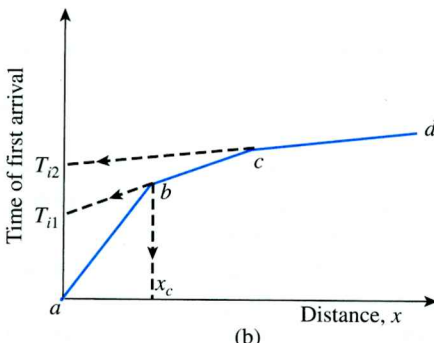
$\gamma$  = unit weight of the medium

$g$  = acceleration due to gravity

$\mu_s$  = Poisson's ratio



(a)



(b)

Figure 2.42 Seismic refraction survey

To determine the velocity  $v$  of  $P$  waves in various layers and the thicknesses of those layers, we use the following procedure:

- Step 1.* Obtain the times of first arrival,  $t_1, t_2, t_3, \dots$ , at various distances  $x_1, x_2, x_3, \dots$  from the point of impact.
- Step 2.* Plot a graph of time  $t$  against distance  $x$ . The graph will look like the one shown in Figure 2.42b.
- Step 3.* Determine the slopes of the lines  $ab, bc, cd, \dots$ :

$$\text{Slope of } ab = \frac{1}{v_1}$$

$$\text{Slope of } bc = \frac{1}{v_2}$$

$$\text{Slope of } cd = \frac{1}{v_3}$$

Here,  $v_1, v_2, v_3, \dots$  are the  $P$ -wave velocities in layers I, II, III, ..., respectively (Figure 2.42a).

- Step 4.* Determine the thickness of the top layer:

$$Z_1 = \frac{1}{2} \sqrt{\frac{v_2 - v_1}{v_2 + v_1}} x_c \quad (2.73)$$

The value of  $x_c$  can be obtained from the plot, as shown in Figure 2.42b.

- Step 5.* Determine the thickness of the second layer:

$$Z_2 = \frac{1}{2} \left[ T_{i2} - 2Z_1 \frac{\sqrt{v_3^2 - v_1^2}}{v_3 v_1} \right] \frac{v_3 v_2}{\sqrt{v_3^2 - v_2^2}} \quad (2.74)$$

Here,  $T_{i2}$  is the time intercept of the line  $cd$  in Figure 2.42b, extended backwards.

(For detailed derivatives of these equations and other related information, see Dobrin, 1960, and Das, 1992).

The velocities of  $P$  waves in various layers indicate the types of soil or rock that are present below the ground surface. The range of the  $P$ -wave velocity that is generally encountered in different types of soil and rock at shallow depths is given in Table 2.12.

In analyzing the results of a refraction survey, two limitations need to be kept in mind:

1. The basic equations for the survey—that is, Eqs. (2.73) and (2.74)—are based on the assumption that the  $P$ -wave velocity  $v_1 < v_2 < v_3 < \dots$ .
2. When a soil is saturated below the water table, the  $P$ -wave velocity may be deceptive.  $P$  waves can travel with a velocity of about 1500 m/sec (5000 ft/sec) through water. For dry, loose soils, the velocity may be well below 1500 m/sec. However, in a saturated condition, the waves will travel through water that is present in the void spaces with a velocity of about 1500 m/sec. If the presence of groundwater has not been detected, the  $P$ -wave velocity may be erroneously interpreted to indicate a stronger material (e.g., sandstone) than is actually present *in situ*. In general, geophysical interpretations should always be verified by the results obtained from borings.

**Table 2.12** Range of *P*-Wave Velocity in Various Soils and Rocks

Type of soil or rock	P-wave velocity	
	m/sec	ft/sec
<i>Soil</i>		
Sand, dry silt, and fine-grained topsoil	200–1000	650–3300
Alluvium	500–2000	1650–6600
Compacted clays, clayey gravel, and dense clayey sand	1000–2500	3300–8200
Loess	250–750	800–2450
<i>Rock</i>		
Slate and shale	2500–5000	8200–16,400
Sandstone	1500–5000	4900–16,400
Granite	4000–6000	13,100–19,700
Sound limestone	5000–10,000	16,400–32,800

### Example 2.1

The results of a refraction survey at a site are given in the following table:

Distance of geophone from the source of disturbance (m)	Time of first arrival (sec × 10 <sup>3</sup> )
2.5	11.2
5	23.3
7.5	33.5
10	42.4
15	50.9
20	57.2
25	64.4
30	68.6
35	71.1
40	72.1
50	75.5

Determine the *P*-wave velocities and the thickness of the material encountered.

### Solution

#### Velocity

In Figure 2.43, the times of first arrival of the *P* waves are plotted against the distance of the geophone from the source of disturbance. The plot has three straight-line segments. The velocity of the top three layers can now be calculated as follows:

$$\text{Slope of segment } 0a = \frac{1}{v_1} = \frac{\text{time}}{\text{distance}} = \frac{23 \times 10^{-3}}{5.25}$$

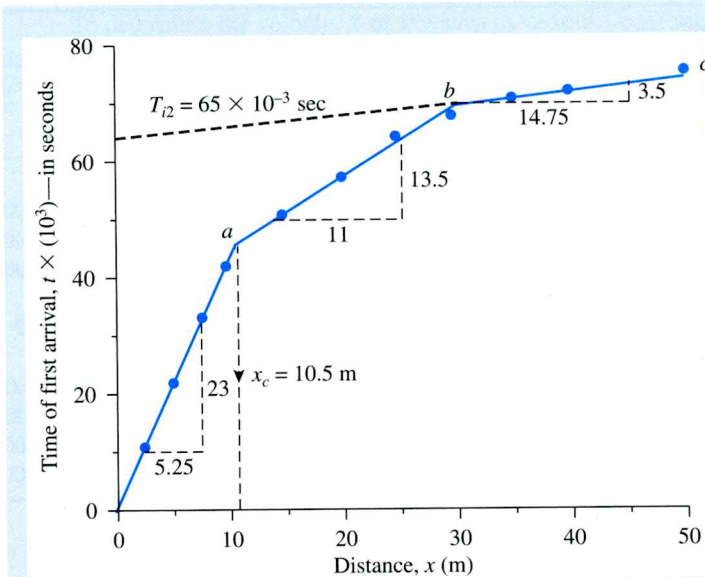


**Figure 2.43** Plot of first arrival time of  $P$  wave versus distance of geophone from source of disturbance

or

$$v_1 = \frac{5.25 \times 10^3}{23} = 228 \text{ m/sec (top layer)}$$

$$\text{Slope of segment } ab = \frac{1}{v_2} = \frac{13.5 \times 10^{-3}}{11}$$

or

$$v_2 = \frac{11 \times 10^3}{13.5} = 814.8 \text{ m/sec (middle layer)}$$

$$\text{Slope of segment } bc = \frac{1}{v_3} = \frac{3.5 \times 10^{-3}}{14.75}$$

or

$$v_3 = 4214 \text{ m/sec (third layer)}$$

Comparing the velocities obtained here with those given in Table 2.12 indicates that the third layer is a *rock layer*.

#### Thickness of Layers

From Figure 2.43,  $x_c = 10.5 \text{ m}$ , so

$$Z_1 = \frac{1}{2} \sqrt{\frac{v_2 - v_1}{v_2 + v_1}} x_c$$

Thus,

$$Z_1 = \frac{1}{2} \sqrt{\frac{814.8 - 228}{814.8 + 228}} \times 10.5 = 3.94 \text{ m}$$

Again, from Eq. (2.74)

$$Z_2 = \frac{1}{2} \left[ T_{i2} - \frac{2Z_1 \sqrt{v_3^2 - v_1^2}}{(v_3 v_1)} \right] \frac{(v_3)(v_2)}{\sqrt{v_3^2 - v_2^2}}$$

The value of  $T_{i2}$  (from Figure 2.43) is  $65 \times 10^{-3}$  sec. Hence,

$$\begin{aligned} Z_2 &= \frac{1}{2} \left[ 65 \times 10^{-3} - \frac{2(3.94)\sqrt{(4214)^2 - (228)^2}}{(4214)(228)} \right] \frac{(4214)(814.8)}{\sqrt{(4214)^2 - (814.8)^2}} \\ &= \frac{1}{2}(0.065 - 0.0345)830.47 = \mathbf{12.66 \text{ m}} \end{aligned}$$

Thus, the rock layer lies at a depth of  $Z_1 + Z_2 = 3.94 + 12.66 = \mathbf{16.60 \text{ m from the surface of the ground.}}$

### Cross-Hole Seismic Survey

The velocity of shear waves created as the result of an impact to a given layer of soil can be effectively determined by the *cross-hole seismic survey* (Stokoe and Woods, 1972). The principle of this technique is illustrated in Figure 2.44, which shows two holes drilled into the ground a distance  $L$  apart. A vertical impulse is created at the bottom of one borehole by means of an impulse rod. The shear waves thus generated are recorded by a vertically sensitive transducer. The velocity of shear waves can be calculated as

$$v_s = \frac{L}{t} \quad (2.75)$$

where  $t$  = travel time of the waves.

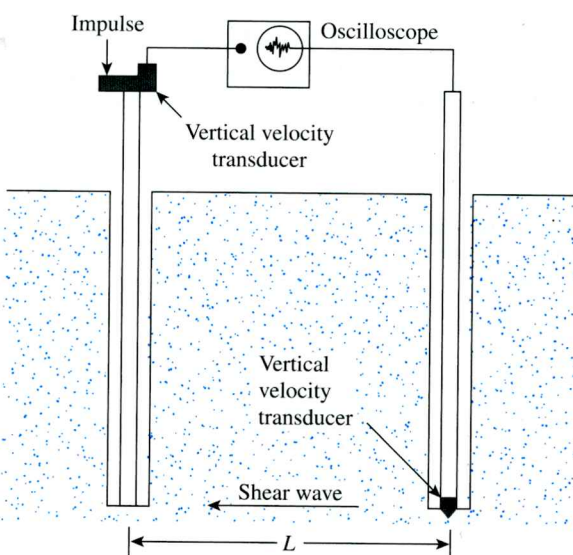


**Figure 2.44** Cross-hole method of seismic survey

The shear modulus  $G_s$  of the soil at the depth at which the test is taken can be determined from the relation

$$v_s = \sqrt{\frac{G_s}{(\gamma/g)}}$$

or

$$G_s = \frac{v_s^2 \gamma}{g} \quad (2.76)$$

where

$v_s$  = velocity of shear waves

$\gamma$  = unit weight of soil

$g$  = acceleration due to gravity

The shear modulus is useful in the design of foundations to support vibrating machinery and the like.

### Resistivity Survey

Another geophysical method for subsoil exploration is the *electrical resistivity survey*. The electrical resistivity of any conducting material having a length  $L$  and an area of cross section  $A$  can be defined as

$$\rho = \frac{RA}{L} \quad (2.77)$$

where  $R$  = electrical resistance.

The unit of resistivity is *ohm-centimeter* or *ohm-meter*. The resistivity of various soils depends primarily on their moisture content and also on the concentration of dissolved ions in them. Saturated clays have a very low resistivity; dry soils and rocks have a high resistivity. The range of resistivity generally encountered in various soils and rocks is given in Table 2.13.

The most common procedure for measuring the electrical resistivity of a soil profile makes use of four electrodes driven into the ground and spaced equally along a straight line. The procedure is generally referred to as the *Wenner method* (Figure 2.45a).

**Table 2.13** Representative Values of Resistivity

Material	Resistivity (ohm · m)
Sand	500–1500
Clays, saturated silt	0–100
Clayey sand	200–500
Gravel	1500–4000
Weathered rock	1500–2500
Sound rock	>5000

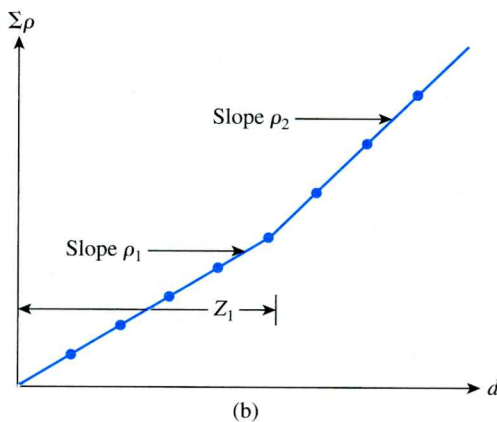
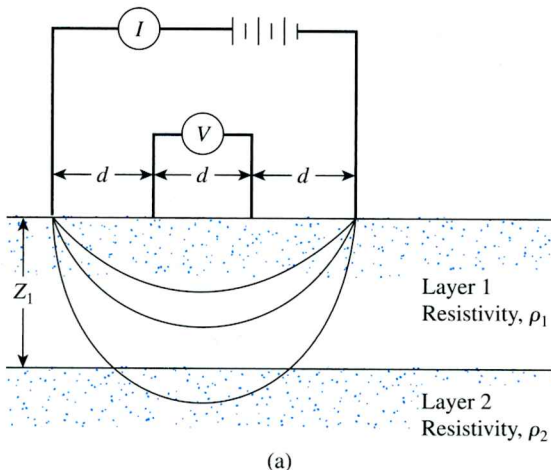


**Figure 2.45** Electrical resistivity survey: (a) Wenner method; (b) empirical method for determining resistivity and thickness of each layer

The two outside electrodes are used to send an electrical current  $I$  (usually a dc current with nonpolarizing potential electrodes) into the ground. The current is typically in the range of 50 to 100 milliamperes. The voltage drop,  $V$ , is measured between the two inside electrodes. If the soil profile is homogeneous, its electrical resistivity is

$$\rho = \frac{2\pi dV}{I} \quad (2.78)$$

In most cases, the soil profile may consist of various layers with different resistivities, and Eq. (2.78) will yield the *apparent resistivity*. To obtain the *actual resistivity* of various layers and their thicknesses, one may use an empirical method that involves conducting tests at various electrode spacings (i.e.,  $d$  is changed). The sum of the apparent resistivities,  $\Sigma\rho$ , is plotted against the spacing  $d$ , as shown in Figure 2.45b. The plot thus obtained has relatively straight segments, the slopes of which give the resistivity of individual layers. The thicknesses of various layers can be estimated as shown in Figure 2.45b.

The resistivity survey is particularly useful in locating gravel deposits within a fine-grained soil.

## 2.27 Subsoil Exploration Report

At the end of all soil exploration programs, the soil and rock specimens collected in the field are subject to visual observation and appropriate laboratory testing. (The basic soil tests were described in Chapter 1.) After all the required information has been compiled, a soil exploration report is prepared for use by the design office and for reference during future construction work. Although the details and sequence of information in such reports may vary to some degree, depending on the structure under consideration and the person compiling the report, each report should include the following items:

1. A description of the scope of the investigation
2. A description of the proposed structure for which the subsoil exploration has been conducted
3. A description of the location of the site, including any structures nearby, drainage conditions, the nature of vegetation on the site and surrounding it, and any other features unique to the site
4. A description of the geological setting of the site
5. Details of the field exploration—that is, number of borings, depths of borings, types of borings involved, and so on
6. A general description of the subsoil conditions, as determined from soil specimens and from related laboratory tests, standard penetration resistance and cone penetration resistance, and so on
7. A description of the water-table conditions
8. Recommendations regarding the foundation, including the type of foundation recommended, the allowable bearing pressure, and any special construction procedure that may be needed; alternative foundation design procedures should also be discussed in this portion of the report
9. Conclusions and limitations of the investigations

The following graphical presentations should be attached to the report:

1. A site location map
2. A plan view of the location of the borings with respect to the proposed structures and those nearby
3. Boring logs
4. Laboratory test results
5. Other special graphical presentations

The exploration reports should be well planned and documented, as they will help in answering questions and solving foundation problems that may arise later during design and construction.

## Problems

- 2.1** For a Shelby tube, given: outside diameter = 3 in. and inside diameter 2.874 in. What is the area ratio of the tube?
- 2.2** A soil profile is shown in Figure P2.2 along with the standard penetration numbers in the clay layer. Use Eqs. (2.8) and (2.9) to determine the variation of  $c_u$  and OCR with depth. What is the average value of  $c_u$  and OCR?

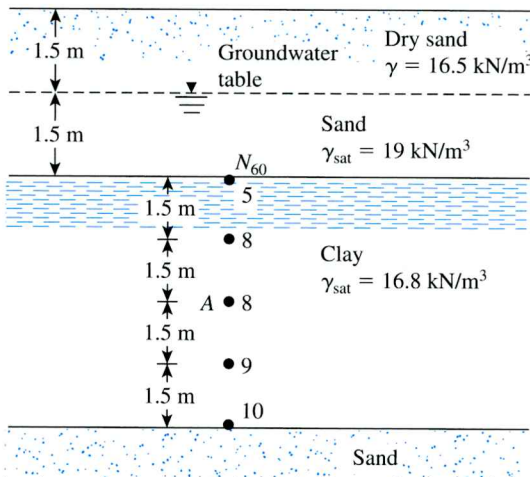


**Figure P2.2**

- 2.3** Following is the variation of the field standard penetration number ( $N_{60}$ ) in a sand deposit:

Depth (m)	$N_{60}$
1.5	6
3	8
4.5	9
6	8
7.9	13
9	14

The groundwater table is located at a depth of 6 m. Given: the dry unit weight of sand from 0 to a depth of 6 m is  $18 \text{ kN/m}^3$ , and the saturated unit weight of sand for depth 6 to 12 m is  $20.2 \text{ kN/m}^3$ . Use the relationship of Skempton given in Eq. (2.12) to calculate the corrected penetration numbers.

- 2.4** For the soil profile described in Problem 2.3, estimate an average peak soil friction angle. Use Eq. (2.28).
- 2.5** Repeat Problem 2.4 using Eq. (2.27).
- 2.6** Refer to Problem 2.3. Using Eq. (2.20), determine the average relative density of sand.
- 2.7** The following table gives the variation of the field standard penetration number ( $N_{60}$ ) in a sand deposit:

Depth (m)	$N_{60}$
1.5	5
3.0	11
4.5	14
6.0	18
7.5	16
9.0	21

The groundwater table is located at a depth of 12 m. The dry unit weight of sand from 0 to a depth of 12 m is  $17.6 \text{ kN/m}^3$ . Assume that the mean grain size ( $D_{50}$ ) of the sand deposit to be about 0.8 mm. Estimate the variation of the relative density with depth for sand. Use Eq. (2.21).

- 2.8** Following are the standard penetration numbers determined from a sandy soil in the field:

Depth (ft)	Unit weight of soil (lb/ft <sup>3</sup> )	$N_{60}$
10	106	7
15	106	9
20	106	11
25	118	16
30	118	18
35	118	20
40	118	22

Using Eq. (2.27), determine the variation of the peak soil friction angle,  $\phi'$ .

Estimate an average value of  $\phi'$  for the design of a shallow foundation.  
(Note: For depth greater than 20 ft, the unit weight of soil is  $118 \text{ lb/ft}^3$ .)

- 2.9** Refer to Problem 2.8. Assume that the sand is clean and normally consolidated. Estimate the average value of the modulus of elasticity between depths of 20 ft and 30 ft.
- 2.10** Following are the details for a soil deposit in sand:

Depth (m)	Effective overburden pressure (kN/m <sup>2</sup> )	Field standard penetration number, $N_{60}$
3.0	55	9
4.5	82	11
6.0	98	12

Assume the uniformity coefficient ( $C_u$ ) of the sand to be 2.8 and an overconsolidation ratio (OCR) of 2. Estimate the average relative density of the sand between the depth of 3 to 6 m. Use Eq. (2.19).

- 2.11** Refer to Figure P2.2. Vane shear tests were conducted in the clay layer. The vane dimensions were  $63.5 \text{ mm } (D) \times 127 \text{ mm } (H)$ . For the test at A, the torque required to cause failure was  $0.051 \text{ N}\cdot\text{m}$ . For the clay, given: liquid limit = 46 and plastic limit = 21. Estimate the undrained cohesion of the clay for use in the design by using Bjerrum's  $\lambda$  relationship [Eq. (2.35a)].
- 2.12** Refer to Problem 2.11. Estimate the overconsolidation ratio of the clay. Use Eqs. (2.37) and (2.38).
- 2.13** **a.** A vane shear test was conducted in a saturated clay. The height and diameter of the vane were 4 in. and 2 in., respectively. During the test, the maximum torque applied was 23 lb-ft. Determine the undrained shear strength of the clay.
- b.** The clay soil described in part (a) has a liquid limit of 58 and a plastic limit of 29. What would be the corrected undrained shear strength of the clay for design purposes? Use Bjerrum's relationship for  $\lambda$  [Eq. (2.35a)].
- 2.14** Refer to Problem 2.13. Determine the overconsolidation ratio for the clay. Use Eqs. (2.37) and (2.40). Use  $\sigma'_0 = 1340 \text{ lb/ft}^2$ .

- 2.15** In a deposit of normally consolidated dry sand, a cone penetration test was conducted. Following are the results:

Depth (m)	Point resistance of cone, $q_c$ (MN/m <sup>2</sup> )
1.5	2.06
3.0	4.23
4.5	6.01
6.0	8.18
7.5	9.97
9.0	12.42

Assuming the dry unit weight of sand to be 16 kN/m<sup>3</sup>, estimate the average peak friction angle,  $\phi'$ , of the sand. Use Eq. (2.48).

- 2.16** Refer to Problem 2.15. Using Eq. (2.46), determine the variation of the relative density with depth.
- 2.17** In the soil profile shown in Figure P2.17, if the cone penetration resistance ( $q_c$ ) at A (as determined by an electric friction-cone penetrometer) is 0.8 MN/m<sup>2</sup>, estimate
- The undrained cohesion,  $c_u$
  - The overconsolidation ratio, OCR
- 2.18** In a pressuremeter test in a soft saturated clay, the measuring cell volume  $V_o = 535 \text{ cm}^3$ ,  $p_o = 42.4 \text{ kN/m}^2$ ,  $p_f = 326.5 \text{ kN/m}^2$ ,  $v_o = 46 \text{ cm}^3$ , and  $v_f = 180 \text{ cm}^3$ . Assuming Poisson's ratio ( $\mu_s$ ) to be 0.5 and using Figure 2.32, calculate the pressuremeter modulus ( $E_p$ ).
- 2.19** A dilatometer test was conducted in a clay deposit. The groundwater table was located at a depth of 3 m below the surface. At a depth of 8 m below the surface, the contact pressure ( $p_o$ ) was 280 kN/m<sup>2</sup> and the expansion stress ( $p_1$ ) was 350 kN/m<sup>2</sup>. Determine the following:
- Coefficient of at-rest earth pressure,  $K_o$
  - Overconsolidation ratio, OCR
  - Modulus of elasticity,  $E_s$
- Assume  $\sigma'_o$  at a depth of 8 m to be 95 kN/m<sup>2</sup> and  $\mu_s = 0.35$ .

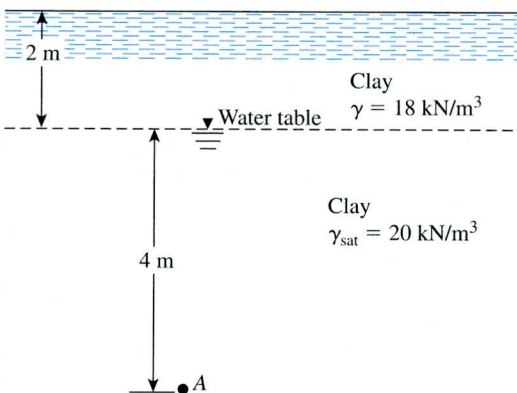


Figure P2.17

- 2.20** A dilatometer test was conducted in a sand deposit at a depth of 6 m. The ground-water table was located at a depth of 2 m below the ground surface. Given, for the sand:  $\gamma_d = 14.5 \text{ kN/m}^3$  and  $\gamma_{\text{sat}} = 19.8 \text{ kN/m}^3$ . The contact stress during the test was  $260 \text{ kN/m}^2$ . Estimate the soil friction angle,  $\phi'$ .
- 2.21** The  $P$ -wave velocity in a soil is 1900 m/sec. Assuming Poisson's ratio to be 0.32, calculate the modulus of elasticity of the soil. Assume that the unit weight of soil is  $18 \text{ kN/m}^3$ .
- 2.22** The results of a refraction survey (Figure 2.42a) at a site are given in the following table. Determine the thickness and the  $P$ -wave velocity of the materials encountered.

Distance from the source of disturbance (m)	Time of first arrival of $P$ -waves (sec $\times 10^3$ )
2.5	5.08
5.0	10.16
7.5	15.24
10.0	17.01
15.0	20.02
20.0	24.2
25.0	27.1
30.0	28.0
40.0	31.1
50.0	33.9

## References

- AMERICAN SOCIETY FOR TESTING AND MATERIALS (2001). *Annual Book of ASTM Standards*, Vol. 04.08, West Conshohocken, PA.
- AMERICAN SOCIETY OF CIVIL ENGINEERS (1972). "Subsurface Investigation for Design and Construction of Foundations of Buildings," *Journal of the Soil Mechanics and Foundations Division*, American Society of Civil Engineers, Vol. 98, No. SM5, pp. 481–490.
- ANAGNOSTOPOULOS, A., KOUKIS, G., SABATAKAKIS, N., and TSIAMBAOS, G. (2003). "Empirical Correlations of Soil Parameters Based on Cone Penetration Tests (CPT) for Greek Soils," *Geotechnical and Geological Engineering*, Vol. 21, No. 4, pp. 377–387.
- BAGUELIN, F., JÉZÉQUEL, J. F., and SHIELDS, D. H. (1978). *The Pressuremeter and Foundation Engineering*, Trans Tech Publications, Clausthal, Germany.
- BALDI, G., BELLOTTI, R., GHIONNA, V., and JAMIOLKOWSKI, M. (1982). "Design Parameters for Sands from CPT," *Proceedings, Second European Symposium on Penetration Testing*, Amsterdam, Vol. 2, pp. 425–438.
- BAZARAA, A. (1967). *Use of the Standard Penetration Test for Estimating Settlements of Shallow Foundations on Sand*, Ph.D. Dissertation, Civil Engineering Department, University of Illinois, Champaign-Urbana, Illinois.
- BJERRUM, L. (1972). "Embankments on Soft Ground," *Proceedings of the Specialty Conference*, American Society of Civil Engineers, Vol. 2, pp. 1–54.
- CRUDEN, D. M., and VARNES, D. J. (1996). "Landslide Types and Processes," *Special Report 247*, Transportation Research Board, pp. 36–75.
- CUBRINOVSKI, M., and ISHIHARA, K. (1999). "Empirical Correlations between SPT  $N$ -Values and Relative Density for Sandy Soils," *Soils and Foundations*, Vol. 39, No. 5, pp. 61–92.
- DAS, B. M. (1992). *Principles of Soil Dynamics*, PWS Publishing Company, Boston.

# 3

## Shallow Foundations: Ultimate Bearing Capacity

### 3.1

#### Introduction

To perform satisfactorily, shallow foundations must have two main characteristics:

1. They have to be safe against overall shear failure in the soil that supports them.
2. They cannot undergo excessive displacement, or settlement. (The term *excessive* is relative, because the degree of settlement allowed for a structure depends on several considerations.)

The load per unit area of the foundation at which shear failure in soil occurs is called the *ultimate bearing capacity*, which is the subject of this chapter.

### 3.2

#### General Concept

Consider a strip foundation with a width of  $B$  resting on the surface of a dense sand or stiff cohesive soil, as shown in Figure 3.1a. Now, if a load is gradually applied to the foundation, settlement will increase. The variation of the load per unit area on the foundation ( $q$ ) with the foundation settlement is also shown in Figure 3.1a. At a certain point—when the load per unit area equals  $q_u$ —a sudden failure in the soil supporting the foundation will take place, and the failure surface in the soil will extend to the ground surface. This load per unit area,  $q_u$ , is usually referred to as the *ultimate bearing capacity of the foundation*. When such sudden failure in soil takes place, it is called *general shear failure*.

If the foundation under consideration rests on sand or clayey soil of medium compaction (Figure 3.1b), an increase in the load on the foundation will also be accompanied by an increase in settlement. However, in this case the failure surface in the soil will gradually extend outward from the foundation, as shown by the solid lines in Figure 3.1b. When the load per unit area on the foundation equals  $q_{u(1)}$ , movement of the foundation will be accompanied by sudden jerks. A considerable movement of the foundation is then required for the failure surface in soil to extend to the ground surface (as shown by the broken lines in the figure). The load per unit area at which this happens is the *ultimate bearing capacity*,  $q_u$ . Beyond that point, an increase in load will be

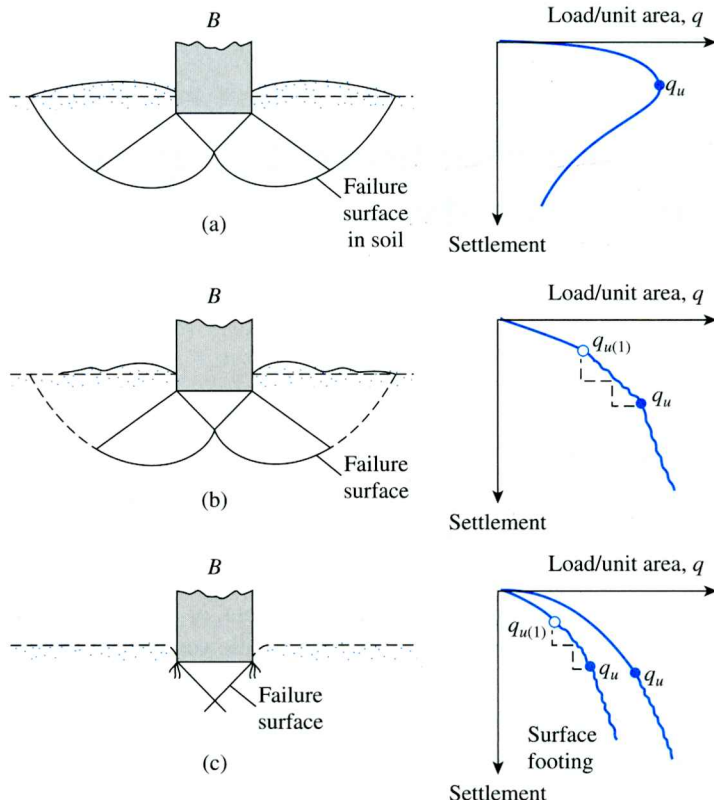


**Figure 3.1** Nature of bearing capacity failure in soil: (a) general shear failure; (b) local shear failure; (c) punching shear failure (Redrawn after Vesic, 1973) (Vesic, A. S. (1973). "Analysis of Ultimate Loads of Shallow Foundations," *Journal of Soil Mechanics and Foundations Division, American Society of Civil Engineers*, Vol. 99, No. SM1, pp. 45–73. With permission from ASCE.)

accompanied by a large increase in foundation settlement. The load per unit area of the foundation,  $q_{u(1)}$ , is referred to as the *first failure load* (Vesic, 1963). Note that a peak value of  $q$  is not realized in this type of failure, which is called the *local shear failure* in soil.

If the foundation is supported by a fairly loose soil, the load-settlement plot will be like the one in Figure 3.1c. In this case, the failure surface in soil will not extend to the ground surface. Beyond the ultimate failure load,  $q_u$ , the load-settlement plot will be steep and practically linear. This type of failure in soil is called the *punching shear failure*.

Vesic (1963) conducted several laboratory load-bearing tests on circular and rectangular plates supported by a sand at various relative densities of compaction,  $D_r$ . The variations of  $q_{u(1)}/\frac{1}{2}\gamma B$  and  $q_u/\frac{1}{2}\gamma B$  obtained from those tests, where  $B$  is the diameter of a circular plate or width of a rectangular plate and  $\gamma$  is a dry unit weight of sand, are shown in Figure 3.2. It is important to note from this figure that, for  $D_r \geq 70\%$ , the general shear type of failure in soil occurs.

On the basis of experimental results, Vesic (1973) proposed a relationship for the mode of bearing capacity failure of foundations resting on sands. Figure 3.3